UNIVERSITY OF CALIFORNIA SAN DIEGO

Injectable Biomaterials for Skeletal Muscle Regeneration

A dissertation submitted in partial satisfaction of the
Requirements for the degree Doctor of Philosophy

in

Bioengineering

by

Jessica Leigh Ungerleider

Committee in Charge:

Professor Karen L. Christman, Chair
Professor Adam J. Engler
Professor Nathan C. Gianneschi
Professor Ehtisham Mahmud
Professor Samuel R. Ward

2018

The Dissertation of Jessica Leigh Ungerleider is approved, and it is acceptable in quality and form for publication on microfilm and electronically:

Chair

University of California San Diego

2018

DEDICATION

To my parents, my brothers, and Mehmet, and in loving memory of Eleanor Ungerleider.

TABLE OF CONTENTS

LIST OF ABBREVIATIONS

ANOVA = Analysis of Variance Test

bFGF = Basic Fibroblast Growth Factor

BM-MSCs = Bone Marrow Mesenchymal Stromal Cells

BM-MNCs = Bone Marrow Mononuclear Cells

CBER = Center for Biologic Evaluation and Research

CDER = Center for Drug Evaluation and Research

CDRH = Center for Devices and Radiological Health

cECM = Cardiac Extracellular Matrix

cGMP = Current Good Manufacturing Practice

CLI = Critical Limb Ischemia

D = Days

DAVID = Database for Annotation, Visualization, and Integrated Discovery

DE = Differentially Expressed

DLS = Dynamic Light Scattering

DMF = Dimethylformamide

DPBS = Dulbecco's Phosphate Buffered Saline

ECM = Extracellular Matrix

EPCs = Endothelial Progenitor Cells

EVE = Ethyl Vinyl Ether

FDA = US Food and Drug Administration

GFP = Green Fluorescent Protein

GLP = Good Laboratory Practice

GMP = Good Manufacturing Practice

H&E = Hematoxylin and Eosin

HA = Hyaluronic Acid

HGF = Hepatocyte Growth Factor

hUC = Human Umbilical Cord Matrix

HUVECs = Human Umbilical Vein Endothelial Cells

IM = Intramuscular

IR = Infrared

ISO = International Standards Office

IV = Intravenous

IVIS = In Vivo Imaging System

LASCA = Laser Speckle Contrast Analysis

LNG = Lung Extracellular Matrix

MI = Myocardial Infarction

MMP = Matrix Metalloproteinase

MPS = Monocyte Phagocytic System

NMR = Nuclear Magnetic Resonance

NP = Nanoparticle

NTF = Normalized Transmission Fluorescence

NTX = Notexin

OCP = Office of Combination Products

OCT = Optimal Cutting Temperature Compound

PAD = Peripheral Artery Disease

PCA = Principal Component Analysis

PLGA = Poly-lactic co-Glycolic Acid

PPA = Peptide Polymer Amphiphile

PRP = Platelet Rich Plasma

QA = Quality Assurance

qPCR = Quantitative Polymerase Chain Reaction

RFD = Request for Designation

ROMP = Ring Opening Metathesis Polymerization

SEC-MALS = Size Exclusion Chromatography – Multi Angle Light Scattering

SDF-1 = Stem Cell Derived Factor

sGAG = Sulfate Glycosaminoglycans

SKM = Skeletal Muscle Matrix

TEM = Transmission Electron Microscopy

US = United States

VEGF = Vascular Endothelial Growth Factor

Wks = Weeks

LIST OF FIGURES AND SCHEMES

LIST OF TABLES

ACKNOWLEDGEMENTS

I would like to thank Karen Christman, my thesis advisor, for her mentorship and guidance over the past five years. I have learned so much from her: about independent and creative thinking, experimental design, administrative and managerial aspects of research, grant-writing, and big picture vision in science. I have evolved significantly as a scientist and as a person throughout this period, and for that I am very grateful to Karen for enabling me to reach my full potential.

I would like to thank all of the members of the Christman lab, past and present, for their guidance, helpful discussions, and friendship. I am especially thankful for Todd Johnson, Jean Wang-Wassenaar, Melissa Hernandez, Mary Nguyen, Roberto Gaetani, Gina Policastro, and Holly Sullivan. I also want to thank my thesis committee members and collaborators for their helpful discussions and guidance through this research endeavor: Nathan Gianneschi, Sam Ward, Shami Mahmud, and Adam Engler. I also could not have done much of this research without the help of my undergraduate collaborators and mentees: Jeanne Li, Dean Elhag, Michelle Wong, Cori Espelian, Eti Sinha, Nicole Friend, Dylan Zawila, Juhi Madan, Neil Aiad, and Emma Zelus.

I am also very appreciative for my collaborators over the years. Specifically, I have really enjoyed working with Jacquelin Kammeyer, Andrea Carlini, Mike Gibbons, Monika Dzieciatkowska, Kristen Stearns-Reider, Ninna Rossen, and the Gianneschi, Ward, and Crosbie-Watson labs.

I also wouldn't have been able to reach this point in life without my loving friends and family. Thanks especially to Diane and Peter Ungerleider, Stephen and Daniel Ungerleider, Jackie Lomboy and Melanie Shields, Arlene, Pam, and Brittney Phillips, Shane and Lily Williams, John and Patricia Phillips, Art Ungerleider, David, Julie, and all of the Ungerleider clan. Forever thankful to Mehmet Badur, and to my bioengineering classmates Aimee Raleigh, Colton Lloyd, Kara Johnson, Mike Gibbons, Ajay Sapre, Ricky O'Laughlin, and Nick Csicsery.

Also to Aimee Raleigh, Mike Gibbons, Sarah Plfedderrer, Colton Lloyd, Casey Parsons, Andy Drummond, Ricky O'Laughlin, Jenna Summerfield, Jacquelin Kammeyer, and Cliff Woodford for keeping Mehmet and I sane.

Chapter 1, in part, is a reprint of the material as it appears in *Stem Cells Translational Medicine*, 2014, 3(9): 1090-1099. The authors are Jessica Ungerleider and Karen Christman. The dissertation author was the primary investigator and author of this paper.

Chapter 2, in full, is a reprint of the material as it appears in *Methods*, 2015, 84: 53-59. The authors are Jessica Ungerleider, Todd Johnson, Nikhil Rao, and Karen Christman. The dissertation author was the primary investigator and author of this paper.

Chapter 3, in part, is a reprint of the material as it appears in *Journal of the American College of Cardiology: Basic to Translational Science*, 2016, 1(1-2): 32-44. The authors include Jessica Ungerleider, Todd Johnson, Melissa Hernandez, Dean Elhag, Rebecca Braden, Monika Dzieciatkowska, Kent Osborn, Kirk Hansen, Ehtisham Mahmud, and Karen Christman. The dissertation author was the primary investigator and co-first author of this paper.

Chapter 4, in full is currently being prepared for submission for publication of the material. The authors are Jessica Ungerleider and Karen Christman. The dissertation author was the primary investigator and author of this material.

Chapter 5, in part, is a reprint of the material as it appears in *Polymer Chemistry*, 2017, 8(34): 5212-5219. The authors are Jessica Ungerleider, Jacquelin Kammeyer, Rebecca Braden, Karen Christman, and Nathan Gianneschi. The dissertation author was the primary investigator and co-first author of this paper.

VITA

2013 Bachelor of Science, University of Virginia

2017 Master of Science, University of California San Diego

2018 Doctor of Philosophy, University of California San Diego

PUBLICATIONS

Ungerleider JL*, Kammeyer JK*, Braden RL, Christman KL, Gianneschi NC. Enzyme-targeted nanoparticles for delivery to ischemic skeletal muscle. *Polymer Chemistry* (2017) 8(34): 5212-5219.

Ungerleider JL*, Johnson TD*, Hernandez MJ, Elhag DI, Braden RL, Dzieciatkowska M, Osborn KG, Hansen KC, Mahmud E, Christman KL. Extracellular matrix hydrogel promotes tissue remodeling, arteriogenesis, and perfusion in a rat hindlimb ischemia model. *Journal of the American College of Cardiology: Basic to Translational Science* (2016) 1(1-2): 32-44.

Ungerleider JL, Johnson TD, Rao N, Christman KL. Synthesis and evaluation of injectable hydrogels for peripheral artery disease. *Methods* (2015) 84: 53-59.

Rao N, Agmon G, Tierney MT, Ungerleider JL, Braden RL, Sacco A, Christman KL. Engineering an injectable muscle-specific microenvironment for improved cell delivery using a nanofibrous extracellular matrix hydrogel. *ACS Nano* (2017) 11: 3851-3859.

Zhang Y, Gao W, Chen Y, Escajadillo T, Ungerleider J, Fang RH, Christman K, Nizet V, Zhang L. Self-assembled colloidal gel using cell membrane-coated nanosponges as building blocks. *ACS Nano* (2017) 11: 11923-11930.

Johnson TD, DeQuach JA, Gaetani R, Ungerleider JL, Elhag D, Nigam V, Behfar A, Christman KL. Human versus porcine tissue sourcing for an injectable myocardial matrix. *Biomaterials Science* (2014) 2: 735-744.

Gaetani R, Ungerleider JL, Christman KL. Acellular injectable biomaterials for treating cardiovascular disease. *Stem Cell and Gene Therapy for Cardiovascular Disease* (2015) Chapter 25.

Ungerleider JL and Christman KL. Injectable biomaterials for the treatment of myocardial infarction and peripheral artery disease: translational challenges and progress. *Stem Cells Translational Medicine* (2014) 3(9): 1090-1099.

ABSTRACT OF THE DISSERTATION

Injectable Biomaterials for Skeletal Muscle Regeneration

By

Jessica Leigh Ungerleider

Doctor of Philosophy in Bioengineering

University of California San Diego, 2018

Professor Karen Christman, Chair

Skeletal muscle injury is a leading cause of diminished quality of life and morbidity in adults, with limited therapeutic interventions. Synthetic and naturally-derived biomaterials provide a potential avenue for novel treatment modalities that address unmet clinical needs. These materials can improve delivery of biological therapeutics or serve as acellular scaffolds for stimulating endogenous tissue repair processes. The goals of this dissertation were to investigate the efficacy of a decellularized skeletal muscle matrix hydrogel in tissue specific

regeneration and to design tunable enzyme-targeted nanoparticles for minimally invasive delivery to ischemic muscle.

An injectable decellularized skeletal muscle matrix hydrogel has previously been developed by our lab as a therapy to improve perfusion to ischemic skeletal muscle in a preclinical peripheral artery disease model. To better understand how the skeletal muscle matrix induces beneficial effects, transcriptomic analysis of matrix or saline-injected muscle was performed in both ischemic and acute muscle regeneration models. We showed that the skeletal muscle matrix increased cell survival, neovascularization, and muscle regeneration and confirmed these pathways through histological analysis at short, medium, and long time points. In acute muscle regeneration, the skeletal muscle matrix increased the density of skeletal muscle progenitors over non-specific controls (lung matrix or saline). This suggests the tissue specific source of the decellularized matrix can have an effect on regenerative pathways.

Enzyme-targeted nanoparticles are an alternative biomaterial approach for more minimally invasive therapeutic delivery as they can be injected intravenously and will target ischemic tissue due to overexpression of matrix metalloproteinases. We were the first group to show minimally invasive targeting of peptide-polymer nanoparticles to ischemic skeletal muscle. We also showed tunable nanoparticle targeting through altering the packing density of enzyme cleavable peptide and the surface charge of the nanoparticles.

Chapter 1

Injectable biomaterials for the treatment of peripheral artery disease: translational challenges and progress

1.1 Introduction

Cardiovascular disease is the leading cause of morbidity and mortality in the US [1]. Although there are about 83.6 million Americans who suffer from the disease in some capacity, there is still no cure for some of the most common cardiovascular events like myocardial infarction (MI) and peripheral artery disease (PAD). PAD is a condition that afflicts 12 to 20 percent of Americans over 65 [2]. Its most common cause is atherosclerosis, but it predominantly afflicts smokers, diabetics, and African Americans. The disease first presents as pain during exercise (also called intermittent claudication) due to chronic plaque build-up and reduced blood flow in peripheral arteries, most commonly in the legs [1]. These patients can exhibit muscle denervation and atrophy in fiber cross-sectional area [3]. Over time, the plaque occludes more of the major arteries and leads to critical limb ischemia (CLI), the most severe form of the disease. CLI affects about a quarter of the overall PAD population. CLI patients present with pain at rest, ulcers or gangrene, and a significant risk of amputation [4]. The skeletal muscle of these patients also exhibits atrophy, denervation, and a loss of type II fibers relative to type I fibers [5–7]. The main treatments include lifestyle changes such as diet and exercise, or pharmacologic interventions to treat the underlying causes of the disease, such as cilostazol. In patients who remain symptomatic, surgical revascularization is an option. However, few patients are eligible for this therapy due to the diffuse nature of the atherosclerotic lesions, and it carries a high failure rate due to restenosis, which is why amputation rates due to PAD have remained relatively unchanged in the last 30 years [8,9]. Thus, there is a strong need for tissue salvage and

restoration of muscle function in these patients. An ideal therapy will increase blood flow to the ischemic tissue and promote regenerative pathways to reduce muscle denervation and atrophy. In this introduction, we will focus on recent developments in the field of injectable biomaterial scaffolds and related regenerative medicine therapies for preventing and/or treating PAD (Figure 1.1). We will then investigate the main obstacles faced by investigators in translating their therapies to the clinic, including regulatory considerations, delivery concerns, and manufacturing-related challenges.

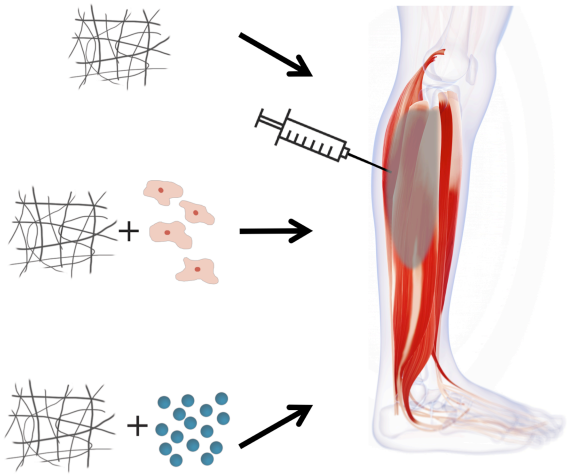

Figure 1.1. Injectable therapies for PAD. Current biomaterial-based regenerative medicine therapies for peripheral artery disease (PAD) involve either a material alone, material plus cells, or material plus other therapeutics (e.g. growth factors). Most studies involve intramuscular injections directly to the site of ischemia.

1.2 Current Biomaterial-based Regenerative Medicine Approaches

Although gene therapy, stem cells, and growth factors have all been studied for PAD, the use of biomaterials either to enhance these therapies or to act as a stand-alone treatment is just beginning to be explored. Thus, in this review we will cover both small and large animal preclinical studies of injectable biomaterials for PAD (Table 1.1).

Table 1.1: Selected Injectable Biomaterials for PAD

Material	Other Therapeutic	Species	Injury model	Delivery Method	Time of treatment post-injury	Time of assessment	Perfusion	Neo-vascularization	Other	Ref.
HA	HUVECs	Mouse	Femoral and iliac artery ligation, excised	IM	1 d	4 wks	Increased	Increased arterioles and capillaries	Increased cell survival	[10]
Collagen	BM-MSCs	Rabbit	Femoral artery excised	IM	10 d	6 and 8 wks	Increased oxygen saturation ratio	Increased arterioles and capillaries		[11]
Hydroxy-apatite nano-particles	BM-MNCs	Mouse	Femoral artery, vein, and side branches excised	IM	Immediate	14 d		Increased arterioles and capillaries	Increased cell survival, VEGF and bFGF levels in tissue	[12]
Glutar-aldehyde-cross-linked gelatin micro-spheres	bFGF	Dog	External iliac artery ligated, femoral artery excised	IM	7 d	30 d		Increased arterioles and capillaries		[13]
Alginate	HGF	Mouse	Femoral artery excised	IM	1 d	9 d	Increased	Increased arterioles		[14]
Alginate micro-spheres in collagen hydrogel	SDF-1	Mouse	Femoral artery ligated	IM	Immediate	2 wks	Increased	Increased arterioles	Increased recruitment of progenitor cells	[15]
Fragmin-protamine micro-particles	bFGF, platelet-rich plasma	Rabbit and Mouse	Femoral artery excised	IM	1 or 10 d	14 or 18 d		Increased arterioles	Improved calf blood pressure	[16,17]
Peptide nano-fibers	Substance P	Mouse	Femoral artery and side branches excised	IM	1 d	4 wks	Increased	Increased arterioles and capillaries	Increased cell survival	[18]
Peptide nano-fibers	VEGF-mimetic epitope	Mouse	Femoral artery excised	IM	3 d	4 wks	Increased	Increased capillaries		[19]
Gold nano-particles	VEGF	Mouse	Femoral artery and vein and iliac artery excised	IV	1 d	40 d	Increased	Increased capillaries		[20]
PLGA micro-particles	VEGF	Mouse	Femoral artery, iliac artery, and branches excised	IM	Immediate	4 wks		Increased arterioles and capillaries		[21]

Table 1.1 continued: Selected Injectable Biomaterials for PAD

Material	Other Therapeutic	Species	Injury model	Delivery Method	Time of treatment post-injury	Time of assessment	Perfusion	Neo-vascularization	Other	Ref.
Dextran and gelatin nano-particles	VEGF	Rabbit	Femoral artery excised, all branches ligated	IM	2 d	30 d	Increased	Increased capillaries		[22]
Fibrin particles		Rabbit	Femoral artery and branches excised	IM	7 d	28 d	Increased	Increased arterioles and capillaries	Improved angio-graphic score and calf blood pressure	[23]
Skeletal muscle ECM Hydrogel		Rat	Femoral artery excised	IM	1 wk	2 wks		Increased arterioles and capillaries	Increased muscle cell infiltration	[24]

IM = intramuscular; IV = intravenous.

1.2.1 Cells and material.

Cell therapy for PAD, compared to MI, has a more singularly angiogenic focus since ischemia is the main etiology of PAD. Tang et al. first injected human umbilical vein endothelial cells (HUVECs) intramuscularly in HA, a pro-angiogenic ECM component. The addition of HA prolonged the degree of cell retention and enhanced the ability of HUVECs to survive and engraft into the endothelium and recruit host smooth muscle cells. The HA plus HUVEC combination also improved limb perfusion and angiogenesis compared to either cells or material alone at a four week time point in a nude mouse hind limb ischemia model [10]. Wang et al. injected autologous bone marrow derived MSCs seeded in a collagen hydrogel in a rabbit model of hind limb ischemia. Their cell-material constructs enhanced angiogenesis and improved hind limb perfusion as measured by oxygen saturation ratio after eight weeks. While collagen alone improved capillary density, the MSC-collagen construct significantly improved mature vessel density and oxygen saturation over cell, material, and saline controls [11]. Another group used a synthetic hydroxyapatite nanoparticle system to deliver BM-MNCs into the murine ischemic limb; they showed increased angiogenesis, arteriogenesis, and cell survival after seven days, which correlated with increased VEGF and basic fibroblast growth factor (bFGF) protein levels in the tissue [12].

1.2.2 Other therapeutics and material.

Perhaps because of the largely paracrine effects seen with many stem cell injections, many groups have looked to embedding growth factors in materials as a way to improve sustained release of angiogenic factors without the complication of using stem cells. The only biomaterials based therapy currently in clinical trials for PAD involves such a sustained release system, using gelatin microspheres to deliver bFGF to ischemic tissue over prolonged periods [25]. Sustained release can improve with crosslinking, as seen with bFGF release over ten days from glutaraldehyde-crosslinked gelatin microspheres in a canine hindlimb ischemia model [13].

Naturally-derived materials have also been shown to sustain release of factors. For example, Ruvinov et al. showed that alginate modified with sulfate improved affinity binding and thus allowed for more sustained release of HGF over seven days, leading to improvements in limb perfusion and mature vessel formation [14]. Kuraitis et al. showed that a combination of two naturally derived materials, alginate microspheres within an injectable collagen hydrogel, prolonged the delivery of stem cell derived factor 1 (SDF-1) over ten days to the ischemic murine hind limb, improving perfusion, arteriole density, and recruitment of GFP-labeled bone marrow progenitor cells. Although collagen alone also significantly improved perfusion and arteriole density over PBS controls, the SDF-1/alginate/collagen system had higher trends in all metrics, and significantly higher arteriole lumen area and recruitment of GFP-labeled bone marrow cells [15]. Other groups have used a fragmin/protamine system to form microparticles that allow for sustained release of bFGF or platelet-rich plasma (PRP) [16]. For example, Fujita et al. showed improved collateral vessel formation and calf blood pressure in a rabbit model of hind limb ischemia due to the PRP-loaded fragmine/protamine microparticles [17]. Furthermore, all three components of their system are currently used for other clinical applications, which would likely facilitate clinical translation. In a completely synthetic system, Kim et al. showed that self-assembling bioactive peptides sustained release of substance P, a neuropeptide involved in wound healing, to recruit host mesenchymal stem cells and improve limb perfusion in a mouse model of hind limb ischemia after four weeks [18]. Webber et al. also designed a synthetic system of peptide amphiphile structures engineered to display a VEGF-mimetic epitope [19]. The construct improved angiogenesis and limb perfusion after three weeks over all material controls. In other synthetic systems, groups have explored the loading of gold [20], PLGA [21], or dextran and gelatin [22] nano- or microparticles with VEGF. These particle systems all demonstrated sustained release of VEGF over 35, 20, or 12 days respectively into the ischemic hind limb and lead to increased angiogenesis and limb perfusion.

1.2.3 Material alone

Although a relatively new approach for the PAD field, injection of materials alone may show particular promise for translatability, as there are fewer issues without additional bioactive components like cells or growth factors. Fan et al. injected fibrin particles intramuscularly in a rabbit model of hindlimb ischemia and showed improved capillary and arteriole density, as well as improved perfusion measured via angiographic score and calf blood pressure ratio after 28 days [23]. In a more recent study, DeQuach et al. were the first group to develop a tissue-specific injectable matrix for hind limb ischemia [24]. This initial study showed that the naturally-derived, decellularized skeletal muscle ECM hydrogel improved neovascularization and muscle cell infiltration into the material after two weeks.

1.3 Translating Injectable Biomaterials to the Clinic: Current Obstacles

Despite promising preclinical results, there are currently no FDA-approved injectable biomaterial products for treating PAD or CLI. The difficulty of bringing a therapy to the market is reflected in the small number of biomaterials that are currently undergoing clinical trials (Figure 1.2). For the heart, only two injectable biomaterials are currently in clinical trials: both are alginate hydrogel systems, one delivered via transcoronary catheter infusion for acute MI [26,27] and the other delivered via direct epicardial injection for dilated cardiomyopathy [28–30]. For PAD, there are several clinical trials for stem cell, growth factor, and gene therapy systems, but none have shown conclusively positive results [31] and only one involved a biomaterial scaffold [25]. This lack of transition from preclinical to clinical studies indicates that there is a heightened need to consider strategies that will better enable translation of injectable biomaterial therapies for MI

and PAD. In designing a material for clinical application, it is important to consider regulatory options, manufacturing strategies, and delivery methods throughout the development of the product. While these design criteria are not always considered in early academic research, attention early on could minimize hurdles later in the path to the clinic.

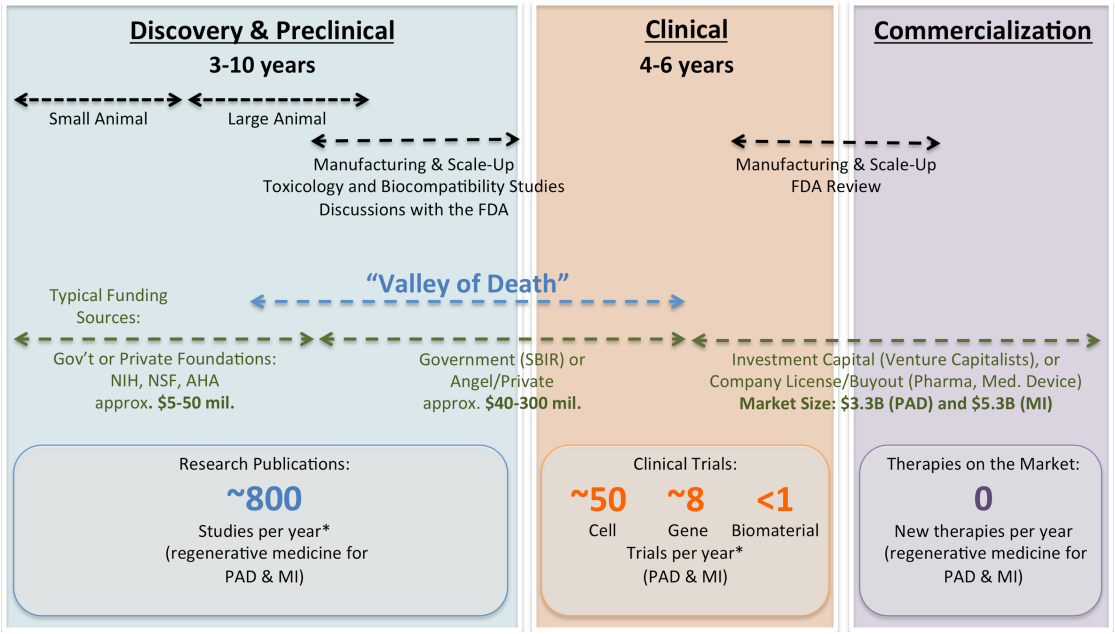

Figure 1.2. Translational pathway. The typical time, cost, relative number of publications, funding sources, and phases of the translational pathway for biomaterial-based therapies for cardiovascular disease are highlighted. * = number of studies in PubMed (preclinical) and ClinicalTrials.Gov (clinical) averaged per year over the past five years, using search terms "cell therapy," "gene therapy," "biomaterials," "myocardial infarction," and "peripheral artery disease." Cost of each phase adapted from [32] for preclinical and clinical phases, [33] for PAD market size, and [34] for MI market size.

1.3.1 Regulatory Challenges

A major obstacle in the translation of biomaterials for cardiovascular disease to the clinic is regulatory approval. Given the diversity of biomaterial therapies described above, it is difficult to classify some products within just one of FDA's regulatory arms. Thus in 2011, the Office of Combination Products (OCP) at the FDA published a draft guidance on classification issues to help resolve this confusion [35]. In it, they focus on the three regulatory classifications: drugs, devices, and biological products. While their definition of drug is very broad (i.e., any substance

used to “affect the structure or any function of the body of man”), their classification of a device is limited to any product that does not “achieve its primary intended purposes through chemical action.” Historically, biomaterial only therapies have largely been classified as devices under this definition; however, in the guidance document, the OCP stresses that any therapy that “depends, even in part, on chemical action within or on the body of man to achieve any one of its primary intended purposes, would not be a device.” Therefore, many biomaterial products are now being designated as biologics in the U.S. While a final guidance has not been issued, the draft guidance gives insight into the current thinking of OCP in regards to product classification, which has an enormous impact on the translatability of a biomaterial therapy because of the drastically different regulatory pathways for each classification. Drugs, regulated through the Center for Drug Evaluation and Research (CDER) and biologics, regulated through the Center for Biologic Evaluation and Research (CBER), must undergo a three phase, 5-10 year process costing hundreds of millions of dollars, while devices regulated by the Center for Devices and Radiological Health (CDRH) have a relatively shorter and less expensive pathway. See [32] for a good review of different costs associated with these pathways. In addition, any product that involves a combination of components regulated by different centers could fall under the OCP, which determines classification and center jurisdiction.

Most therapies described in this review could potentially fall under multiple classifications due to their complex nature in combining biomaterial therapies with cells, growth factors, or other therapeutics. While more components may have desirable synergistic effects, the addition of each component can add time, cost, and regulatory hurdles to getting that therapy to market. Combination therapies can require extensive preclinical testing examining each component of the product, including the recommended testing for cell and gene therapies [36], as well as assessing the safety of the biomaterial scaffold, which often involves assessing biocompatibility of the scaffold alone using ISO-10993 biocompatibility tests. While biomaterial only therapies can be advantageous in this regard, the main mechanism of action of materials in ischemic

limbs is still unclear, which leads to ambiguity in regulatory classification. It is important for researchers to consider these regulatory hurdles as early as possible when designing a new therapy. Given the uncertainties with regulatory classification and its impact on product development, early interactions with the relevant centers at the FDA and if necessary, submission of a "Request for Designation" (RFD) to OCP are recommended.

1.3.2 Delivery Challenges

Another translational concern is the delivery method of the biomaterial therapy. Specifically, the way the biomaterial is delivered can impact the ease of obtaining regulatory approval and the likelihood of the therapy being adopted by hospitals into clinical workflows and protocols. In peripheral artery disease, delivery has its own set of challenges. Many groups inject intramuscularly adjacent to the site of femoral artery resection in animal models; however, in a human patient, the gradual onset of plaque build up, claudication (pain), and ischemia means that there is no acute injury site to be targeted. Still, in clinical trials most groups tend to inject cell therapies intramuscularly at many sites in the quadriceps or gastrocnemius muscles, intra-arterially or intravenously [31]. Problems with intramuscular injections are the limited biodistribution of factors like gene plasmids, growth factors, or biomaterials, and limited knowledge about the most effective delivery locations within the muscle. Some populations of stem cells, such as endothelial progenitor cells (EPCs), have been shown to migrate more extensively in ischemic tissue than in healthy tissue, specifically towards sites of ischemia [37]. However, multiple injection sites raises concerns regarding systemic exposure of the potential therapy and intra-arterial and intravenous injections are not always an option for patients with severe vessel blockage. For this reason, dosing and delivery mechanism will be important questions to answer before any therapy for PAD can translate successfully to the clinic.

1.3.3 Manufacturing Challenges

Another concern with the translatability of biomaterials to the clinic is their ability to be scaled up to a "current good manufacturing practice" (cGMP) process. Specifically, naturally-derived biomaterials and cell therapies can have issues with batch-to-batch variability, scaling up, and efficiencies. The material content and properties of a naturally-derived biomaterial can depend on the tissue source for biomaterials derived from animal tissue. Although a certain composition is typically conserved from specimen to specimen, there can be variability due to tissue species, age, or health status of the animal or human from which the tissue is derived. For example, human versus porcine myocardial matrices were found to have different material properties and compositions, and specifically the human matrices had high levels of patient-to-patient variability [38]. A study of human pericardium-derived matrices also showed this patient-to-patient variability in material characterization; however, the researchers concluded that this variability *in vitro* did not affect gelation *in vivo*, thus not denying its potential as an autologous biomaterial therapy [39]. Host age also has an impact on mechanical properties of the biomaterial, as younger source tissue appears to facilitate a more constructive tissue remodeling response than older source tissue [40,41].

Scaling up production from bench to manufacturing plant can also have large implications for any cell- or material-based therapy. See Abbasalizadeh and Baharvand [42] and Giancola et al. [43] for a review of cGMP practices for cell therapies. Scaling up a manufacturing process to a sufficient batch size and according to cGMP practice can take significantly longer than expected. The act of scaling up a manufacturing process can also have impacts on yield efficiencies of sensitive processes like cell encapsulation. For example, even at the bench level some groups have trouble getting encapsulation efficiencies above 20 percent [44]. Thus, any process with more stable components may be easier to scale up than components like growth factors, which may have an unstable shelf life, and stem cells, which require intensive work to reach appropriate batch sizes for commercial and clinical applications. Moreover, the cost of

scaling up a manufacturing process from bench to plant should not be neglected. While having detailed knowledge about cGMP guidelines is outside the realm of most academic labs, a basic understanding of the differences between a lab bench and cGMP process can facilitate more rapid translation to the clinic.

1.3.4 Other Challenges

In terms of translatability, a challenge for developing new treatments for critical limb ischemia will be the consensus of a working animal model. Depending on the severity of the surgical procedure, the animal can heal significantly on its own. For this reason, studies in rats, mice and rabbits may have more significantly positive results than what is actually seen in clinical trials (see [31] for an extensive review on the clinical trial landscape for PAD). Furthermore, treatment timelines for PAD preclinical models also typically mimic the acute or sub-acute stage of the disease instead of chronic PAD, which is the more common indication to treat in clinical trials. This mismatch between animal model and clinical treatment timelines can give unrealistic results for the efficacy of an injectable biomaterial therapy.

1.4 Future Directions: Designing a Translatable Biomaterial

All of the above challenges are vital to clinical translation yet can be overlooked in academic settings. Oftentimes there is attrition when translating therapies between the bench to the clinic, called “the valley of death” (Figure 1.2). In recent years the “valley of death” has widened since venture capitalists and strategic partners (i.e. big pharma or medical device companies) typically want to see patient data (often Phase II data) before they are willing to invest in a new technology. Designing better preclinical studies in academic labs can facilitate bridging this gap. For example, designing studies that appropriately mimic the timing and delivery route of a material therapy, as well as developing technologies that can be readily

translated to a GMP process and current clinical delivery modalities can facilitate entering clinical trials. While good laboratory practice (GLP) studies [45] in full compliance with 21 CFR 58 are difficult to accomplish in an academic setting, it is possible for academic labs to conduct studies in the "spirit of GLP", which can be FDA compliant [36], and have less documentation and no quality assurance (QA) oversight. Therefore appropriately designing and documenting studies, particularly large animal studies, can accelerate translation, decrease the amount of funding necessary to translate a therapy into patients, and give a technology a better chance at crossing the valley of death.

Although there have been many novel approaches to the field of regenerative medicine for cardiovascular disease in the past ten years, we are still waiting for an effective treatment to reach patients. Initially, the field trended towards using different variations of cell and gene or protein therapies. However, more recently the potential of biomaterials to sustain release and prolong survival of factors and cells has been harnessed with significant gains in preclinical treatment efficacies. Still, the complex nature of these therapies and the subsequent challenges in regulatory approval, manufacturing, and delivery have likely hindered biomaterial-based therapies from proceeding in large numbers to the clinic. The recent trend of stand alone biomaterials, which can act on endogenous cells, avoids many of the regulatory complexities and could reduce some of the concerns with manufacturing and delivery mechanism. Despite these challenges, the field of injectable biomaterial-based regenerative medicine therapies for cardiovascular disease has significant potential to help a large number of patients, and as the first injectable biomaterials progress through clinical trials, it is anticipated that more will soon advance through the translational pathway.

1.5 Thesis Outline

This thesis is broken into four subsequent chapters. Chapter 2 presents methods for the fabrication and characterization of decellularized hydrogels to treat PAD and MI. Injectable

decellularized hydrogels are more commonly being explored for their pro-regenerative characteristics upon injection *in situ* in cardiovascular and musculoskeletal diseases, and it is important to optimize the design considerations in the fabrication methods of the material and to standardize characterization assays of these biologic-based materials. Chapter 3 outlines the short term dynamic transcriptomic study of the mechanism of action of a decellularized skeletal muscle matrix hydrogel (SKM). The decellularized SKM hydrogel increased cell survival, vascularization, skeletal muscle progenitor density, and cell migration compared to saline control in a rat hindlimb ischemia model. The SKM hydrogel also decreased apoptosis and neuronal cell death and altered pathways related to inflammation and metabolism. Chapter 4 investigates the tissue specific importance of decellularized extracellular matrix hydrogels for skeletal muscle regeneration. The skeletal muscle matrix hydrogel showed the most improvements in skeletal muscle progenitor recruitment, fiber cross sectional area, and gene expression related to muscle contractility followed by lung matrix and saline. Chapter 5 demonstrates the proof-of-concept of tunable enzyme-targeted nanoparticles as a drug delivery vehicle for targeting to ischemic muscle. Targeting was tuned by altering the enzyme-cleavable peptide density and the surface charge of the nanoparticles, paving the way for future minimally invasive drug delivery efficacy studies.

Chapter 1, in part, is a reprint of the material as it appears in *Stem Cells Translational Medicine*, 2014, 3(9): 1090-1099. The authors are Jessica Ungerleider and Karen Christman. The dissertation author was the primary investigator and author of this paper.

1.6 References

1. Go, A. S., Mozaffarian, D., Roger, V. L., Benjamin, E. J., Berry, J. D., Borden, W. B., Bravata, D. M., Dai, S., Ford, E. S., Fox, C. S., Franco, S., Fullerton, H. J., Gillespie, C., Hailpern, S. M., Heit, J. A., Howard, V. J., Huffman, M. D., Kissela, B. M., Kittner, S. J., *et al.* Heart disease and stroke statistics--2013 update: a report from the American Heart Association. *Circulation* **127,** e6–e245 (2013).

2. Ostchega, Y., Paulose-Ram, R., Dillon, C. F., Gu, Q. & Hughes, J. P. Prevalence of

peripheral arterial disease and risk factors in persons aged 60 and older: data from the National Health and Nutrition Examination Survey 1999-2004. *J Am Geriatr Soc* **55,** 583–589 (2007).

3. Regensteiner, J. G., Wolfel, E. E., Brass, E. P., Carry, M. R., Ringel, S. P., Hargarten, M. E., Stamm, E. R. & Hiatt, W. R. Chronic changes in skeletal muscle histology and function in peripheral arterial disease. *Circulation* **87,** 413–421 (1993).

4. Norgren, L., Hiatt, W. R., Dormandy, J. A., Nehler, M. R., Harris, K. A., Fowkes, F. G. & Group, T. I. W. Inter-Society Consensus for the Management of Peripheral Arterial Disease (TASC II). *J Vasc Surg* **45 Suppl S,** S5-67 (2007).

5. Hedberg, B., Angquist, K. A. & Sjostrom, M. Peripheral arterial insufficiency and the fine structure of the gastrocnemius muscle. *Int Angiol* **7,** 50–59 (1988).

6. Hedberg, B., Angquist, K. A., Henriksson-Larsen, K. & Sjostrom, M. Fibre loss and distribution in skeletal muscle from patients with severe peripheral arterial insufficiency. *Eur J Vasc Surg* **3,** 315–322 (1989).

7. Makitie, J. Peripheral neuromuscular system in peripheral arterial insufficiency. *Scand J Rheumatol Suppl* 157–162 (1979).

8. White, C. J. & Gray, W. A. Endovascular therapies for peripheral arterial disease: an evidence-based review. *Circulation* **116,** 2203–2215 (2007).

9. Tongers, J., Roncalli, J. G. & Losordo, D. W. Therapeutic angiogenesis for critical limb ischemia: microvascular therapies coming of age. *Circulation* **118,** 9–16 (2008).

10. Tang, Z. C., Liao, W. Y., Tang, A. C., Tsai, S. J. & Hsieh, P. C. The enhancement of endothelial cell therapy for angiogenesis in hindlimb ischemia using hyaluronan. *Biomaterials* **32,** 75–86 (2011).

11. Wang, J., Cui, W., Ye, J., Ji, S., Zhao, X., Zhan, L., Feng, J., Zhang, Z. & Zhao, Y. A cellular delivery system fabricated with autologous BMSCs and collagen scaffold enhances angiogenesis and perfusion in ischemic hind limb. *J Biomed Mater Res A* **100,** 1438–1447 (2012).

12. Mima, Y., Fukumoto, S., Koyama, H., Okada, M., Tanaka, S., Shoji, T., Emoto, M., Furuzono, T., Nishizawa, Y. & Inaba, M. Enhancement of cell-based therapeutic angiogenesis using a novel type of injectable scaffolds of hydroxyapatite-polymer nanocomposite microspheres. *PLoS One* **7,** e35199 (2012).

13. Zhao, Y., Liu, Z., Pan, C., Li, Z., Zhou, J., Wang, J., Yin, Z. & Wang, X. Preparation of gelatin microspheres encapsulated with bFGF for therapeutic angiogenesis in a canine ischemic hind limb. *J Biomater Sci Polym Ed* **22,** 665–682 (2011).

14. Ruvinov, E., Leor, J. & Cohen, S. The effects of controlled HGF delivery from an affinity-binding alginate biomaterial on angiogenesis and blood perfusion in a hindlimb ischemia model. *Biomaterials* **31,** 4573–4582 (2010).

15. Kuraitis, D., Zhang, P., Zhang, Y., Padavan, D. T., McEwan, K., Sofrenovic, T., McKee, D., Zhang, J., Griffith, M., Cao, X., Musaro, A., Ruel, M. & Suuronen, E. J. A stromal cell-

derived factor-1 releasing matrix enhances the progenitor cell response and blood vessel browth in ischaemic skeletal muscle. *Eur Cell Mater* **22,** 109–123 (2011).

16. Nakamura, S., Ishihara, M., Takikawa, M., Kishimoto, S., Isoda, S., Fujita, M., Sato, M. & Maehara, T. Attenuation of limb loss in an experimentally induced hindlimb ischemic model by fibroblast growth factor-2/fragmin/protamine microparticles as a delivery system. *Tissue Eng Part A* **18,** 2239–2247 (2012).

17. Fujita, M., Horio, T., Kishimoto, S., Nakamura, S., Takikawa, M., Nakayama, T., Yamamoto, Y., Shimizu, M., Hattori, H., Tachibana, S. & Ishihara, M. Effects of platelet-rich plasma-containing fragmin/protamine microparticles in enhancing endothelial and smooth muscle cell growth and inducing collateral vessels in a rabbit model of hindlimb ischemia. *J Biomed Mater Res B Appl Biomater* **101,** 36–42 (2013).

18. Kim, J. H., Jung, Y., Kim, B. S. & Kim, S. H. Stem cell recruitment and angiogenesis of neuropeptide substance P coupled with self-assembling peptide nanofiber in a mouse hind limb ischemia model. *Biomaterials* **34,** 1657–1668 (2013).

19. Webber, M. J., Tongers, J., Newcomb, C. J., Marquardt, K. T., Bauersachs, J., Losordo, D. W. & Stupp, S. I. Supramolecular nanostructures that mimic VEGF as a strategy for ischemic tissue repair. *Proc Natl Acad Sci U S A* **108,** 13438–13443 (2011).

20. Kim, J., Cao, L., Shvartsman, D., Silva, E. A. & Mooney, D. J. Targeted Delivery of Nanoparticles to Ischemic Muscle for Imaging and Therapeutic Angiogenesis. *Nano Let.* **11,** 694–700 (2011).

21. Lee, J., Bhang, S. H., Park, H., Kim, B. S. & Lee, K. Y. Active blood vessel formation in the ischemic hindlimb mouse model using a microsphere/hydrogel combination system. *Pharm Res* **27,** 767–774 (2010).

22. Xie, J., Wang, H., Wang, Y., Ren, F., Yi, W., Zhao, K., Li, Z., Zhao, Q., Liu, Z., Wu, H., Gu, C. & Yi, D. Induction of angiogenesis by controlled delivery of vascular endothelial growth factor using nanoparticles. *Cardiovasc Ther* **31,** e12-8 (2013).

23. Fan, C., Gao, P., Gu, Y., Tang, X., Liu, J., Wei, J., Inoue, K. & Zhu, D. Therapeutic angiogenesis by intramuscular injection of fibrin particles into ischaemic hindlimbs. *Clin. Exp. Pharmacol. Physiol.* **33,** 617–622 (2006).

24. DeQuach, J. A., Lin, J. E., Cam, C., Hu, D., Salvatore, M., Sheikh, F. & Christman, K. L. Injectable skeletal muscle matrix hydrogel promotes neovascularization and muscle cell infiltration in a hindlimb ischemia model. *Eur Cell Mater* **23,** 400–412 (2013).

25. Marui, A., Tabata, Y., Kojima, S., Yamamoto, M., Tambara, K., Nishina, T., Saji, Y., Inui, K., Hashida, T., Yokoyama, S., Onodera, R., Ikeda, T., Fukushima, M. & Komeda, M. A Novel Approach to Therapeutic Angiogenesis for Patients With Critical Limb Ischemia by Sustained Release of Basic Fibroblast Growth Factor Using Biodegradable Gelatin Hydrogel: An Initial Report of the Phase I-IIa Study . *Circ J* **71,** 1181–1186 (2007).

26. Inc, I. H. NCT01226563. IK-5001 for the Prevention of Remodeling of the Ventricle and Congestive Heart Failure after Acute Myocardial Infarction (PRESERVATION 1). *clinicaltrials.gov*

27. Ltd, B. NCT00557531. Safety and Feasibility of the Injectable BL-1040 Implant. *clinicaltrials.gov*

28. Inc, L. H. NCT01311791. A Randomized, Controlled Study to Evaluate Algisyl-LVR as a Method of Left Ventricular Augmentation for Heart Failure (AUGMENT-HF). *clinicaltrials.gov*

29. Inc, L. H. NCT00847964. Safety and Feasibility of Algisyl-LVR as a Method of Left Ventricular Restoration in Patients With DCM Undergoing Open-heart Surgery. *clinicaltrials.gov*

30. Lee, R. J., Hinson, A., Helgerson, S., Bauernschmitt, R. & Sabbah, H. N. Polymer-based restoration of left ventricular mechanics. *Cell Transpl.* **22,** 529–533 (2013).

31. Ouma, G. O., Jonas, R. A., Usman, M. H. & Mohler 3rd, E. R. Targets and delivery methods for therapeutic angiogenesis in peripheral artery disease. *Vasc Med* **17,** 174–192 (2012).

32. Pashuck, E. T. & Stevens, M. M. Designing Regenerative Biomaterial Therapies for the Clinic. *Sci Transl Med* **4,** (2012).

33. Group, M. R. US Peripheral Vascular Device Market to Grow Strongly to $3.3 Billion by 2017. (2013).

34. Wood, L. Research and Markets: Myocardial Infarction (MI) Therapeutics - Pipeline Assessment and Market Forecasts to 2018. *Bus. Wire* (2012).

35. Products, F. and D. A. O. of C. Draft Guidance for Industry and FDA Staff: Classification of Products as Drugs and Devices and Additional Product Classification Issues. (2011).

36. Research, F. and D. A. C. for B. E. and. Guidance for Industry: Preclinical Assessment of Investigational Cellular and Gene Therapy Products. (2013).

37. Agudelo, C. A., Tachibana, Y., Hurtado, A. F., Ose, T., Iida, H. & Yamaoka, T. The use of magnetic resonance cell tracking to monitor endothelial progenitor cells in a rat hindlimb ischemic model. *Biomaterials* **33,** 2439–2448 (2012).

38. Johnson, T. D., DeQuach, J. A., Gaetani, R., Ungerleider, J., Elhag, D., Nigam, V., Behfar, A. & Christman, K. L. Human versus porcine tissue sourcing for an injectable myocardial matrix hydrogel. *Biomater. Sci.* 60283D (2014). doi:10.1039/c3bm60283d

39. Seif-Naraghi, S. B., Horn, D., Schup-Magoffin, P. A., Madani, M. M. & Christman, K. L. Patient-to-patient variability in autologous pericardial matrix scaffolds for cardiac repair. *J Cardiovasc Transl Res* **4,** 545–556 (2011).

40. Sicari, B. M., Johnson, S. A., Siu, B. F., Crapo, P. M., Daly, K. A., Jiang, H., Medberry, C. J., Tottey, S., Turner, N. J. & Badylak, S. F. The effect of source animal age upon the in vivo remodeling characteristics of an extracellular matrix scaffold. *Biomaterials* **33,** 5524–5533 (2012).

41. Tottey, S., Johnson, S. A., Crapo, P. M., Reing, J. E., Zhang, L., Jiang, H., Medberry, C. J., Reines, B. & Badylak, S. F. The effect of source animal age upon extracellular matrix scaffold properties. *Biomaterials* **32,** 128–136 (2011).

42. Abbasalizadeh, S. & Baharvand, H. Technological progress and challenges towards cGMP manufacturing of human pluripotent stem cells based therapeutic products for allogeneic and autologous cell therapies. *Biotechnol Adv* **31,** 1600–1623 (2013).

43. Giancola, R., Bonfini, T. & Iacone, A. Cell therapy: cGMP facilities and manufacturing. *Muscles. Ligaments Tendons J.* **2,** 243–247 (2012).

44. Mayfield, A. E., Tilokee, E. L., Latham, N., McNeill, B., Lam, B. K., Ruel, M., Suuronen, E. J., Courtman, D. W., Stewart, D. J. & Davis, D. R. The effect of encapsulation of cardiac stem cells within matrix-enriched hydrogel capsules on cell survival, post-ischemic cell retention and cardiac function. *Biomaterials* **35,** 133–142 (2014).

45. Seiler, J. P. *Good Laboratory Practice - the Why and the How*. (Springer-Verlag, 2005).

Chapter 2

Fabrication and Characterization of Injectable Hydrogels Derived from Decellularized Skeletal and Cardiac Muscle

2.1 Introduction

Cardiovascular disease is the leading cause of death in the United States [1]. One consequence of cardiovascular disease, myocardial infarction (MI), afflicts more than 900,000 Americans annually and can lead to heart failure and death. MI is caused by acute occlusion of a coronary artery, leading to myocardial ischemia, cardiomyocyte necrosis, collagen scar formation, and subsequent diminished pump function [2]. The only treatments for heart failure post-MI are either a heart transplant or a mechanical left ventricular (LV) assist device, and no current therapy prevents negative left ventricular remodeling and heart failure. As such, the five-year mortality rate post-MI is 50 percent [1]. Another manifestation of cardiovascular disease, peripheral artery disease (PAD) is a cardiovascular condition that afflicts 12 to 20 percent of Americans over age 65 [3], which is caused by atherosclerosis and leads to decreased blood flow and eventual amputation in the lower limbs as described in Chapter 1. In both instances, atherosclerosis leads to acute or chronic muscle ischemia, followed by negative remodeling and fibrosis. Thus, an ideal therapy would encourage positive remodeling post-ischemia and prevent chronic ischemia and inflammation from leading to overall tissue damage and failure over time.

Direct injection of growth factors [4,5], cells [6], and gene therapy[7,8] are some examples of tissue engineering approaches used to stimulate angiogenesis in the ischemic limb or heart. Recently, biomaterial scaffolds have begun to be used for their potential in prolonging the release of angiogenic factors and for their inherent ability to encourage tissue-scale regeneration (outlined in Chapter 1). Briefly, naturally-derived [4,5,9,10] and synthetic [11,12] hydrogel

scaffolds have been tested for their ability to recruit endogenous progenitor cells and promote tissue remodeling post-ischemia. While promising results have been seen, with material delivery of growth factors or stem cells[13–16], the expensive nature of preparing such a combination product and sub-optimal clinical trial results have halted these therapies' progression to market[17]. In contrast, material-alone therapies have significant potential for many translational reasons, including minimally invasive delivery and reduced costs compared to a cell- or growth factor-based therapy[18]. In particular, injectable hydrogels derived from decellularized muscle ECM, have shown significant potential for treating both MI and PAD. Singelyn et al. first showed the capability of a decellularized cardiac ECM hydrogel to increase vascular cell migration *in vitro* and vessel density *in vivo* [19]. The material has since shown efficacy to increase cardiac muscle, reduce fibrosis, and improve cardiac function post-MI in small and large preclinical animal models [20,21] and is now planned for testing in a Phase I clinical trial (clinicaltrials.gov: NCT02305602). DeQuach et al. showed skeletal muscle progenitor recruitment and neovascularization due to injection of a skeletal muscle ECM hydrogel alone in a preclinical model of hindlimb ischemia, thus indicating the potential for ECM hydrogels to be used alone to treat PAD and regenerate ischemic damaged skeletal muscle[10].

In this chapter, we present detailed methods for fabricating injectable hydrogels derived from either decellularized cardiac or skeletal muscle extracellular matrix (ECM). We also present methods, which we recommend should be performed on each batch of material prior to *in vitro* or *in vivo* use, to ensure limited batch-to-batch variability and more consistent results.

2.2 Materials and Methods

2.2.1 Fabrication of injectable hydrogels

2.2.1.1 - Day 0 – Initial Tissue Processing

Tissue specific injectable hydrogels were derived from either porcine myocardium or skeletal muscle. In order to fabricate a sterile material, all steps in the protocol were conducted

with sterile solutions and autoclaved beakers or in a biosafety cabinet where possible. Decellularization was accomplished with a 1% wt/vol sodium dodecyl sulfate (SDS) solution, made by adding appropriate volumes of 20x PBS, 10x SDS, and ultrapure water. The psoas muscle or heart was harvested from Yorkshire farm pigs weighing 30-45 kg. Note that larger animals or other sources of skeletal muscle are more likely to have greater interstitial adipose tissue within the muscle, which interferes with tissue processing. The skeletal muscle was obtained and isolated from skin, superficial fat, and fascia, leaving only the homogenous skeletal muscle tissue behind. For cardiac ECM fabrication, the left ventricle (LV) free wall and septum were isolated from the right ventricular free wall, atria, and valves by blunt dissection and cleared of any fat or fascia. Papillary muscles and chordae tendinae in the LV lumen were also removed, leaving only myocardium remaining. Muscle was cut into regularly sized cubes approximately 3-5 mm (skeletal muscle, Figure 1A) or 2 mm (cardiac muscle) per side at the smallest, as tissue is prone to degradation and collapse during decellularization. A larger piece of muscle was set aside for histological analysis as a “before decellularization” sample. Tissue was weighed and divided into 1L autoclaved beakers with 20-35 g of tissue in each beaker, and ultrapure water was added to a total volume of 800mL and spun with a stir bar at 125 rpm for 30-45 minutes. Tissue was strained in an autoclaved fine mesh strainer, rinsed under ultrapure water, and returned to the beaker. Previously mixed 1% SDS solution was added to the beaker so that the total volume of tissue and SDS was 800 mL and was stirred at 125 rpm for 2 hours as an initial rinse. Again, after 2 hours the tissue was rinsed in the fine mesh strainer with ultrapure water and returned to the beaker, also rinsed with ultrapure water. Fresh 1% SDS was added to the beaker to a final volume of 800 mL. Four mL of 10,000 U Penicillin/Streptimycin (PenStrep) was then added to each beaker, giving a final working concentration of 50 U PenStrep in 1% SDS. The beaker was kept sealed with a square of parafilm and the tissue was spun at 125 rpm for 24 hours.

2.2.1.2 - Day 1-5 – SDS solution changes

Tissue was strained and the beaker/stir bar were thoroughly rinsed with ultrapure water. On the first day only, larger pieces of tissue were more finely cut into smaller pieces to ensure consistent rates of decellularization (larger pieces tended to have a deeper red or pink center after the first day of decellularization, Figure 2.1B). Tissue was returned to the beaker and fresh 1% SDS was added to 800 mL with 4 mL 10,000 U PenStrep. Through this process, beakers were kept covered with parafilm whenever possible to reduce the risk of contamination. Rinses and solution changes were repeated every 24 hours until the tissue was completely white, usually 3-4 days (Figure 2.1C). Remaining ECM was spun for an extra 24 hour period to ensure full decellularization. Additional days of solution changes were minimized once tissue was fully white to avoid degradation and loss of ECM proteins. Cardiac ECM was then processed starting with the water rinse step (2.2.1.4), while skeletal muscle was processed first with the IPA lipid removal step (2.2.1.3).

2.2.1.3 - IPA Lipid Removal (skeletal muscle ECM only)

The presence of lipids after decellularization could inhibit subsequent gelation of the digested material, and therefore an isopropyl alcohol (IPA) lipid removal step was implemented only for fattier skeletal muscle tissue. After final SDS solution change, ECM was rinsed in the mesh strainer with ultrapure water and the beaker and stir bar were rinsed thoroughly to remove any trace SDS. ECM was spun in ultrapure water at 800 mL total volume for 2 hours to remove residual SDS. Up to 5 beakers of rinsed ECM were placed into a single clean 1L beaker with a clean stir bar. In a fume hood, IPA was added up to 400 mL total volume. The beaker was sealed with parafilm and spun at 125 rpm for 12-24 hours.

2.2.1.4 - Water Rinse, Freezing, Milling

ECM was rinsed in ultrapure water and for skeletal muscle ECM, used IPA was properly disposed of as hazardous waste. Both skeletal and cardiac muscle ECM was spun in 800 mL ultrapure water at 125 rpm for 30-45 minutes to remove residual SDS and IPA from ECM. ECM was rinsed and fresh ultrapure water was added and spun at 125 rpm for an additional 24 hours. ECM was thoroughly rinsed with ultrapure water in the mesh strainer and added to new autoclaved 1L bottle with ultrapure water up to 800 mL total volume. The lid was tightly sealed and the bottle was shaken vigorously for 30 seconds. The bottle and ECM were strained and rinsed several times to remove residual SDS; this shaking step was repeated at least twice until no bubbles persisted after 30 seconds of vigorous shaking. ECM was evenly divided into 50 mL conicals, which were filled to less than 20 mL. A few pieces of ECM were prepared for histological analysis to compare to the pre-decellularization sample (see 2.2.2.2). The 50 mL conicals were frozen at -80 °C, with the conicals laid on their side and the ECM evenly distributed along the length of the conical for more uniform freezing and subsequent lyophilization. Frozen ECM was lyophilized and milled (Wiley Mini-Mill, #40 or #60 filter) to generate a particulate for subsequent protease digestion. ECM was milled in larger batches (greater than 1 gram) to avoid significant ECM loss within the mill mechanism.

2.2.1.5 - Pepsin Digestion

In order to liquefy the ECM, milled ECM was partially digested in pepsin (protocol modified from [22]). All steps with open vials were performed in a biosafety cabinet. Fresh pepsin was dissolved in 0.1 M HCl at 1 mg/ml through shaking for 5-10 minutes. While pepsin was shaking, approximately 20 to 30 mg of milled ECM were added to a 20 mL scintillation vial with a small stir bar. Once dissolved the pepsin solution was sterile filtered with a 0.22 µm filter and added to the ECM vial to reach a concentration of 10 mg ECM / 1 mL pepsin solution. The closed vial was then placed on a stir plate (~60-120 rpm) for 48 hours at room temperature. To

ensure the entire material was digested in the pepsin solution, material on the sides of the vial was gently scraped down with a spatula one or two times during the 48 hour digestion. After 48 hours, the liquid ECM was titrated to pH 7.4, 1x PBS and a final material concentration of 6 mg ECM/ml. First, pH was titrated to 7.4 by adding sterile 1 M NaOH (1/10 the acidic liquid ECM volume) and by adding subsequent volumes of sterile 1 M NaOH or 0.1 M HCl after measuring pH of the well-mixed solution. Then, salt concentration was titrated to a final concentration of 1x PBS by adding 1/9 of the resulting liquid ECM volume of sterile 10x PBS. Finally, a sufficient volume of sterile 1x PBS was added to reach a final ECM concentration of 6 mg/ml, based off of the initial mass of ECM added. Material was then aliquoted, frozen and lyophilized for long term storage for up to one year at -80°C. When ready for use, lyophilized ECM was resuspended in an equivalent volume of sterile water for use. For example, if the aliquot was a 600 µl aliquot of the original batch of digested and titrated ECM, 600 µL of sterile water was added and mixed until homogeneous by pipetting up and down repeatedly. There was some material loss due to bubbles forming upon mixing, so approximately 10% additional material than required was aliquoted.

2.2.2 In vitro characterization of injectable hydrogels

2.2.2.1 - Gelation Test

Each batch of decellularized ECM was characterized to ensure minimal batch-to-batch variability. First, gelation was tested by adding 500 µL of resuspended digested ECM to a 4 mL scintillation vial and incubating at 37°C for 1 hour. If material did not flow upon tilting the vial, a gel was formed.

2.2.2.2 – Decellularization Verification

Histology

Sufficient decellularization was first verified through hematoxylin and eosin staining and Hoechst staining. Briefly, fresh and final samples were either fresh frozen by freezing in Tissue-Tek OCT (Fisher-Scientific, Waltham, MA) or fixed in 10% formalin for 24 hours and paraffin-embedded. Samples were sectioned in 10 µm thick slices and whole mounted on slides. Hematoxylin and eosin staining was performed on both fresh and final samples (fresh frozen or paraffin-embedded) in order to assess morphology of the decellularized ECM as well as nuclear hematoxylin-labeled content of the fresh and final tissue. Fluorescent nuclear staining was performed by acetone-fixing both fresh and final slides (fresh frozen) for 1.5 minutes, followed by three 5 minute 1x PBS washes and 10 minutes of incubation in Hoechst 33342 (diluted by adding 1 µL of Hoechst 33342 in 10 mL DI water, Life Technologies, Grand Island, NY). After incubation, samples were kept with minimal light exposure, washed again 3 times for 5 minutes in 1x PBS, and cover slips were mounted using Fluormount. H&E stained slides were imaged on a Leica Aperio ScanScope CS^2 at 20x magnification (Leica Biosystems, Buffalo Grove, IL), and Hoechst-labeled slides were imaged on a Carl Zeiss Observer D1. Images were acquired at 10x with an equivalent exposure time for both fresh and final samples for comparison (usually about 40 ms).

dsDNA quantification

Double stranded DNA (dsDNA) was quantified to further determine the extent of decellularization. DNA was isolated from digested and lyophilized 1 mg aliquots of ECM using a standard kit (we suggest NucleoSpin, Macherey-Nagel, Bethlehem, PA). Lyophilized ECM aliquots were resuspended in lysis buffer T1 and proteinase-K by pipetting up and down multiple times, and DNA was isolated according to kit instructions. Proteinase-K digestion of the material was confirmed by a visually clear solution before running ECM through the remainder of the

NucleoSpin kit. NanoDrop (Thermo Scientific, Waltham, MA) readings were conducted on eluted DNA to confirm a DNA concentration of zero, since DNA remaining in the ECM should be below the detectable threshold of NanoDrop spectrophotometers. PicoGreen fluorescent reporter was used (Life Technologies, Grand Island, NY) to more precisely quantify dsDNA content according to kit instructions with 100 µL of eluted sample DNA.

2.2.2.3 – Material Composition

sGAG quantification

Sulfated glycosaminoglycans (sGAGs) were quantified in both cardiac and skeletal muscle ECM using the 1,9-dimethylmethylene blue dye (DMMB) assay (modified from [23]). Chondroitan sulfate dilutions from 0 to 50 µg per 100 µL in a 1.5 mL Eppendorf tube were used to create a standard curve. Resuspended digested ECM at 6 mg/mL was run in triplicate samples of 100 µL per Eppendorf tube. Working solution was made fresh by combining 5 mL of formate solution (2.5g sodium formate in 240 mL 1 M guanidine hydrochloride (GuHCl) and 2.795 mL of 85% formic acid), 1.25 mL of 0.64 mg DMMB/mL ethanol, and ultrapure water to a total volume of 25 mL. Decomplexation solution was made by combining 2.05 g sodium acetate, 200 mL ultrapure water, 50 mL 1-propanol, and 250 mL of 8 M GuHCl. Working solution was added to each sample or standard concentration tube (1 mL/tube), and tubes were vortexed at level 3.5 for 30 minutes. Tubes were then centrifuged for 10 minutes at 12,000 rpm in a microcentrifuge to collect a pellet of precipitated DMMB-sGAG complex. If no pellet formed in the standard tubes, the entire protocol was restarted with fresh standard solutions. Supernatant was carefully aspirated so as not to disturb the pellet. Then, the pellet was gently broken up by slowly pipetting with 1 mL of decomplexation solution. Tubes were again vortexed at level 3.5 for 30 minutes. Solutions were confirmed to be homogenous with the pellet fully dissolved. Absorbance was then read at 656 nm on a plate reader by pipetting 100 µL in triplicate into a 96

well plate. Chondroitan sulfate concentrations were plotted against absorbance to calculate a standard curve for determination of sGAG concentration in resuspended ECM samples.

Protein content

Resuspended ECM was run on SDS-polyacrylamide gel electrophoresis (SDS-PAGE) gel to assess protein fragment content. Rat tail collagen I at 2.5 mg/mL (Life Technologies, Grand Island, NY) was run on adjacent wells to compare ECM protein content, as collagen is the main protein component of decellularized ECM hydrogels [25]. Gels were run using the general protocol from the Invitrogen NuPage® kit (Life Technologies, Grand Island, NY). Digested ECM was resuspended and 7.5 µL were added to each running sample. To each sample was also added 3.75 µL of NuPAGE LDS 4x Sample Buffer, 1.5 µL NuPAGE 10x Reducing Agent, and 2.25 µL DI water, to a final volume of 15 µL. Samples were heated at 70°C in a water bath or heating block for 10 minutes to denature proteins. Running buffer was made by mixing 50 mL of 20x NuPAGE SDS Running Buffer with 950 mL DI water. For the upper buffer chamber, 200 mL of the Running Buffer was set aside and 500 µL NuPAGE Antioxidants was added within 30 minutes of running the gel. The remaining running buffer (~600 mL) was added to the outer chamber of an assembled mini cell, and the 200 mL of running buffer with antioxidants was loaded into the inner chamber. In each well of a 12% Tris-Acetate gel, 10 µL of each sample was added. We recommend running resuspended 6 mg/ml ECM samples mixed in the above ratios with 2.5 mg/mL collagen I in the same ratios (7.5 µL of sample added to the mixture) for comparative analysis. The gel was run at a constant voltage (200 V) for approximately 50 minutes, or until dye reached the bottom of the gel. Gel was removed from the cartridge and stained with Imperial Protein Stain overnight on a shaker plate in a fume hood. The stained gel was then rinsed with ultrapure water for 2-3 hours, or until bands became distinct. Placing a Kim-Wipe in the container with the gel and the water helped absorb more of the Imperial Protein Stain.

2.2.2.4 – Mechanical Properties

Resuspended ECM was tested via rheometry in liquid form for complex viscosity and gel form for storage and loss moduli. Samples were run on a parallel plate rheometer (ARG2 Rheometer, TA Instruments, New Castle, DE). For complex viscosity measurements, 200 µL resuspended liquid ECM was pipetted into the center of the parallel plate geometry. Plate temperature was fixed at 25°C and gap height was set to 500 µm to ensure the liquid filled the entire gap between plates. Material was run in a flow procedure programmed with frequencies ranging from 0.1 – 100 Hz. For storage and loss moduli, lyophilized ECM was resuspended in DI water and 500 µL was pipetted carefully into a 4 mL scintillation vial to avoid bubble formation. ECM was gelled for 24 hours at 37°C. Samples were run with the plate pre-set to 37°C. Samples were carefully transferred from the 4 mL scintillation vial to the parallel plate; if gels were broken, the gel was discarded and another gel was used, as any impurities or tears in the gel can affect the measured mechanical properties. Excess water used to help transfer the gel from the vial to the plate was also carefully removed from the gel by using a Kim Wipe. Gap height was set to 1200 µm in order to ensure the gel filled the entire gap between the parallel plates and an oscillatory frequency sweep was run from 0.1 to 100 rad/s to measure the storage and loss moduli. The maximum suggested gap height for running gels of this size is 1500 µm.

2.2.2.5 – Structural Properties

Scanning electron microscopy (SEM) was performed on gelled ECM material. Resuspended ECM aliquots of 100 µL each were pipetted into a 96 well plate in triplicate while avoiding bubble formation. Aliquots were allowed to gel at 37°C for 24 hours and then a solution of 4% paraformaldehyde and 4% glutaraldehyde in DI water was pipetted on top of each gel for 24 hours. Fixative was added on top of each gel in the 96 well plate, or if gels were carefully transferred to a 12 or 24 well plate, the larger well size allowed for submergence on all sides for improved uniform fixation. Gels were then dehydrated in graduated rinses of ethanol. Fixed and

dehydrated gels were dried and sputter coated as previously published [24]. Briefly, the critical point dryer (Leica EM CPD300, Leica, Vienna) was set to perform 40 exchange cycles of CO_2 at medium speed and 40% stirring. Before sputter coating, samples were carefully pulled apart with tweezers to expose the gels' inner nano-fiber architecture. Samples were sputter coated with 7 nm of platinum (Leica SCD, Leica, Vienna) and imaged on an FE-SEM at 0.6 kV using the in-lens SE1 detector (Sigma VP, Zeiss Ltd, Cambridge, UK).

2.3 Results and Discussion

To demonstrate ways to characterize decellularized porcine cardiac and skeletal muscle ECM, we present a variety of characterization assays for naturally derived ECM hydrogels. These include assessing histology, DNA content, sulfated glycosaminoglycan (sGAG) content, mechanical properties (viscosity and storage and loss moduli), protein content, and nanoscale architecture. It is important to quantify these material characteristics in order to ensure minimal batch-to-batch variability for consistent behavior in *in vitro* or *in vivo* applications.

H&E was conducted on fresh frozen or fixed and paraffin embedded 10 μm sections of "fresh" tissue and "final" ECM for each round of decellularization to verify that the decellularization process was thorough (Figure 2.1). Hoechst staining was conducted on fresh frozen 10 μm sections and imaged at constant exposure time to verify absence of nuclear content as indicated by lack of blue staining in "final" samples (Figure 2.2). Investigators should look for cellular content in the final product, such as hematoxylin or Hoechst positive staining, which is indicative of nuclei or residual DNA. The ECM alone should be light pink stained fibers on H&E (see Figure 2.2 B, F). Batches with unsuccessful cellular removal should not be used for *in vivo* applications especially, as cellular content can elicit a negative immune response in host tissue [25].

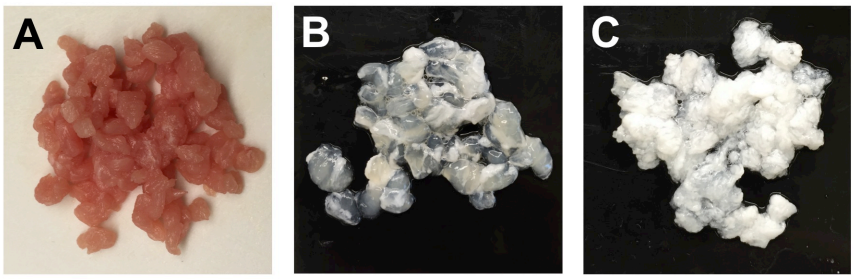

Figure 2.1: Decellularization Process. (A) Images of freshly cubed porcine skeletal muscle. (B) Tissue after the first day in 1% SDS. (C) Final ECM after complete decellularization. Note larger pieces of ECM maintain an opaque, pink-tinted center after the first day of SDS rinsing (B), indicating incomplete decellularization.

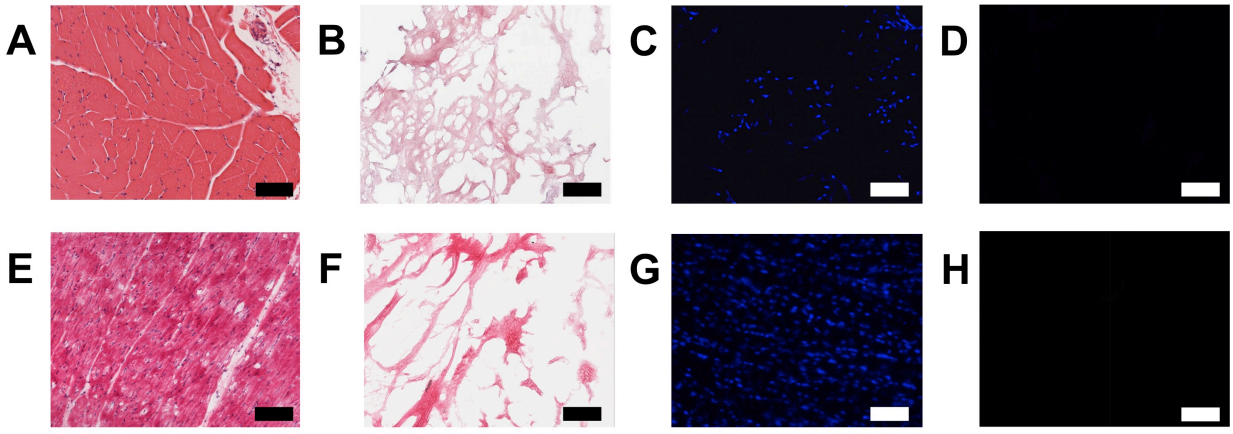

Figure 2.2: Decellularization Verification. Hematoxylin and eosin staining shows fresh (A, E) and decellularized (B, F) cross sections of porcine skeletal and cardiac muscle, respectively. Nuclei (purple) are clearly present in fresh, but not final samples. Hoechst 33342 staining shows fresh (C, G) and decellularized (D, H) cross sections of skeletal and cardiac muscle, respectively. Nuclei (blue) are clearly present in fresh, but not final samples. Scale bars are 100 μm.

DNA content was measured by isolating DNA from the ECM using a standard DNA isolation kit and a fluorescent reporter with a standard curve (PicoGreen kit), demonstrating a range from 0.1 to 5 ng dsDNA/mg ECM for both skeletal muscle and cardiac sources. Measuring double stranded DNA (dsDNA) content is important because it gives an approximation of the quantitative extent of decellularization. Removing cellular content is vital to decrease the negative immune response *in vivo,* as both allogeneic and xenogeneic biomaterials have the ability to elicit an immune response upon injection [25]. It is useful to

compare measurements to a known standard, such as dsDNA content found in a variety of decellularization methods published by Reing et al [26]. Although the protocol in this study typically produces a dsDNA content an order of magnitude lower, Reing et al. suggested that 50 ng dsDNA/mg ECM should be the threshold limit for DNA content. There may be slight differences in DNA content from batch to batch or depending on the tissue source, but as long as the content is lower than the suggested threshold, the material can be considered effectively devoid of cellular content. Batch to batch or tissue source variability in dsDNA content may be due to slight differences in processing. For example, slightly different SDS exposure times or additional processing steps such as IPA rinsing may alter decellularization extent.

sGAG content was quantified with the DMMB assay, with some modifications from a previously published protocol [23], in order to account for specific ECM differences. For both muscle ECM hydrogels, sGAG content ranged from approximately 5 to 15 μg sGAGs/mg ECM. sGAGs are growth factor binding moieties that may lend desired bioactivity to any naturally derived matrix for their ability to bind and prolong release of regenerative cytokines, either those secreted *in vivo* or exogenously delivered [27]. Although the decellularization process can wash away sGAGs [26], it is useful to quantify the remaining GAG content to compare decellularization methods or optimize a naturally derived hydrogel for a given delivery application.

PAGE shows a qualitative measure of the material protein content and extent of protease digestion. Collagen is the main content of muscle ECM-derived hydrogels, so rat tail collagen I was run in an adjacent lane to compare the characteristic bands (Figure 2.3). We found that 2.5 mg/mL of collagen I shows the most similar protein fragment concentrations in PAGE to 6 mg/mL of resuspended digested ECM. Figure 2.3 also shows one example of the batch-to-batch variability than can be possible with ECM hydrogels derived from different porcine donors. Lanes 1, 2, and 3 each show each a different sample of three batched skeletal muscle ECM donors. Batching material from multiple donors helps ensure consistent material properties, but batched ECM can still be compared with assays such as PAGE by the presence

or differing intensities of some bands. For example, batch 1 shows a higher concentration of protein fragments from 90-100 kDa than either batch 2 or 3 (Figure 2.3). For both muscle ECM hydrogels, the PAGE should display characteristic collagen bands as well as faint bands below 20 kDa, confirming sufficient partial digestion of the ECM by pepsin. For a more thorough analysis of the protein content, mass spectrometry can be conducted on digested material to characterize protein fractions. Furthermore, current research has identified novel methods of quantifying relative protein abundance with mass spectrometry and stable isotope labeled peptide standards [28,29].

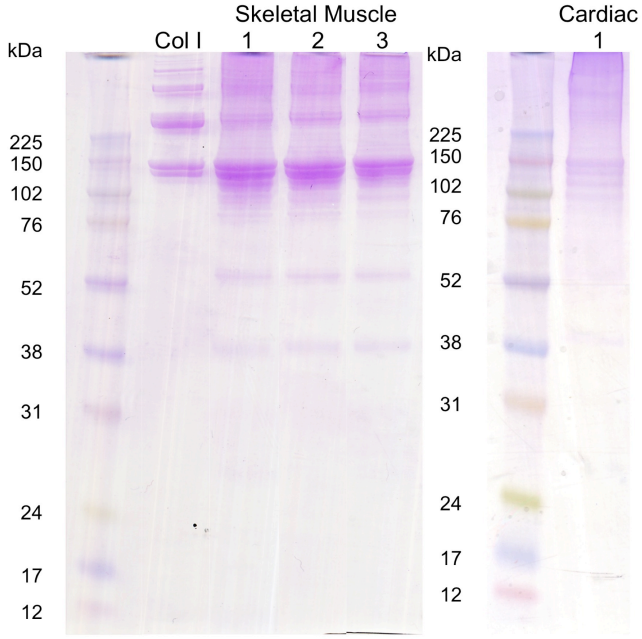

Figure 2.3: Material Characterization. PAGE gel showing collagen I (Col), multiple batches (1, 2, and 3) of digested skeletal muscle ECM, and a single batch of digested cardiac ECM.

Quantifying mechanical properties is vital to assess the physical characteristics of naturally derived ECM hydrogels. Although they can be tissue-specific regarding biochemical composition, decellularized hydrogels are typically weaker than the tissues from which they are derived [30,31]. This can vary due to the harshness of the decellularization method[26]. Shear storage and loss moduli can indicate the stiffness of the gel. Example traces for both muscle ECM hydrogels are shown in Figure 4A and B. Reported at 1 rad/s, values for storage modulus typically range between 5 and 10 Pa and loss modulus between 1 and 5 Pa [10,30,31]. Quantifying complex viscosity also shows the potential of the material for injectability and/or catheter delivery. The material should be shear thinning at frequencies from 0.1 – 100 Hz with complex viscosities of approximately 1 to 0.02 Pa-s (Figure 2.4 C, D)[24]. Since the cardiac and skeletal muscle ECM materials are shear thinning, they are well suited to be delivered in a narrow catheter with high shear rates. Storage and loss modulus as well as complex viscosity can all be quantified on a parallel plate rheometer.

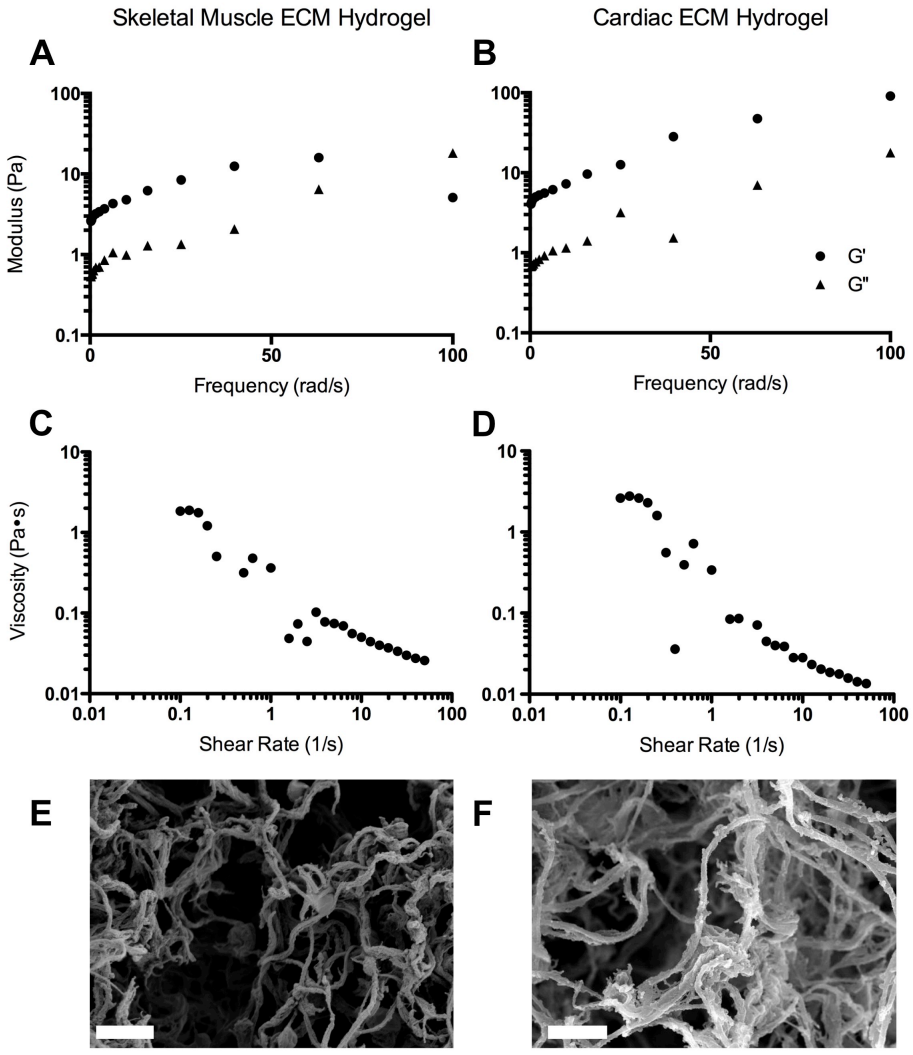

Figure 2.4: Mechanical and Structural Properties. Sample rheometer frequency sweep for storage (G') and loss (G") moduli for skeletal muscle ECM (A) and cardiac ECM (B) hydrogels. Sample complex viscosity traces for liquid skeletal muscle ECM (C) and cardiac ECM (D). SEM shows nanoscale architecture of skeletal muscle ECM (E) and cardiac ECM (F) hydrogels. Scale bar is 1 μm.

SEM can be performed to visualize the nanoscale architecture of ECM hydrogels. This three dimensional nanoscale architecture is important for cell attachment and migration through the scaffold. Although the ECM was partially digested, which allowed it to be injectable, the ECM reassembled into a three dimensional nanofibrous network upon gelation at physiologic temperature and pH. Porous nanofibrous architecture may be desirable to resemble the native ECM conditions, as the main ECM component, collagen, forms a nanofibrous architecture *in*

vivo[32,33]. Fiber diameters can also affect the mechanical properties and self assembly of the hydrogel; we have found that fibers with diameters between 30 – 250 nm and an average diameter of 100 nm form upon self-assembly of the muscle ECM hydrogels [30]. Figure 2.4E and F display example SEM images for the skeletal muscle and cardiac ECM hydrogels.

The final, decellularized ECM hydrogel can be used for a variety of applications. A benefit of the lyophilized digested ECM is that it has a long shelf life if stored frozen and can be quickly prepared for injection by thorough resuspension in sterile water. The shear thinning property and solution-to-gel transformation at 37°C both allow for injection and gelation *in situ* at body temperature. This allows for direct injection of the material into a tissue-specific location, such as the skeletal muscle ECM hydrogel injected intramuscularly for PAD applications, or the cardiac ECM hydrogel injected into the left ventricle via catheter for cardiac repair after MI. For example, we have shown the potential of the skeletal muscle-specific ECM hydrogel to improve neovascularization and muscle proliferation in a rat model of hindlimb ischemia [10]. Our cardiac ECM hydrogel has been shown to increase cell migration *in vitro* [19]; it also promoted tissue repair and increased cardiac function after one and three months in small and large animal models *in vivo*[20,21]. This general process for generating and characterizing ECM hydrogels can also be performed on many other tissue types, such as brain [34], adipose [35], bone [36], and skin [37], to develop tissue specific injectable hydrogels for a variety of *in vitro* and *in vivo* tissue engineering applications. The overall goal of the injectable ECM hydrogels is to provide biochemical cues that are specific to the tissue, which is being regenerated, as well as a physical scaffold to support cell infiltration.

2.4 Conclusions

We have shown that naturally derived ECM hydrogels can be fabricated through detergent based decellularization and enzymatic digestion, and subsequently characterized through a variety of mechanical and biochemical techniques. Once fabricated and properly

characterized, these tissue-specific hydrogels can be used in a variety of applications for tissue regeneration and repair *in vivo* or probing tissue-specific cell interactions *in vitro.* We will demonstrate some of the *in vivo* applications of these injectable hydrogels in skeletal muscle regeneration for PAD in Chapters 3 and 4.

Chapter 2, in full, is a reprint of the material as it appears in *Methods*, 2015, 84: 53-59. The authors are Jessica Ungerleider, Todd Johnson, Nikhil Rao, and Karen Christman. The dissertation author was the primary investigator and author of this paper.

2.5 References

1. Go, A. S., Mozaffarian, D., Roger, V. L., Benjamin, E. J., Berry, J. D., Borden, W. B., Bravata, D. M., Dai, S., Ford, E. S., Fox, C. S., Franco, S., Fullerton, H. J., Gillespie, C., Hailpern, S. M., Heit, J. A., Howard, V. J., Huffman, M. D., Kissela, B. M., Kittner, S. J., *et al.* Heart disease and stroke statistics--2013 update: a report from the American Heart Association. *Circulation* **127,** e6–e245 (2013).

2. Sutton, M. G. S. J. & Sharpe, N. Left Ventricular Remodeling After Myocardial Infarction : Pathophysiology and Therapy. *Circulation* **101,** 2981–2988 (2000).

3. Ostchega, Y., Paulose-Ram, R., Dillon, C. F., Gu, Q. & Hughes, J. P. Prevalence of peripheral arterial disease and risk factors in persons aged 60 and older: data from the National Health and Nutrition Examination Survey 1999-2004. *J Am Geriatr Soc* **55,** 583–589 (2007).

4. Ruvinov, E., Leor, J. & Cohen, S. The effects of controlled HGF delivery from an affinity-binding alginate biomaterial on angiogenesis and blood perfusion in a hindlimb ischemia model. *Biomaterials* **31,** 4573–4582 (2010).

5. Kawamura, I., Takemura, G., Tsujimoto, A., Watanabe, T., Kanamori, H., Esaki, M., Kobayashi, H., Takeyama, T., Kawaguchi, T., Goto, K., Maruyama, R., Fujiwara, T., Fujiwara, H., Tabata, Y. & Minatoguchi, S. Treatment of leg ischemia with biodegradable gelatin hydrogel microspheres incorporating granulocyte colony-stimulating factor. *J Cardiovasc. Pharmacol.* **57,** 416–423 (2011).

6. Powell, R. J., Comerota, A. J., Berceli, S. A., Guzman, R., Henry, T. D., Tzeng, E., Velazquez, O., Marston, W. A., Bartel, R. L., Longcore, A., Stern, T. & Watling, S. Interim analysis results from the RESTORE-CLI, a randomized, double-blind multicenter phase II trial comparing expanded autologous bone marrow-derived tissue repair cells and placebo in patients with critical limb ischemia. *J Vasc Surg* **54,** 1032–1041 (2011).

7. Powell, R. J., Goodney, P., Mendelsohn, F. O., Moen, E. K., Annex, B. H. & Investigators, H. G. F. T. Safety and efficacy of patient specific intramuscular injection of HGF plasmid gene therapy on limb perfusion and wound healing in patients with ischemic lower

extremity ulceration: results of the HGF-0205 trial. *J Vasc Surg* **52,** 1525–1530 (2010).

8. Shigematsu, H., Yasuda, K., Iwai, T., Sasajima, T., Ishimaru, S., Ohashi, Y., Yamaguchi, T., Ogihara, T. & Morishita, R. Randomized, double-blind, placebo-controlled clinical trial of hepatocyte growth factor plasmid for critical limb ischemia. *Gene Ther* **17,** 1152–1161 (2010).

9. Fan, C., Gao, P., Gu, Y., Tang, X., Liu, J., Wei, J., Inoue, K. & Zhu, D. Therapeutic angiogenesis by intramuscular injection of fibrin particles into ischaemic hindlimbs. *Clin. Exp. Pharmacol. Physiol.* **33,** 617–622 (2006).

10. DeQuach, J. A., Lin, J. E., Cam, C., Hu, D., Salvatore, M., Sheikh, F. & Christman, K. L. Injectable skeletal muscle matrix hydrogel promotes neovascularization and muscle cell infiltration in a hindlimb ischemia model. *Eur Cell Mater* **23,** 400–412 (2013).

11. Webber, M. J., Tongers, J., Newcomb, C. J., Marquardt, K. T., Bauersachs, J., Losordo, D. W. & Stupp, S. I. Supramolecular nanostructures that mimic VEGF as a strategy for ischemic tissue repair. *Proc Natl Acad Sci U S A* **108,** 13438–13443 (2011).

12. Lin, Y. D., Luo, C. Y., Hu, Y. N., Yeh, M. L., Hsueh, Y. C., Chang, M. Y., Tsai, D. C., Wang, J. N., Tang, M. J., Wei, E. I., Springer, M. L. & Hsieh, P. C. Instructive nanofiber scaffolds with VEGF create a microenvironment for arteriogenesis and cardiac repair. *Sci Transl Med* **4,** 146ra109 (2012).

13. Tongers, J., Roncalli, J. G. & Losordo, D. W. Therapeutic angiogenesis for critical limb ischemia: microvascular therapies coming of age. *Circulation* **118,** 9–16 (2008).

14. Rane, A. A. & Christman, K. L. Biomaterials for the treatment of myocardial infarction: a 5-year update. *J Am Coll Cardiol* **58,** 2615–2629 (2011).

15. Akhyari, P., Kamiya, H., Haverich, A., Karck, M. & Lichtenberg, A. Myocardial tissue engineering: the extracellular matrix. *Eur J Cardiothorac Surg* **34,** 229–241 (2008).

16. Segers, V. F. & Lee, R. T. Biomaterials to enhance stem cell function in the heart. *Circ Res* **109,** 910–922 (2011).

17. Ouma, G. O., Jonas, R. A., Usman, M. H. & Mohler 3rd, E. R. Targets and delivery methods for therapeutic angiogenesis in peripheral artery disease. *Vasc Med* **17,** 174–192 (2012).

18. Ungerleider, J. L. & Christman, K. L. Concise review: Injectable biomaterials for the treatment of myocardial infarction and peripheral artery disease: translational challenges and progress. *Stem Cells Trans Med* **3,** 1–10 (2014).

19. Singelyn, J. M., DeQuach, J. A., Seif-Naraghi, S. B., Littlefield, R. B., Schup-Magoffin, P. A. & Christman, K. L. Naturally derived myocardial matrix as an injectable scaffold for cardiac tissue engineering. *Biomaterials* **30,** 5409–5416 (2009).

20. Seif-Naraghi, S. B., Singelyn, J. M., Salvatore, M., Osborn, K. G., Wang, J., Sampat, U., Kwan, O. L., Strachan, G. M., Wong, J., Schup-Magoffin, P. A., Braden, R. L., Bartels, K., DeQuach, J. A., Preul, M., Kinsey, A. M., Demaria, A. N., Dib, N. & Christman, K. L. Safety and Efficacy of an Injectable Extracellular Matrix Hydrogel for Treating Myocardial

Infarction. *Sci Transl Med* **5,** 173ra25 (2013).

21. Singelyn, J. M., Sundaramurthy, P., Johnson, T. D., Schup-Magoffin, P. J., Hu, D. P., Faulk, D. M., Wang, J., Mayle, K. M., Bartels, K., Salvatore, M., Kinsey, A. M., Demaria, A. N., Dib, N. & Christman, K. L. Catheter-deliverable hydrogel derived from decellularized ventricular extracellular matrix increases endogenous cardiomyocytes and preserves cardiac function post-myocardial infarction. *J Am Coll Cardiol* **59,** 751–763 (2012).

22. Freytes, D. O., Martin, J., Velankar, S. S., Lee, A. S. & Badylak, S. F. Preparation and rheological characterization of a gel form of the porcine urinary bladder matrix. *Biomaterials* **29,** 1630–1637 (2008).

23. Barbosa, I., Garcia, S., Barbier-Chassefiere, V., Caruelle, J. P., Martelly, I. & Papy-Garcia, D. Improved and simple micro assay for sulfated glycosaminoglycans quantification in biological extracts and its use in skin and muscle tissue studies. *Glycobiology* **13,** 647–653 (2003).

24. Johnson, T. D., DeQuach, J. A., Gaetani, R., Ungerleider, J., Elhag, D., Nigam, V., Behfar, A. & Christman, K. L. Human versus porcine tissue sourcing for an injectable myocardial matrix hydrogel. *Biomater. Sci.* 60283D (2014). doi:10.1039/c3bm60283d

25. Badylak, S. F. Decellularized allogeneic and xenogeneic tissue as a bioscaffold for regenerative medicine: factors that influence the host response. *Ann Biomed Eng* **42,** 1517–1527 (2014).

26. Reing, J., Brown, B. N., Daly, K. A., Freund, J. M., Gilbert, T. W., Hsiong, S., Huber, A., Kullas, K. E., Tottey, S., Wolf, M. T. & Badylak, S. F. The effects of processing methods upon mechanical and biologic properties of porcine dermal extracellular matrix scaffolds. *Biomaterials* **31,** 8626–8633 (2010).

27. Seif-Naraghi, S. B., Horn, D., Schup-Magoffin, P. J. & Christman, K. L. Injectable extracellular matrix derived hydrogel provides a platform for enhanced retention and delivery of a heparin-binding growth factor. *Acta Biomater* **8,** 3695–3703 (2012).

28. Hill, R. C., Calle, E. A., Dzieciatkowska, M., Niklason, L. E. & Hansen, K. C. Quantification of Extracellular Matrix Proteins from a Rat Lung Scaffold to Provide a Molecular Readout for Tissue Engineering. *Mol. Cell. Proteomics* (2015). doi:10.1074/mcp.M114.045260

29. Beynon, R. J., Doherty, M. K., Pratt, J. M. & Gaskell, S. J. Multiplexed absolute quantification in proteomics using artificial QCAT proteins of concatenated signature peptides. *Nat Meth* **2,** 587–589 (2005).

30. Johnson, T. D., Lin, S. Y. & Christman, K. L. Tailoring material properties of a nanofibrous extracellular matrix derived hydrogel. *Nanotechnology* **22,** 494015 (2011).

31. Singelyn, J. M. & Christman, K. L. Modulation of material properties of a decellularized myocardial matrix scaffold. *Macromol Biosci* **11,** 731–738 (2011).

32. Rosenblatt, J., Devereux, B. & Wallace, D. G. Injectable collagen as a pH-sensitive hydrogel. *Biomaterials* **15,** 985–995 (1994).

33. Williams, B. R., Gelman, R. A., Poppke, D. C. & Piez, K. A. Collagen Fibril Formation: Optimal in vitro conditions and preliminary kinetic results. *J Biol. Chem* **253,** 6578–6585 (1978).

34. DeQuach, J. A., Yuan, S. H., Goldstein, L. S. & Christman, K. L. Decellularized porcine brain matrix for cell culture and tissue engineering scaffolds. *Tissue Eng Part A* **17,** 2583–2592 (2011).

35. Young, D. A., Bajaj, V. & Christman, K. L. Decellularized adipose matrix hydrogels stimulate in vivo neovascularization and adipose formation. *J Biomed Mater Res A* **102,** 1641–1651 (2014).

36. Sawkins, M. J., Bowen, W., Dhadda, P., Markides, H., Sidney, L. E., Taylor, A. J., Rose, F. R. A. J., Badylak, S. F., Shakesheff, K. M. & White, L. J. Hydrogels derived from demineralized and decellularized bone extracellular matrix. *Acta Biomater* **9,** 7865–7873 (2013).

37. Wolf, M. T., Daly, K. A., Brennan-Pierce, E. P., Johnson, S. A., Carruthers, C. A., D'Amore, A., Nagarkar, S. P., Velankar, S. S. & Badylak, S. F. A hydrogel derived from decellularized dermal extracellular matrix. *Biomaterials* **33,** 7028–7038 (2012).

Chapter 3

Extracellular Matrix Hydrogel Promotes Tissue Remodeling, Arteriogenesis, and Perfusion in a Rat Hindlimb Ischemia Model

3.1 Introduction

Nearly 30 million patients in North American and Europe have been diagnosed with peripheral artery disease (PAD) [1]. A major consequence of untreated PAD is lower extremity amputations due to decreased limb perfusion, and an estimated 120,000 and 100,000 patients in the U.S. and Europe, respectively, suffer this extreme outcome annually [2]. Endovascular revascularization [3] is the only current surgical treatment, but 40% of patients with critical limb ischemia (CLI) are left with no options due to extreme tissue damage and/or diffuse atherosclerotic disease [4,5]. Even with revascularization, the rate of amputation remains high [6]. Therefore, there is an extreme need for alternative limb salvage therapies for PAD patients.

Regenerative medicine has shown promise as a potential treatment for PAD, including cell [7–9], growth factor [10–12], or bioactive material delivery systems [13–15]. An ideal therapy should ameliorate tissue ischemia, and some strategies have shown promise by delivering angiogenic or vasodilatory factors. Despite these efforts, no PAD therapy has been approved due to suboptimal results.

As highlighted in previous chapters, biomaterial-alone approaches are becoming more prevalent in the field of regenerative medicine for their ability to improve damaged tissue regeneration in heart failure, skeletal muscle pathology, and many other disease applications [15–18]. This approach is cost-efficient, has an increased shelf life, and is associated with fewer

ethical concerns compared to cell or growth factor based therapies (see Chapter 1). While injectable biomaterial alone approaches have been explored to treat ischemic cardiac muscle [19], they have not been extensively explored for treating the ischemic skeletal muscle associated with PAD. When designed appropriately, injectable biomaterials can be employed to create new scaffolds that recruit endogenous cells to repair damaged tissue.

Our group previously developed an injectable hydrogel derived from decellularized porcine skeletal muscle extracellular matrix (SKM) (Chapter 2) [15]. Preliminary histological analysis within the local region of the injected biomaterial in a mild rodent hindlimb ischemia model suggested that this acellular approach has the potential to not only stimulate vessel growth, but could also aid in treating the muscle atrophy associated with PAD. A functional perfusion study also showed that SKM increased blood flow to the ischemic limb over saline controls, and end point-histology demonstrated this was through arteriogenesis (Figure 3.1) [20]. The material had been degraded by 35 days post-injection, and there was no evidence of chronic inflammation due to the injection. Furthermore, muscle morphology of the SKM-injected muscle was significantly improved over saline controls and not dissimilar from healthy muscle (Figure 3.1).

The goal of this study was to investigate the dynamic changes due to SKM injection in a rat hindlimb ischemia model in order to better understand the tissue wide effects of biomaterial injection in a regeneration context.

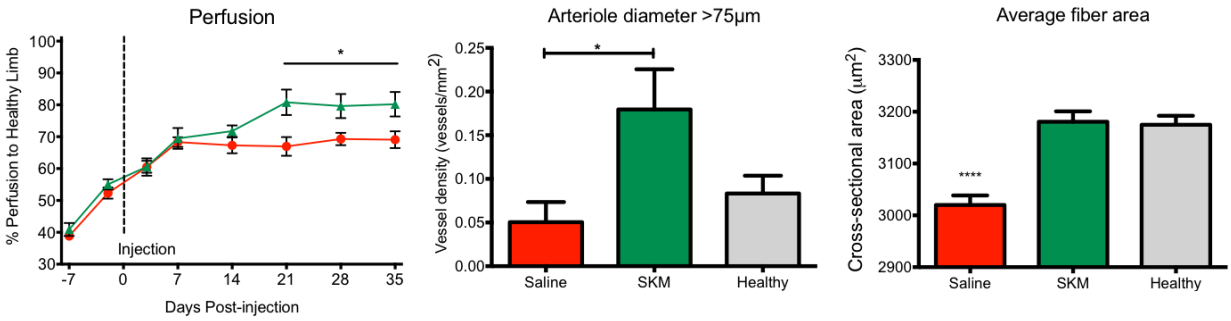

Figure 3.1: SKM hydrogel increases perfusion, arteriogenesis, and muscle remodeling at 35 days post-injection. Left: perfusion post-hindlimb ischemia (day -7) and post-treatment (day 0) with SKM or saline as measured by laser speckle contrast analysis. Middle: density of large arterioles (>75 µm in diameter) in gracilis muscle at 35 days post-injection. Right: muscle fiber cross sectional area in gracilis muscle at 35 days post-injection. *p<0.05, ****p<0.0001 compared to saline.

3.2 Materials and Methods

3.2.1 ECM hydrogel development and characterization

The methods for producing the porcine skeletal muscle matrix (SKM) were modified from our previously published protocol [15,21]. Briefly, psoas muscle was harvested from Yorkshire farm pigs, approximately 30-45 kg, immediately after euthanasia. All dermal tissue, subcutaneous fat and connective tissue were dissected away. The tissue was then chopped into small cubed pieces about 3-5 mm in length and rinsed in water for 30-45 min. After rinsing, the tissue was spun in 1% (w/v) sodium dodecyl sulfate (SDS) (Fischer Scientific, Fair Lawn, NJ) in phosphate buffered saline (PBS) with 0.5% penicillin streptomycin (PS) of 10,000 U/mL (Gibco, Life Technologies, Grand Island, NY) for 2 hours. The tissue was then rinsed and transferred to new SDS solution with PS for 3-5 days with daily solution changes to remove the cellular content. Once fully white, the tissue was rinsed in ultra pure water for 2 hours and then placed into isopropyl alcohol (IPA) (Fischer Scientific, Fair Lawn, NJ) for 18-24 hours for lipid removal. Finally the tissue was rinsed in water for 24 hours following by 2-5 additional rinses in water, freezing at -80 °C, and lyophilizing. The lyophilized material was then milled into a fine powder

using a Wiley® Mini-Mill and a #40 sieve. ECM samples from three different pigs were combined to form a batched material that was used for all analysis and testing.

SKM was digested using a previously described protocol [15]. Briefly, the powder form was digested at 10 mg/mL in a solution of pepsin at 1 mg/mL (Sigma, St. Louis, MO) in 0.1 M HCl for 48 hours. Once digested into a liquid form, the material was brought to a pH of 7.4 on ice while stirring using chilled 1.0 M NaOH. Next, the salt concentration was adjusted to 1x PBS by addition of 10x PBS. Finally, the ECM concentration was lowered to 6 mg of ECM/ml with 1x PBS. All solutions used were sterile filtered and pre-chilled in an ice and water slurry. The material was then frozen and lyophilized for storage in at -80 °C. Upon use, the material was thawed and brought back to a material concentration of 6 mg of ECM/mL with sterile ultra pure water.

The dsDNA content was isolated (n=3) using a NucleoSpin® Tissue kit (Macherey-Nagel, Duren, Germany). The nucleic acid composition was quantified (n=3) with a Thermo Scientific NanoDrop 2000c spectrophotometer and the dsDNA content was measured (n=3) by using a Quint-iT^{TM} PicoGreen® dsDNA Assay Kit (Invitrogen, Eugene, OR). Sulfated glycosaminoglycan (sGAG) content was quantified (n=3) with a previously published DMMB protocol [22,23]. Rheology of the SKM hydrogel was quantified using an AR-G2 Rheometer on 500 µl gels at 37ºC with a gap height of 1000 µm and a 2.5% strain using a frequency sweep protocol (100 rad/s to 0.25 rad/s oscillatory) and storage and loss moduli were reported at 1 Hz.

Samples were prepared for LC-MS/MS following a previously published protocol [24]. Briefly, milled ECM samples were chemically digested in 100 mM CNBr in 86% TFA. The samples were digested according to the FASP protocol using a 10 kDa molecular weight cutoff filter. Samples were supplemented with $^{13}C_6$ labeled QconCAT peptides and digested using the FASP method as previously described [25]. High pH reversed phase chromatography was performed on a Gemini C18, 50 × 2 mm column using 20 mM ammonium bicarbonate (pH 10)

as mobile phase (A) and 20 mM ammonium bicarbonate and 75% ACN (pH 10) as mobile-phase B. Global LC-MS/MS was performed on 6 fractions using the LTQ-FT Ultra Hybrid ion cyclotron resonance mass spectrometer (Thermo Fisher Scientific) and Selected Reaction Monitoring (SRM) was performed on the QTRAP®5500 triple quadrupole mass spectrometer (ABSciex). Nano-flow reverse phase LC-MS/MS was performed on both systems using a capillary Agilent 1200 HPLC system. Instrument parameters and run conditions and bioinformatics analysis were performed as previously described [25]. MS/MS data of Skeletal Muscle Matrix sample were searched against the *Sus scrofa* protein sequences database from the UniProtKB/Swiss-Prot database and MS/MS data of Umbilical Cord Matrix sample were searched against the *Homo Sapiens* protein sequences database from the UniProtKB/Swiss-Prot (release October 2014, containing 20,268 proteins). Peptide identifications were accepted if they could be established at >95.0% probability as specified by the Peptide Prophet algorithm. Protein identifications were accepted if they could be established at >99.0% probability and contained at least two identified unique peptides. All data files generated on the triple quadrupole mass spectrometer during LC-SRM analyses were imported to Skyline v2.2 software [26] for data processing. Transition quality, peak shape, and peak area boundaries were manually validated. The peak integration was done automatically by the software, using Savitzky–Golay smoothing, and all the data were manually inspected to confirm correct peak detection.

3.2.2 Hindlimb ischemia surgery and biomaterial injection

All experiments in this study were performed in accordance with the guidelines established by the Institutional Animal Care and Use Committee at the University of California, San Diego, and the American Association for Accreditation of Laboratory Animal Care. Studies were done with 24 female Sprague Dawley (SD) rats ranging in weights of 220-265 g.

For the hindlimb ischemia surgery (day -7), animals were anesthetized with 2.5% Isoflurane gas using a Kent Scientific PhysioSuite™ ventilator system. Unilateral ischemia damage was applied to the animals' right limb by ligation and removal of segments from the femoral artery and vein starting proximal to the epigastric artery as described previously [27,28]. First, the surgical site was shaved and cleaned with betadine and isopropanol along with delivery of 1% licocaine subcutaneously along the incision site. The targeted vessels were visualized by creating an incision overlying the proximal, medial portion of the right hindlimb. The femoral artery and vein were dissected away from the femoral nerve and ligated to target the proximal removal of a 2 cm segment. Any major branches along the 2 cm segment, including the epigastric artery, were cauterized or ligated before excision to minimize bleeding. The entry incision through the skin was then closed using a mattress suture (5-O silk). Postoperatively, all animals were regularly monitored and analgesia (Buprenorphine at 0.05 mg/kg) was administered immediately upon regaining consciousness.

Animals were arbitrarily selected for treatment with SKM hydrogel (n=6 per timepoint) or saline (n=6 per timepoint) (out to day 3 and day 10 post-injection). The injection site was prepared by shaving if needed followed by cleaning with betadine and isopropanol. A single injection of 150 µL was performed using a 27 G needle into the gracilis muscle [29,30].

3.2.3 Histological analysis

On day 3 or 10 the injected hindlimb Gracilis muscle and corresponding healthy Gracilis muscle tissue was excised. The tissue was placed in physiological orientation and morphology on a filter paper and flash frozen in isopentane chilled with liquid nitrogen. The tissue was then blocked in OCT to allow for transverse sectioning of the tissue and flash frozen again in isopentane chilled with liquid nitrogen. Sections of 10 µm thickness were taken at seven different locations evenly spaced spanning the majority of the muscle segment. All histological

imaging was done with either a Leica Aperio ScanScope® CS^2 or a Leica Ariol®. Tissue was stained with Hematoxylin and Eosin (H&E) for histological analysis. Immunohistochemistry was used to stain vessels, laminin, and skeletal muscle progenitors. Arterioles were labeled with an alpha-smooth muscle actin (αSMA) antibody (Dako, Carpinteria, California; 1:75) and an Alexa Fluor 488 conjugated secondary antibody (Invitrogen, Carlsbad, California; 1:500), and nuclei were counterstained with Hoechst 33342. Arterioles were quantified from surveying 8 randomly selected 10x images from 5 different slides distributed evenly throughout the length of the muscle per limb for a total of 40 images per sample. For arterioles with a diameter of over 10 μm the major axis, minor axis, and total internal lumen area were measured with ImageJ (NIH, Bethesda, MD). Arteriole diameter was reported as the average of the major and minor axis. Capillaries were stained using Alkaline Phosphatase chromagen (BCIP/NBT) (Abcam, Cambridge, MA) staining on fresh frozen slides. Capillary density was automatically quantified using a custom assay as part of the Leica Ariol® system and was applied to 10 randomly selected 20x regions from 5 slides per sample distributed evenly throughout the length of the muscle. Skeletal muscle progenitor cell density was quantified through Pax-7 staining with an anti-Pax-7 primary antibody (abcam, Boston, Massachusetts, 1:100) and an Alexa Fluor 568 conjugated secondary antibody (Invitrogen, Carlsbad, California, 1:500) and nuclei were counterstained with Hoechst 33342. The percent of Pax-7 positive nuclei was calculated by visual colocalization and nuclear counting using the Leica Ariol® system from 3 randomly selected 10x regions from 3 different slides per sample spanning the majority of the muscle.

3.2.4 Microarray analysis and qPCR

GeneChip Rat Gene ST 2.0 microarrays (Affymetrix) were run on SKM and saline-injected gracilis muscles at both 3 and 10 days post-injection (n=6 rats per group per timepoint, n=3 arrays per group per timepoint). RNA was isolated from flash-frozen skeletal muscle with

Trizol (Life Technologies) and cleaned with on-column DNase treatment (Qiagen). Two animals were pooled for each array to reduce animal-to-animal variability. Data was normalized with Vampire Analysis. Data was processed with PANTHER using Entrez IDs for Gene Ontology molecular function and biological pathway ID lists using all genes with a p-value below 0.05 from Vampire Analysis. Pathways were generated through the use of Qiagen's Ingenuity Pathway Analysis (IPA, Qiagen Redwood City, www.qiagen.com/ingenuity) using all genes and fold changes with a p-value below 0.05 from Vampire Analysis.

cDNA libraries were synthesized from total RNA pooled from the same donors as for microarray analysis with 1 µg total RNA, SuperScript III RNA Polymerase (Invitrogen), and random hexamers. PCR primers (Invitrogen) were selected using NCBI PrimerBlast and validated by running qPCR reactions at a gradient of melt temperatures (55 to 65°C) and verifying normal melt curves and amplification curves. Primer forward and reverse sequences are summarized in Table 3.9. PCR reactions were assembled using 1:20 dilution of cDNA, Power SYBR© Master Mix (Applied Biosystems), and 1 µM forward and reverse primers.

3.2.5 Statistical analysis

Global proteomics data was directly exported and normalized to sample maximum. Peak area ratios for the SRM data was normalized to an internal standard spike, and then coefficients of variance were determined between the biological replicates. Histology was analyzed with a Student's *t*-test. Raw intensity values from Affymetrix microarrays were normalized and statistically compared with Vampire Analysis algorithm using an FDR of 0.1. P values and activation z scores for Ingenuity pathways were calculated as previously described [31]. Data are means ± SEM unless otherwise noted. Significance was accepted at $P<0.05$.

3.3 Results

3.3.1 SKM hydrogel retains complex proteomic composition

SKM hydrogel was fabricated and characterized using previously published methods. Material was sufficiently decellularized as evidenced by low DNA content. SKM maintained sulfated glycosaminoglycans (sGAGs), which are important for binding of endogenous growth factors upon injection. Hydrogels formed *in vitro* had acceptable rheological properties (Table 3.1). SKM material maintained a complex proteomic composition, which was quantified using targeted proteomics (Table 3.2) and verified using global proteomics (Table 3.3).

Table 3.1: Biochemical and mechanical properties of SKM hydrogel.

Assay	Value (mean +/- standard deviation)
DNA content (ng dsDNA per mg ECM)	1.09 +/- 0.09
sGAG content (µg sGAGs per mg ECM)	6.14 +/- 0.25
Storage Modulus (G', Pa) at 1 rad/s	4.295
Loss Modulus (G", Pa) at 1 rad/s	1.061

Table 3.2: ECM protein concentration in porcine skeletal muscle matrix. Absolute quantification of 49 ECM, ECM associated, and common cellular contaminant proteins.

Protein Abundance in Porcine Skeletal Muscle Matrix [nmol/g]			
Protein	***GENE***	***Functional Classification***	***Average***
Collagen alpha-1(IV) chain(Arresten/Core Protein)	COL4A1	Basement Membrane	106.72
Collagen alpha-1/5(IV) chain(Arresten/Core Protein)	COL4A1/5	Basement Membrane	81.80
Collagen alpha-2(IV) chain(Canstatin/Core Protein)	COL4A2	Basement Membrane	44.08
Laminin alpha-2	LAMA2	Basement Membrane	0.15
Laminin Beta-1	LAMB1	Basement Membrane	0.09
Laminin Beta-2	LAMB2	Basement Membrane	0.25
Laminin Gamma-1	LAMC1	Basement Membrane	1.25
Nidogen-1	NID1	Basement Membrane	0.04
Perlecan	HSPG2	Basement Membrane	6.07
Actin (All Isoforms)	ACT	Cytoskeletal	1.56
Actin, cytoplasmic 1/2	ACTB	Cytoskeletal	0.16
Myosin(Myosin-3,4,6,7)	MYH	Cytoskeletal	2.50
Transglutaminase 2	TGM2	ECM regulator	0.03
Collagen alpha-1(XII) chain	COL12A1	FACIT Collagen	0.39
Collagen alpha-1(XIV) chain	COL14A1	FACIT Collagen	0.68
Collagen alpha-1(I) chain	COL1A1	Fibrillar Collagen	1158.09
Collagen alpha-1(V) chain	COL5A1	Fibrillar Collagen	19.69
Collagen alpha-2(I) chain	COL1A2	Fibrillar Collagen	810.89
Collagen alpha-2(V) chain	COL5A2	Fibrillar Collagen	6.28

Table 3.2 continued: ECM protein concentration in porcine skeletal muscle matrix. Absolute quantification of 49 ECM, ECM associated, and common cellular contaminant proteins.

Protein Abundance in Porcine Skeletal Muscle Matrix [nmol/g]			
Protein	***GENE***	***Functional Classification***	***Average***
Collagen alpha-1(VI) chain	COL6A1	Matricellular	6.83
Collagen alpha-2(VI) chain	COL6A2	Matricellular	4.72
Collagen alpha-3(VI) chain	COL6A3	Matricellular	9.62
Dermatopontin	DPT	Matricellular	6.16
Emilin 1	EMILIN1	Matricellular	0.08
Fibronectin 1	FN1	Matricellular	11.17
Fibulin 1	FBLN1	Matricellular	0.04
Fibulin 3	EFEMP1	Matricellular	0.51
Fibulin 5	FBLN5	Matricellular	0.29
Lumican	LUM	Matricellular	7.51
Periostin	POSTN	Matricellular	0.15
Thrombospondin 1	THBS1	Matricellular	0.06
TnxB Protein	TNXB	Matricellular	0.04
Versican	VCAN	Matricellular	0.07
Glyceraldehyde-3-phosphate dehydrogenase	GAPDH	Other Cellular	0.75
Extracellular Matrix Protein 1	ECM1	Other ECM	0.05
Galectin-1	LGALS1	Other ECM	0.04
Transforming growth factor-beta-induced protein ig-h3	TGFBI	Secreted	0.51
Biglycan	BGN	Structural ECM	0.04
Fibrillin 1	FBN1	Structural ECM	6.17
Fibrillin 2	FBN2	Structural ECM	0.47
Fibromodulin	FMOD	Structural ECM	0.27

Table 3.2 continued: ECM protein concentration in porcine skeletal muscle matrix. Absolute quantification of 49 ECM, ECM associated, and common cellular contaminant proteins.

Protein Abundance in Porcine Skeletal Muscle Matrix [nmol/g]			
Protein	***GENE***	***Functional Classification***	***Average***
Microfibrillar-associated protein 2	MFAP2	Structural ECM	1.12

Table 3.3: Top 20 proteins of porcine skeletal muscle matrix by global proteomics. Table represents top 20 proteins identified based on the number of unique peptide spectral matches from global LC-MS/MS for a given protein.

Proteins	***Gene***	***Functional Classification***	***Accession Number***	***Unique PSM's***
Perlecan	HSPG2	Basement Membrane	F1SU03	18
Laminin subunit gamma-1	LAMC1	Basement Membrane	F1S663	8
Myosin-4	MYH4	Cytoskeletal	Q9TV62	59
Myosin-binding protein C, fast-type	MYBPC2	Cytoskeletal	F1RH19	9
Collagen alpha-1(XIV) chain	COL14A1	FACIT Collagen	F1S285	9
Collagen alpha-2(I) chain	COL1A2	Fibrillar Collagen	F1SFA7	184
Collagen alpha-1(I) chain	COL1A1	Fibrillar Collagen	P02453	113
Collagen alpha-1(III) chain	COL3A3	Fibrillar Collagen	F1RYI8	85
Collagen alpha-1(V) chain	COL5A1	Fibrillar Collagen	F1S021	8
Collagen alpha-2(V) chain	COL5A2	Fibrillar Collagen	F1RXW0	7
Collagen alpha-3(VI) chain	COL6A3	Matricellular	I3LUR7	52
Collagen alpha-1(IV) chain	COL4A2	Matricellular	F1RLL9	37
Collagen alpha-2(IV) chain	COL4A1	Matricellular	F1RLM1	25
Lumican	LUM	Matricellular	F1SQ09	18
Fibronectin	FN1	Matricellular	F1SS24	17
Collagen alpha-2(VI) chain	COL6A2	Matricellular	I3LQ84	15
Calcium-transporting ATPase	ATP2A1	Plasma membrane	F1RFH9	9
Serum albumin	ALB	Secreted	F1RUN2	7
Fibrillin-1	FBN1	Structural ECM	Q9TV36	68
Elastin	ELN	Structural ECM	G8FUN3	5

3.3.2 SKM hydrogel improved perfusion and muscle remodeling through increased density of larger arterioles and recruitment of skeletal muscle progenitors

We sought to analyze the temporal changes following skeletal muscle ECM hydrogel injection. We performed a hindlimb ischemia study, comparing saline and SKM injections at 3 and 10 days post-injection (day 10 and day 17 post-surgery, respectively). There were no significant differences in capillary density, arteriole density, or arteriole diameter between saline and SKM treated muscles at these early time points (Figure 3.2 A-F). However, similar to the previous experiment at day 35, density of arterioles >75 μm trended higher in SKM injected animals at both 3 and 10 days post-injection (Figure 3.2 G,H).

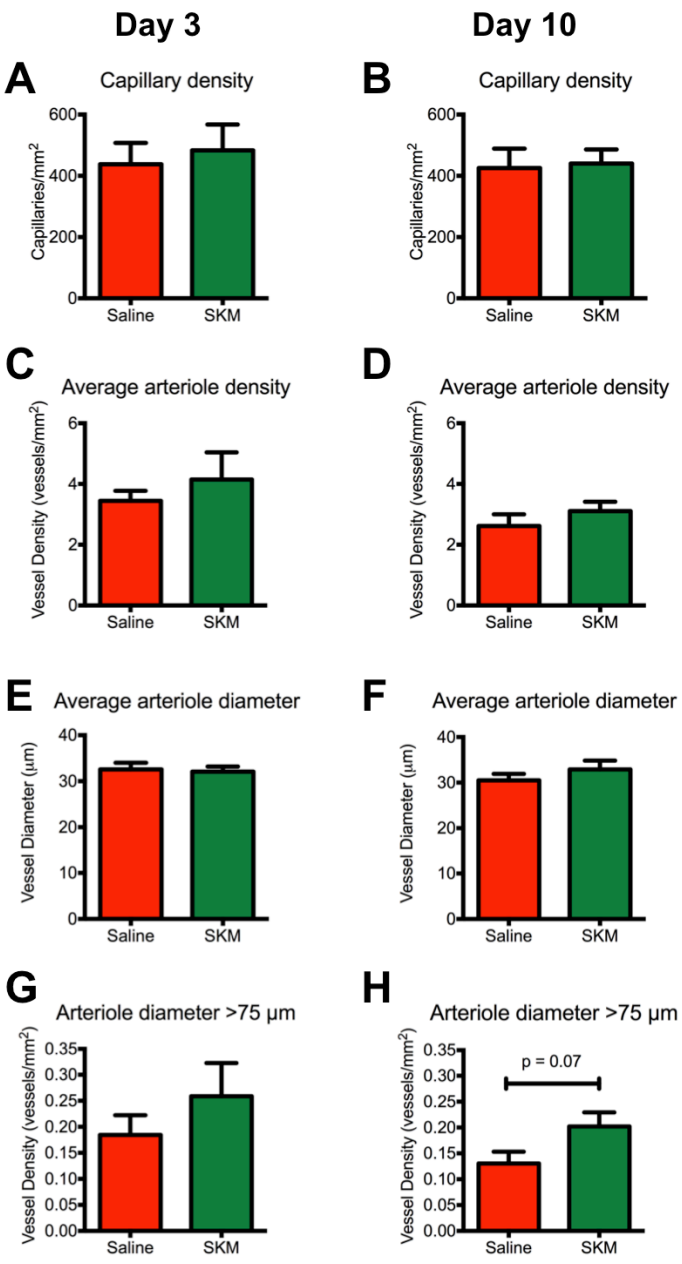

Figure 3.2: Short term histological assessment of arteries and capillaries. Histological analysis taken at Day 3 (**A, C, E, G**) and Day 10 (**B, D, F, H**) post-injection. There were no differences in capillary density (A, B), arteriole density (C, D), or average arteriole diameter (E, F) between SKM and saline at these early timepoints, but the density of arterioles with diameter > 75 µm (**E,F**) trended higher in the SKM (n=6) group compared to saline (n=6).

Due to improvements in muscle remodeling at day 35 post-injection, we analyzed tissue at day 3 and 10 post-injection for infiltration of skeletal muscle progenitors. Pax-7 is a transcription factor involved in early stage muscle lineage commitment in skeletal muscle satellite cells [32]. Analysis of percentage of Pax-7 positive nuclei showed the impact of SKM injection on the gracilis muscle near the material. At day 3, SKM injected muscles had a significantly higher percentage of Pax-7$^+$ nuclei compared to saline ($p < 0.05$), but by day 10 Pax-7$^+$ nuclei dropped to more quiescent levels (Figure 3.3).

Figure 3.3: Short term histological assessment of skeletal muscle progenitor cells. (**A**) Representative image of Pax-7$^+$ (red) and Hoechst 33342 (blue) co-staining in SKM-injected gracilis muscle. Scale bar is 50 μm and Pax-7$^+$ nuclei are indicated by white arrows. There were significantly more Pax-7$^+$ cells as a percentage of total nuclei in SKM (n=6) versus saline (n=6) injected muscles at day 3 (**B**), but this returned to quiescent levels by day 10 (**C**). *P = 0.0096. Data from the healthy limb is shown as a reference.

3.3.3 SKM hydrogel promotes a pro-regenerative environment

We further investigated the mechanism of action of the SKM hydrogel through whole transcript array analysis. Using a false discovery rate of $q < 0.1$, there were 561 significantly differentially regulated genes between saline and SKM in the gracilis at 3 days and 16 genes at 10 days (See [20] Table S5 for significant gene list). At 3 days post-injection, Ingenuity Pathway Analysis showed shifts in the inflammatory response and lipid and carbohydrate metabolism, and increases in muscle development and cell survival with SKM (Table 3.4).

Table 3.4: Significantly altered pathways in SKM relative to saline injected muscle at 3 and 10 days post-injection, as determined by Ingenuity Pathway Analysis.

Day 3 up-regulated pathways				
Category	**Annotation**	**p-value**	**z-score**	**# Molecules**
Lipid Metabolism, Small Molecule Biochemistry	conversion of lipid	0.0112	1.387	5
Cellular Development, Cellular Growth and Proliferation, Hematological System Development and Function	proliferation of lymphocytes	0.0027	1.381	9
Cell Death and Survival	cell survival	0.0272	0.96	21
Cellular Compromise, Inflammatory Response	degranulation of leukocyte cell lines	<0.001	0.748	8
Cell Morphology, Cellular Function and Maintenance	transmembrane potential of mitochondria	0.0021	0.706	9
Cell Signaling, Molecular Transport, Vitamin and Mineral Metabolism	quantity of Ca2+	0.0396	0.699	16
Carbohydrate Metabolism	uptake of monosaccharide	0.0233	0.653	8
Cellular Function and Maintenance	endocytosis	0.0075	0.555	11
Cellular Development, Cellular Growth and Proliferation, Organ Development, Skeletal and Muscular System Development and Function, Tissue Development	proliferation of muscle cells	<0.001	0.486	22
Cell Morphology, Skeletal and Muscular System Development and Function	contractility of muscle cells	0.0115	0.305	4
Day 3 down-regulated pathways				
Category	**Annotation**	**p-value**	**z-score**	**# Molecules**
Cell-To-Cell Signaling and Interaction	activation of cells	0.0161	-2.919	15
Cell Death and Survival	necrosis	0.0139	-2.126	58
Cell Signaling, Post-Translational Modification	tyrosine phosphorylation of protein	0.0401	-2	4

Table 3.4 continued: Significantly altered pathways in SKM relative to saline injected muscle at 3 and 10 days post-injection, as determined by Ingenuity Pathway Analysis.

Day 3 down-regulated pathways				
Category	**Annotation**	**p-value**	**z-score**	**# Molecules**
Cell Death and Survival	neuronal cell death	0.0011	-1.949	36
Cardiovascular System Development and Function, Organismal Development	vasculogenesis	0.0029	-1.604	15
Cell Death and Survival	apoptosis	<0.0001	-1.484	75
Cellular Movement	cell movement	<0.001	-1.39	43
Cell Signaling, Molecular Transport, Small Molecule Biochemistry, Vitamin and Mineral Metabolism	release of Ca2+	0.0486	-1.154	6
Cardiovascular System Development and Function, Organismal Development	angiogenesis	0.0050	-1.107	19
Cellular Assembly and Organization, Cellular Function and Maintenance	organization of cytoskeleton	0.0127	-0.905	45
Day 10 up-regulated pathways				
Category	**Annotation**	**p-value**	**z-score**	**# Molecules**
Cellular Movement	cell movement	0.0089	1.709	7
Cellular Movement	migration of cells	0.0453	1.455	5
Cardiovascular System Development and Function, Organismal Development	vasculogenesis	0.0037	1	4
Cellular Growth and Proliferation	proliferation of cells	<0.00001	0.986	20
Inflammatory Response	inflammatory response	0.0125	0.447	5
Cell Morphology, Cellular Assembly and Organization, Cellular Development, Cellular Growth and Proliferation, Nervous System Development and Function, Tissue Development	outgrowth of neurites	<0.001	0.447	6

Table 3.4 continued: Significantly altered pathways in SKM relative to saline injected muscle at 3 and 10 days post-injection, as determined by Ingenuity Pathway Analysis.

Day 10 up-regulated pathways				
Category	**Annotation**	**p-value**	**z-score**	**# Molecules**
Cardiovascular System Development and Function, Organismal Development	angiogenesis	0.0023	0.277	5
Day 10 down-regulated pathways				
Category	**Annotation**	**p-value**	**z-score**	**# Molecules**
Cell Death and Survival	cell death	<0.001	-0.977	15
Cell Death and Survival	apoptosis	0.0050	-0.594	11

Furthermore, there was down-regulation of genes related to cell death, response to hypoxia, ECM and cytoskeletal organization, and blood vessel development. At 10 days post-injection, there continued to be a shift in the inflammatory response and down-regulation of cell death as well as upregulation of cell adhesion and motility, ECM organization, blood vessel development, and neural system development pathways. Gene ontology analysis also showed differences in many molecular functions and biological processes, such as binding (GO:0005488), catalytic activity (GO:0003824), metabolic process (GO:0008152), developmental process (GO:0032502), and immune system process (GO:0002376), between groups at both time points (Table 3.5-3.8). Microarray analysis was validated with qPCR of key genes (Figure 3.4, Table 3.9).

Table 3.5: Gene ontological molecular function analysis of differentially expressed genes at three days.

	Upregulated in Matrix (day 3) Tot genes: 611 Tot hits: 572		**Upregulated in Saline (day 3) Tot genes: 311 Tot hits: 323**	
Molecular Function	**Number of IDs**	**% (tot hits)**	**Number of IDs**	**% (tot hits)**
transporter activity (GO:0005215)	31	5.40%	32	9.90%
translation regulator activity (GO:0045182)	5	0.90%	1	0.30%
protein binding transcription factor activity (GO:0000988)	4	0.70%	4	1.20%
enzyme regulator activity (GO:0030234)	33	5.80%	15	4.60%
catalytic activity (GO:0003824)	190	33.20%	87	26.90%
receptor activity (GO:0004872)	74	12.90%	43	13.30%
nucleic acid binding transcription factor activity (GO:0001071)	32	5.60%	16	5.00%
antioxidant activity (GO:0016209)	3	0.50%	--	--
structural molecule activity (GO:0005198)	36	6.30%	--	--
binding (GO:0005488)	164	28.70%	91	28.20%
channel regulator activity (GO:0016247)	--	--	1	0.30%
structural molecule activity (GO:0005198)	--	--	33	10.20%

Table 3.6: Gene ontological biological process analysis of differentially expressed genes at three days.

	Upregulated in Matrix (day 3) Tot genes: 611 Tot hits: 1056		**Upregulated in Saline (day 3) Tot genes: 311 Tot hits: 626**	
Biological Process	**Number of IDs**	**% (tot hits)**	**Number of IDs**	**% (tot hits)**
cellular component organization or biogenesis (GO:0071840)	39	3.70%	31	5.00%
cellular process (GO:0009987)	213	20.20%	141	22.50%
localization (GO:0051179)	83	7.90%	59	9.40%
apoptotic process (GO:0006915)	21	2.00%	5	0.80%
reproduction (GO:0000003)	10	0.90%	5	0.80%
biological regulation (GO:0065007)	108	10.20%	66	10.50%
response to stimulus (GO:0050896)	99	9.40%	44	7.00%
developmental process (GO:0032502)	71	6.70%	54	8.60%
multicellular organismal process (GO:0032501)	47	4.50%	27	4.30%
locomotion (GO:0040011)	4	0.40%	1	0.20%
biological adhesion (GO:0022610)	19	1.80%	30	4.80%
metabolic process (GO:0008152)	267	25.30%	131	20.90%
growth (GO:0040007)	1	0.10%	--	--
immune system process (GO:0002376)	74	7.00%	32	5.10%

Table 3.7: Gene ontological molecular function analysis of differentially expressed genes at ten days.

	Upregulated in Matrix (day 10) Tot genes: 68 Tot hits: 60		**Upregulated in Saline (day 10) Tot genes: 13 Tot hits: 16**	
Molecular Function	**Number of IDs**	**% (tot hits)**	**Number of IDs**	**% (tot hits)**
nucleic acid binding transcription factor activity (GO:0001071)	1	1.70%	2	12.50%
binding (GO:0005488)	20	33.30%	3	18.80%
receptor activity (GO:0004872)	12	20.00%	1	6.30%
enzyme regulator activity (GO:0030234)	2	3.30%	--	--
structural molecule activity (GO:0005198)	8	13.30%	1	6.30%
catalytic activity (GO:0003824)	15	25.00%	7	43.80%
antioxidant activity (GO:0016209)	1	1.70%	1	6.30%
transporter activity (GO:0005215)	1	1.70%	1	6.30%

Table 3.8: Gene ontological biological process analysis of differentially expressed genes at ten days.

	Upregulated in Matrix (day 10) Tot genes: 68 Tot hits: 149		**Upregulated in Saline (day 10) Tot genes: 13 Tot hits: 28**	
Biological Process	**Number of IDs**	**% (tot hits)**	**Number of IDs**	**% (tot hits)**
cellular component organization or biogenesis (GO:0071840)	5	3.40%	1	3.60%
cellular process (GO:0009987)	28	18.80%	5	17.90%
localization (GO:0051179)	10	6.70%	2	7.10%
apoptotic process (GO:0006915)	2	1.30%	1	3.60%
biological regulation (GO:0065007)	11	7.40%	3	10.70%
response to stimulus (GO:0050896)	16	10.70%	1	3.60%
developmental process (GO:0032502)	15	10.10%	4	14.30%
multicellular organismal process (GO:0032501)	7	4.70%	1	3.60%
locomotion (GO:0040011)	2	1.30%	--	--
biological adhesion (GO:0022610)	6	4.00%	--	--
metabolic process (GO:0008152)	26	17.40%	8	28.60%
immune system process (GO:0002376)	21	14.10%	2	7.10%

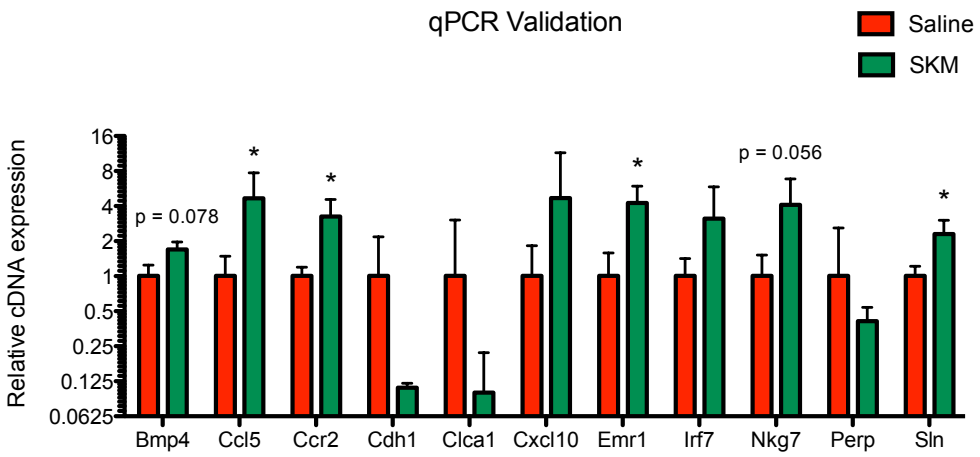

Figure 3.4: PCR validation of microarray results. Differentially expressed genes between SKM and saline were quantified with quantitative RT-PCR (n=3). *P < 0.05.

Table 3.9: qPCR primers for microarray validation.

Gene Name	**Sequence (5' -> 3')**
Bmp4 forward	TGGACACCTCATCACACGACTA
Bmp4 reverse	GCGACGGCAGTTCTTATTCTTC
Ccl5 forward	TTGTCACTCGAAGGAACCGC
Ccl5 reverse	TGAGTGGGAGTAGGGGGTTG
Ccr2 forward	CTTGTGGCCCTTATTTTCCA
Ccr2 reverse	AGATGAGCCTCACAGCCCTA
Cdh1 forward	AGGAGCTGACAAACCCCCTG
Cdh1 reverse	CCAGAGGCTGCGTCACTTTC
Clca1 forward	AATTGGGCCCAGGTGCATTA
Clca1 reverse	GGTACAAGCAACACGAGCA
Clx10 forward	GGGCCATAGGAAAACTTGAAATC
Clx10 reverse	CATTGTGGCAATGATCTCAACAT
Emr1 forward	CCTTGCCTGCTTCTTCTGGATG
Emr1 reverse	AGCATCTTGATGTTGCGAGAGC
Irf7 forward	TGGCAGATGGAAGCTACC
Irf7 reverse	GGCTATACAGGAACACGC
Nkg7 forward	GTGAGCTTCCTGGTTCTGTC
Nkg7 reverse	GAGAAGAATGTCTGGACCTG
Perp forward	CTCGCACTGGCTGCTGTATT
Perp reverse	GCCATAGGCCCAGTTGTAGA
Sln forward	GGTGTGCACTCAGAAGTCCTCC
Sln reverse	GAAGCTCAGGGCACACAGCAG

3.4 Discussion

Various neovascularization therapeutic approaches including cells, growth factors, and gene therapies have been explored, but have been met with mixed results in clinical trials for treating patients with CLI associated with PAD [33]. A biomaterial only therapeutic approach could have several advantages compared to the existing paradigm including off-the-shelf availability, reduced cost, and the ability to stimulate endogenous cell recruitment over multiple days or weeks. In this study, we demonstrate one of the first pieces of evidence of mechanism of action of an injectable ECM based hydrogel for treating PAD by unbiased dynamic transcriptomic analysis and confirmatory histology and PCR.

Previous studies have demonstrated the efficacy of the skeletal muscle matrix to improve functional blood perfusion in a chronic rat hindlimb ischemia study. The increase in perfusion and restoration of hindlimb perfusion kinetics directly correlated with end point (Day 35 post-injection) histological quantification, which showed an increased density of arterioles with diameters >75 μm throughout the whole muscle, suggesting that the biomaterial therapy acts via promoting arteriogenesis rather than angiogenesis since capillary density was not increased at any of the investigated time points. Other studies have indicated that a therapy impacting arteriogenesis rather than angiogenesis may be more desirable for CLI patients [34,35]. The SKM hydrogel treated animals also had restored muscle morphology at day 35 post-injection.

We show through a targeted ECM proteomics approach that SKM has a distinct ECM component signatures despite being predominantly composed of collagen I. This may be important for muscle regeneration, given evidence in the literature correlating differential ECM composition with human myoblast proliferation [36]. When we examined the ischemic muscle shortly after injection of the SKM hydrogel, we found an increase in Pax-7^{+} skeletal muscle progenitor cells. Pax-7 is upregulated in regenerating muscle, but usually is expressed in about

5% of nuclei in quiescent muscle [32]. This suggests that the SKM hydrogel is causing early stimulation of muscle regeneration through recruitment of satellite cells within the first week of material injection, which may have resulted in the improved measures of muscle health we observed at 35 days post-injection.

We chose to further investigate dynamic changes in the global transcriptome due to SKM hydrogel injection. Although microarray analysis has previously been employed to characterize the pre-clinical hindlimb ischemia model [37,38] and human PAD patients [39], no studies have investigated the effect of therapeutic interventions using this global unbiased analysis. At day 3, comparisons between SKM and saline controls showed that the SKM hydrogel promoted cell survival pathways, immune response, and muscle proliferation and contractility while at day 10 the upregulated pathways shifted emphasis to vascular development, neuron outgrowth, and cell motility. Genes associated with extracellular matrix were downregulated at day 3 but became upregulated at day 10. This correlates with other studies of transcriptomic effects of skeletal muscle regeneration, which show that ECM being upregulated at later time points is associated with tissue repair, cell migration, and myogenic development [40]. Interestingly, apoptosis and response to hypoxia were strongly downregulated at both time points, suggesting a pro-survival and regenerative response of the SKM material compared to the saline control across the entire muscle. These results suggest that the SKM hydrogel produces functional outcomes through altering key pathways associated with inflammatory response, cell death and survival, metabolism, and vessel and muscle development.

3.4.1 Study Limitations

Limitations of this study are due to the inherent weaknesses of hindlimb ischemia preclinical models for modeling PAD and CLI. Unfortunately, no preclinical model fully mimics

all aspects of PAD or CLI. In particular, all hindlimb ischemia models are acute models, while PAD is a chronic condition [41]. The standard models for PAD and CLI are rodent models, which due to young age and healthy collateral architecture often heal to a great extent without any therapeutic interventions [41,42]. Even large animal models and other rodent models that mimic aspects of the patient population, such as hyperhomocysteinemia, diabetes, hypercholesterolemia, and/or aging, still show collateral vessel formation [41]. To partially address these limitations, we selected a vessel ligation and excision protocol, which resulted in chronically reduced perfusion (~65%) and muscle atrophy (reduced muscle fiber cross sectional area). While our model did not have accompanying necrosis of the toes or feet, it permitted us to inject the biomaterials 7 days post-ischemic injury to allow the acute response from the surgery to resolve prior to treatment. The small scale is another limitation of these animal models. Here we delivered a single bolus into the ischemic damaged region, whereas in human patients multiple injections would be utilized.

3.4.2 Conclusions

In conclusion, we have shown the short term dynamic effects of an injectable skeletal muscle matrix material in a rat hindlimb ischemia study. Improved arteriogenesis and skeletal muscle progenitor cell recruitment at shorter time points and gene expression differences related to inflammatory response, blood vessel and muscle tissue development, apoptosis, cell survival, and metabolism give evidence of a transcriptome-wide improvement in tissue regeneration due to the SKM hydrogel.

Chapter 3, in part, is a reprint of the material as it appears in *Journal of the American College of Cardiology: Basic to Translational Science*, 2016, 1(1-2): 32-44. The authors include Jessica Ungerleider, Todd Johnson, Melissa Hernandez, Dean Elhag, Rebecca Braden, Monika

Dzieciatkowska, Kent Osborn, Kirk Hansen, Ehtisham Mahmud, and Karen Christman. The dissertation author was the primary investigator and co-first author of this paper.

3.5 References

1. Hirsch, A. T., Haskal, Z. J., Hertzer, N. R., Bakal, C. W., Creager, M. A., Halperin, J. L., Hiratzka, L. F., Murphy, W. R., Olin, J. W., Puschett, J. B., Rosenfield, K. A., Sacks, D., Stanley, J. C., Taylor Jr., L. M., White, C. J., White, J., White, R. A., Antman, E. M., Smith Jr., S. C., *et al.* ACC/AHA 2005 Practice Guidelines for the management of patients with peripheral arterial disease (lower extremity, renal, mesenteric, and abdominal aortic): a collaborative report from the American Association for Vascular Surgery/Society for Vascular Sur. *Circulation* **113,** e463-654 (2006).

2. Lawall, H., Bramlage, P. & Amann, B. Stem cell and progenitor cell therapy in peripheral artery disease. A critical appraisal. *Thromb. Haemost.* **103,** 696–709 (2010).

3. Adam, D. J., Beard, J. D., Cleveland, T., Bell, J., Bradbury, A. W., Forbes, J. F., Fowkes, F. G., Gillepsie, I., Ruckley, C. V, Raab, G., Storkey, H. & participants, B. trial. Bypass versus angioplasty in severe ischaemia of the leg (BASIL): multicentre, randomised controlled trial. *Lancet* **366,** 1925–1934 (2005).

4. Dormandy, J., Heeck, L. & Vig, S. The fate of patients with critical leg ischemia. *Semin Vasc Surg* **12,** 142–147 (1999).

5. Marston, W. A., Davies, S. W., Armstrong, B., Farber, M. A., Mendes, R. C., Fulton, J. J. & Keagy, B. A. Natural history of limbs with arterial insufficiency and chronic ulceration treated without revascularization. *J Vasc Surg* **44,** 108–114 (2006).

6. Isner, J. M. & Rosenfield, K. Redefining the treatment of peripheral artery disease. Role of percutaneous revascularization. *Circulation* **88,** 1534–1557 (1993).

7. Tang, Z. C., Liao, W. Y., Tang, A. C., Tsai, S. J. & Hsieh, P. C. The enhancement of endothelial cell therapy for angiogenesis in hindlimb ischemia using hyaluronan. *Biomaterials* **32,** 75–86 (2011).

8. de Nigris, F., Williams-Ignarro, S., Sica, V., D'Armiento, F. P., Lerman, L. O., Byrns, R. E., Sica, G., Fiorito, C., Ignarro, L. J. & Napoli, C. Therapeutic effects of concurrent autologous bone marrow cell infusion and metabolic intervention in ischemia-induced angiogenesis in the hypercholesterolemic mouse hindlimb. *Int J Cardiol* **117,** 238–243 (2007).

9. Powell, R. J., Comerota, A. J., Berceli, S. A., Guzman, R., Henry, T. D., Tzeng, E., Velazquez, O., Marston, W. A., Bartel, R. L., Longcore, A., Stern, T. & Watling, S. Interim analysis results from the RESTORE-CLI, a randomized, double-blind multicenter phase II trial comparing expanded autologous bone marrow-derived tissue repair cells and placebo in patients with critical limb ischemia. *J Vasc Surg* **54,** 1032–1041 (2011).

10. Powell, R. J., Goodney, P., Mendelsohn, F. O., Moen, E. K., Annex, B. H. & Investigators,

H. G. F. T. Safety and efficacy of patient specific intramuscular injection of HGF plasmid gene therapy on limb perfusion and wound healing in patients with ischemic lower extremity ulceration: results of the HGF-0205 trial. *J Vasc Surg* **52,** 1525–1530 (2010).

11. Shigematsu, H., Yasuda, K., Iwai, T., Sasajima, T., Ishimaru, S., Ohashi, Y., Yamaguchi, T., Ogihara, T. & Morishita, R. Randomized, double-blind, placebo-controlled clinical trial of hepatocyte growth factor plasmid for critical limb ischemia. *Gene Ther* **17,** 1152–1161 (2010).

12. Kawamura, I., Takemura, G., Tsujimoto, A., Watanabe, T., Kanamori, H., Esaki, M., Kobayashi, H., Takeyama, T., Kawaguchi, T., Goto, K., Maruyama, R., Fujiwara, T., Fujiwara, H., Tabata, Y. & Minatoguchi, S. Treatment of leg ischemia with biodegradable gelatin hydrogel microspheres incorporating granulocyte colony-stimulating factor. *J Cardiovasc. Pharmacol.* **57,** 416–423 (2011).

13. Ruvinov, E., Leor, J. & Cohen, S. The effects of controlled HGF delivery from an affinity-binding alginate biomaterial on angiogenesis and blood perfusion in a hindlimb ischemia model. *Biomaterials* **31,** 4573–4582 (2010).

14. Jay, S. M., Shepherd, B. R., Andrejecsk, J. W., Kyriakides, T. R., Pober, J. S. & Saltzman, W. M. Dual delivery of VEGF and MCP-1 to support endothelial cell transplantation for therapeutic vascularization. *Biomaterials* **31,** 3054–3062 (2010).

15. DeQuach, J. A., Lin, J. E., Cam, C., Hu, D., Salvatore, M., Sheikh, F. & Christman, K. L. Injectable skeletal muscle matrix hydrogel promotes neovascularization and muscle cell infiltration in a hindlimb ischemia model. *Eur Cell Mater* **23,** 400–412 (2013).

16. Singelyn, J. M., Sundaramurthy, P., Johnson, T. D., Schup-Magoffin, P. J., Hu, D. P., Faulk, D. M., Wang, J., Mayle, K. M., Bartels, K., Salvatore, M., Kinsey, A. M., Demaria, A. N., Dib, N. & Christman, K. L. Catheter-deliverable hydrogel derived from decellularized ventricular extracellular matrix increases endogenous cardiomyocytes and preserves cardiac function post-myocardial infarction. *J Am Coll Cardiol* **59,** 751–763 (2012).

17. Seif-Naraghi, S. B., Singelyn, J. M., Salvatore, M., Osborn, K. G., Wang, J., Sampat, U., Kwan, O. L., Strachan, G. M., Wong, J., Schup-Magoffin, P. A., Braden, R. L., Bartels, K., DeQuach, J. A., Preul, M., Kinsey, A. M., Demaria, A. N., Dib, N. & Christman, K. L. Safety and Efficacy of an Injectable Extracellular Matrix Hydrogel for Treating Myocardial Infarction. *Sci Transl Med* **5,** 173ra25 (2013).

18. Kuraitis, D., Ebadi, D., Zhang, P., Rizzuto, E., Vulesevic, B., Padavan, D. T., Al Madhoun, A., McEwan, K. A., Sofrenovic, T., Nicholson, K., Whitman, S. C., Mesana, T. G., Skerjanc, I. S., Musaro, A., Ruel, M. & Suuronen, E. J. Injected matrix stimulates myogenesis and regeneration of mouse skeletal muscle after ischaemic injury. *Eur Cell Mater* **24,** 175–176 (2012).

19. Rane, A. A. & Christman, K. L. Biomaterials for the treatment of myocardial infarction: a 5-year update. *J Am Coll Cardiol* **58,** 2615–2629 (2011).

20. Ungerleider, J. L., Johnson, T. D., Hernandez, M. J., Elhag, D. I., Braden, R. L., Dzieciatkowska, M., Osborn, K. G., Hansen, K. C., Mahmud, E. & Christman, K. L. Extracellular Matrix Hydrogel Promotes Tissue Remodeling, Arteriogenesis, and

Perfusion in a Rat Hindlimb Ischemia Model. *J Am Coll Cardiol Basic Transl Sci* **1,** 32–44 (2016).

21. DeQuach, J. A., Mezzano, V., Miglani, A., Lange, S., Keller, G. M., Sheikh, F. & Christman, K. L. Simple and high yielding method for preparing tissue specific extracellular matrix coatings for cell culture. *PLoS One* **5,** e13039 (2010).

22. Johnson, T. D., DeQuach, J. A., Gaetani, R., Ungerleider, J., Elhag, D., Nigam, V., Behfar, A. & Christman, K. L. Human versus porcine tissue sourcing for an injectable myocardial matrix hydrogel. *Biomater. Sci.* 60283D (2014). doi:10.1039/c3bm60283d

23. Barbosa, I., Garcia, S., Barbier-Chassefiere, V., Caruelle, J. P., Martelly, I. & Papy-Garcia, D. Improved and simple micro assay for sulfated glycosaminoglycans quantification in biological extracts and its use in skin and muscle tissue studies. *Glycobiology* **13,** 647–653 (2003).

24. Johnson, T. D., Hill, R. C., Dzieciatkowska, M., Nigam, V., Behfar, A., Christman, K. L. & Hansen, K. C. Quantification of decellularized human myocardial matrix: a comparison of six patients. *Clin Proteom* **in press,** (2015).

25. Hill, R. C., Calle, E. A., Dzieciatkowska, M., Niklason, L. E. & Hansen, K. C. Quantification of Extracellular Matrix Proteins from a Rat Lung Scaffold to Provide a Molecular Readout for Tissue Engineering. *Mol. Cell. Proteomics* (2015). doi:10.1074/mcp.M114.045260

26. MacLean, B., Tomazela, D. M., Shulman, N., Chambers, M., Finney, G. L., Frewen, B., Kern, R., Tabb, D. L., Liebler, D. C. & MacCoss, M. J. Skyline: an open source document editor for creating and analyzing targeted proteomics experiments. *Bioinformatics* **26,** 966–968 (2010).

27. Couffinhal, T., Silver, M., Kearney, M., Sullivan, A., Witzenbichler, B., Magner, M., Annex, B., Peters, K. & Isner, J. M. Impaired Collateral Vessel Development Associated With Reduced Expression of Vascular Endothelial Growth Factor in ApoE-/- Mice. *Circulation* **99,** 3188–3198 (1999).

28. Borselli, C., Storrie, H., Benesch-Lee, F., Shvartsman, D., Cezar, C., Lichtman, J. W., Vandenburgh, H. H. & Mooney, D. J. Functional muscle regeneration with combined delivery of angiogenesis and myogenesis factors. *Proc. Natl. Acad. Sci.* **107,** 3287–3292 (2010).

29. Cho, S.-W., Moon, S.-H., Lee, S.-H., Kang, S.-W., Kim, J., Lim, J. M., Kim, H.-S., Kim, B.-S. & Chung, H.-M. Improvement of Postnatal Neovascularization by Human Embryonic Stem Cell–Derived Endothelial-Like Cell Transplantation in a Mouse Model of Hindlimb Ischemia. *Circulation* **116,** 2409 (2007).

30. Zhang, Z., Slobodianski, A., Ito, W. D., Arnold, A., Nehlsen, J., Weng, S., Lund, N., Liu, J., Egana, J., Lohmeyer, J. A., Muller, D. F. & Machens, H. Enhanced collateral growth by double transplantation of gene-nucleofected fibroblasts in ischemic hindlimb of rats. *PLoS One* **6,** e19192 (2011).

31. Kramer, A., Green, J., Pollard, J. & Tugendreich, S. Causal analysis approaches in Ingenuity Pathway Analysis. *Bioinformatics* **30,** 523–530 (2014).

32. Seale, P., Sabourin, L. A., Girgis-Gabardo, A., Mansouri, A., Gruss, P. & Rudnicki, M. A. Pax7 Is Required for the Specification of Myogenic Satellite Cells. *Cell* **102,** 777–786 (2000).

33. Ouma, G. O., Jonas, R. A., Usman, M. H. & Mohler 3rd, E. R. Targets and delivery methods for therapeutic angiogenesis in peripheral artery disease. *Vasc Med* **17,** 174–192 (2012).

34. Buschmann, I. & Schaper, W. Arteriogenesis Versus Angiogenesis: Two Mechanisms of Vessel Growth. *Physiology* **14,** 121–125 (1999).

35. Scholz, D., Ziegelhoeffer, T., Helisch, A., Wagner, S., Friedrich, C., Podzuweit, T. & Schaper, W. Contribution of Arteriogenesis and Angiogenesis to Postocclusive Hindlimb Perfusion in Mice. *J. Mol. Cell. Cardiol.* **34,** 775–787 (2002).

36. Ferreira, M. M., Dewi, R. E. & Heilshorn, S. C. Microfluidic analysis of extracellular matrix-bFGF crosstalk on primary human myoblast chemoproliferation, chemokinesis, and chemotaxis. *Integr Biol* **7,** 569–579 (2015).

37. Paoni, N. F., Peale, F., Wang, F., Errett-Baroncini, C., Steinmetz, H., Toy, K., Bai, W., Williams, P. M., Bunting, S., Gerritsen, M. E. & Powell-Braxton, L. Time course of skeletal muscle repair and gene expression following acute hind limb ischemia in mice. *Physiol Genomics* **11,** 263–272 (2002).

38. Lee, C. W., Stabile, E., Kinnaird, T., Shou, M., Devaney, J. M., Epstein, S. E. & Burnett, M. S. Temporal patterns of gene expression after acute hindlimb ischemia in mice: insights into the genomic program for collateral vessel development. *J Am Coll Cardiol* **43,** 474–482 (2004).

39. Tuomisto, T. T., Rissanen, T. T., Vajanto, I., Korkeela, A., Rutanen, J. & Yla-Herttuala, S. HIF-VEGF-VEGFR-2, TNF-alpha and IGF pathways are upregulated in critical human skeletal muscle ischemia as studied with DNA array. *Atherosclerosis* **174,** 111–120 (2004).

40. Goetsch, S. C., Hawke, T. J., Gallardo, T. D., Richardson, J. A. & Garry, D. J. Transcriptional profiling and regulation of the extracellular matrix during muscle regeneration. *Physiol Genomics* **14,** 261–271 (2003).

41. Waters, R. E., Terjung, R. L., Peters, K. & Annex, B. Preclinical models of human peripheral arterial occlusive disease: implications for investigation of therapeutic agents. *J Appl Physiol* **97,** 773–780 (2004).

42. Landazuri, N., Joseph, G., Guldberg, R. E. & Taylor, W. R. Growth and regression of vasculature in healthy and diabetic mice after hindlimb ischemia. *Am J Physiol Regul Integr Comp Physiol* **202,** R48–R56 (2012).

Chapter 4

Tissue specific muscle extracellular matrix hydrogel improves skeletal muscle regeneration *in vivo* over non-matched tissue sources

4.1 Introduction

Acute and chronic muscle injuries are common ailments, often caused by physical trauma or as a co-morbidity of lifestyle diseases. Skeletal muscle repair is a complex regenerative process, requiring exquisite spatiotemporal coordination of many cellular subtypes in a complex inflammatory milieu. Dysregulation of this process prevents functional repair of muscle due to improper myofibril function and organization. Activation of quiescent stem cell populations, rapid proliferation of myocytes, and differentiation into multi-cellular myotubes is required for this repair to occur. However improper myogenesis and inflammation is associated with aging and various disease states[1]. A critical need exists for therapeutic interventions to guide this process.

Decellularized extracellular matrix (ECM) hydrogels show great promise in a variety of regenerative medicine applications [2,3]. Their retention of the complex distribution of native ECM proteins and proteoglycans is able to effectively guide cell fate decisions. Additionally, solubilized ECM hydrogels, while they do not retain the tissue's native 3D ultrastructure, reassemble into a hydrogel at physiological temperature, pH, and salt concentration and form a nanofibrous matrix with similar architecture to native tissue. Due to their ability to form a hydrogel supportive matrix *in situ,* injectable ECM hydrogels are translationally attractive for applications where minimally invasive delivery is desirable (injections over a wide area or difficult to access location). ECM hydrogels have shown efficacy in preclinical models of

myocardial infarction[2] and peripheral artery disease[3], and *in vitro* 3D microenvironmental drug screening models[4].

The classic approach is to use an ECM hydrogel where the source tissue that is decellularized is typically the same tissue to which the treatment is applied. While studies have investigated the merit of using tissue specific ECM sources *in vitro* [5–11], the importance of tissue specificity has not been definitively assessed *in vivo.* Some groups have compared different ECM materials for esophageal[12] or skeletal muscle repair[3], but the control "non-matched" ECM sources were not properly controlled for form (intact patch versus solubilized hydrogel) or ECM age and decellularization method (thus complication the question of young versus old ECM and effect of decellularization method on biological outcomes *in vivo*). We hypothesized, in a muscle regeneration model, that a tissue specific ECM hydrogel improves regeneration and function through preferentially stimulating physiologically relevant processes (e.g. progenitor cell proliferation and differentiation). In this study we show that skeletal muscle ECM hydrogels benefit skeletal muscle regeneration over non-matched tissue sources (lung) via stimulation of skeletal muscle progenitor recruitment and increased muscle growth.

4.2 Methods

4.2.1 ECM fabrication and characterization

ECM hydrogels were fabricated and characterized using previously published methods [3,13]. Briefly, skeletal muscle or lung tissue from 3 month old pigs was harvested and chopped into small pieces. Tissue was rinsed in ultrapure water for 30 minutes followed by ~4 days of rinsing in 1% (skeletal muscle) or 0.1% (lung) sodium dodecyl sulfate with periodic solution changes. Skeletal muscle material was finally rinsed in isopropanol for 18 hours to remove interstitial fat. Decellularization was confirmed with H&E staining (not shown). Final material was lyophilized, milled into a fine powder, and digested for 48 hours in 1 mg/ml pepsin in 0.1M HCl.

Digests were neutralized and lyophilized at 6 mg/ml. QconCAT proteomics were performed on the milled material pre-digestion as previously described [14]. Rheometry was performed using an AR-G2 rheometer on 500 µL gels at 37 ºC with a 1000 µm gap height and 2.5% strain for shear moduli and on 200 µL liquid ECM with a 500 µm gap height at 25 ºC for complex viscosity measurements.

4.2.2 NTX injury

Male 8 week old C57BL/6 animals were injured using a notexin acute muscle injury model. Notexin (10µg/mL, Latoxan) was injected in a single injection of 20 µL into the mid-belly of the right tibialis anterior (TA) muscle. Left TAs served as noninjected and uninjured controls. After 2 days, animals were injected with a single 20 µL injection of either saline, skeletal muscle ECM, or lung ECM (n=7 per group at each time point). Animals were then harvested either 3, 7, or 12 days post-treatment. TA muscles were laid on filter paper to orient fibers and flash frozen in liquid nitrogen. Muscles were then frozen again in OCT for cryosectioning along the short axis. During cryosectioning, tissue was either mounted on slides (10µm thick sections) or collected for RNA isolation at 3 locations spanning the muscle.

4.2.3 Immunohistochemistry

Cryosections were fixed with 4% paraformaldehyde and blocked with 1% bovine serum albumin, 0.3% Triton-X, and 5% goat serum. Primary antibodies against laminin (1:100, abcam), embryonic myosin heavy chain (1:10, DSHB), alpha smooth muscle actin (1:50, abcam), CD31 (1:75, BD Pharmagen), Pax7 (1:2, DSHB), myogenin (1:100, abcam), and Ki67 (1:1000, abcam) were incubated overnight at 4ºC. Secondary antibodies (AlexaFluor goat IgG against rabbit [laminin, α-SMA, Ki67, myogenin], mouse [eMHC, Pax7], or rat [CD31]).

4.2.4 RNA sequencing

RNA was isolated using Trizol and cleaned using Qiagen DNase clean-up per the manufacturer's instructions. The Institute for Genomic Medicine at UCSD conducted all quality checks, library prep, and sequencing of the RNA samples. Briefly, RINe was measured using an Agilent Bioanalyzer, libraries were prepared using Illumina's mRNA stranded library prep kit, and libraries were sequenced to a depth of approximately 25 million reads on a HiSeq flow lane. Quality of sequencing was verified with FastQC. Fastq files were aligned to the Ensembl mouse genome (Grcm38 version 84) using HiSat 2 [15] and counted using StringTie [16,17]. Counts were statistically analyzed using the DESeq2 package [18]. Differentially expressed genes were defined as genes with adjusted Benjamini-Hochberg p-value less than 0.1 and absolute value of log fold change greater than 0.6. Differentially expressed genes were assigned to biological pathways using DAVID functional annotation clustering [19,20].

4.3 Results

4.3.1 Tissue-of-origin alters composition of tissue-specific injectable hydrogels

To understand how tissue-of-origin alters muscle repair, we developed injectable hydrogels from two orthogonal sources – skeletal muscle and lung. Lung was chosen as a non-matched tissue control as it is distinct from skeletal muscle in both developmental origin and tissue function. Both injectable hydrogels were decellularized using detergent methods and were controlled for donor characteristics (i.e. species, age).

Common characterization assays – DNA content, sulfated glycosaminoglycan content, and rheology – show that all three ECM hydrogels are sufficiently decellularized and have similar viscoelastic properties (Figure 4.1). In collaboration with the Hansen lab at CU Denver, 53 of the most common ECM and cellular contaminant proteins were quantified using stable isotope labeled quantitative concatenated (QconCAT) peptides and LC-MS analysis (Table 4.1)

to compare the relative abundance of proteins in the ECM scaffolds. While both ECM scaffolds contained mostly collagen I (65-80% by molar fraction), each scaffold had a complex and unique composition of ECM proteins. Importantly, collagen VI composition is different between the materials, which has been shown to have an effect on skeletal muscle progenitor cell renewal *in vivo* [21]. This demonstrates strong evidence that the large variety in ECM composition between each material will impact tissue specific cellular responses *in vivo.*

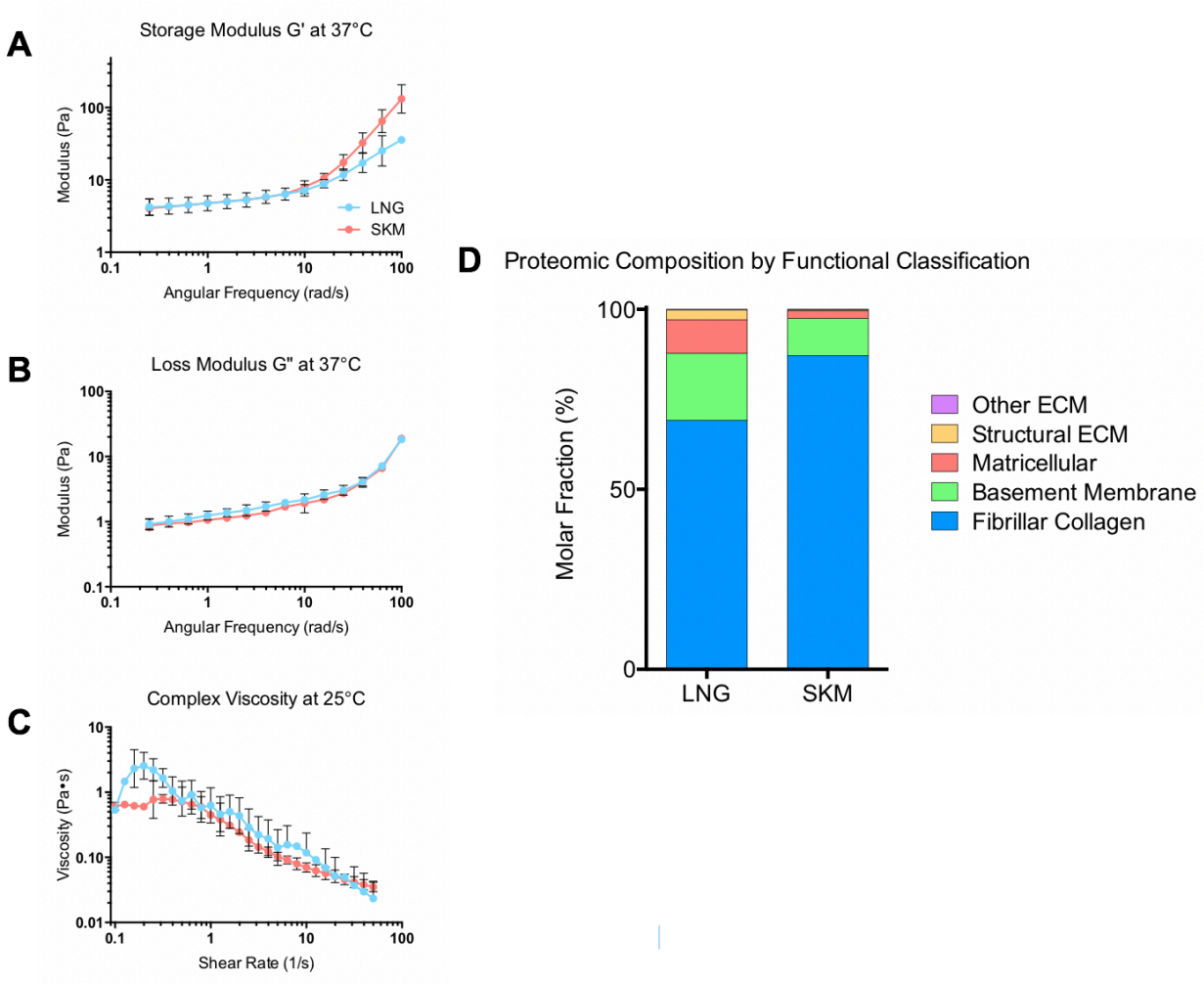

Figure 4.1. ECM hydrogel characterization. (A,B) Storage and loss modulus of lung (LNG) and skeletal muscle (SKM) ECM hydrogels. (C) Complex viscosity indicates materials are shear thinning. (D) Quantitative mass spectrometry of proteomic composition of ECM hydrogels by molar fraction and functional classification.

Table 4.1: Quantitative proteomics of decellularized ECM from different tissues of origin.

Protein Abundance in Matrix (Molar Fraction)				
Protein	***GENE***	***Functional Classification***	***Lung Average***	***Skeletal Muscle Average***
Collagen alpha-1(IV) chain(Arresten/Core Protein)	COL4A1*	Basement Membrane	2.41%	4.66%
Collagen alpha-1/5(IV) chain(Arresten/Core Protein)	COL4A1/5*	Basement Membrane	10.03%	3.57%
Collagen alpha-2(IV) chain(Canstatin/Core Protein)	COL4A2*	Basement Membrane	1.60%	1.92%
Laminin alpha-2	LAMA2	Basement Membrane	0.00%	0.01%
Laminin alpha-4	LAMA4	Basement Membrane	0.00%	0.00%
Laminin Beta-1	LAMB1	Basement Membrane	0.04%	0.00%
Laminin Beta-2	LAMB2	Basement Membrane	0.13%	0.01%
Laminin Gamma-1	LAMC1	Basement Membrane	2.88%	0.05%
Nidogen-1	NID1	Basement Membrane	0.87%	0.00%
Agrin	AGRN	Basement Membrane	0.00%	0.00%
Collagen alpha-5(IV) chain	COL4A5	Basement Membrane	0.37%	0.00%
Perlecan	HSPG2	Basement Membrane	0.32%	0.26%
Actin (All Isoforms)	ACT	Cytoskeletal	0.08%	0.07%
Actin, cytoplasmic 1/2	ACTB	Cytoskeletal	0.10%	0.01%
Spectrin alpha chain, non-erythrocytic 1	SPTA2	Cytoskeletal	0.00%	0.00%
Vimentin	VIM	Cytoskeletal	0.00%	0.00%
Myosin(Myosin-3,4,6,7)	MYH*	Cytoskeletal	0.00%	0.11%
Tubulin beta-4B chain(4b & 5 chain)	TUBB*	Cytoskeletal	0.03%	0.00%
Lysyl oxidase-like 1	LOXL1	ECM regulator	0.09%	0.00%
Transglutaminase 2	TGM2	ECM regulator	0.00%	0.00%
Collagen alpha-1(XII) chain	COL12A1	FACIT Collagen	0.00%	0.02%
Collagen alpha-1(XIV) chain	COL14A1	FACIT Collagen	0.01%	0.03%
Collagen alpha-1(I) chain	COL1A1	Fibrillar Collagen	43.21%	50.52%
Collagen alpha-1(V) chain	COL5A1	Fibrillar Collagen	1.73%	0.86%
Collagen alpha-2(I) chain	COL1A2	Fibrillar Collagen	23.66%	35.37%
Collagen alpha-2(V) chain	COL5A2	Fibrillar Collagen	0.52%	0.27%

Table 4.1 continued: Quantitative proteomics of decellularized ECM from different tissues of origin.

Protein Abundance in Matrix (Molar Fraction)				
Protein	***GENE***	***Functional Classification***	***Lung Average***	***Skeletal Muscle Average***
Collagen alpha-1(VI) chain	COL6A1	Matricellular	2.82%	0.30%
Collagen alpha-1(XVIII) chain	COL18A1	Matricellular	0.01%	0.00%
Collagen alpha-2(VI) chain	COL6A2	Matricellular	3.00%	0.21%
Collagen alpha-3(VI) chain	COL6A3	Matricellular	2.28%	0.42%
Dermatopontin	DPT	Matricellular	0.52%	0.27%
Emilin 1	EMILIN1	Matricellular	0.11%	0.00%
Fibronectin 1	FN1	Matricellular	0.20%	0.49%
Fibulin 1	FBLN1	Matricellular	0.00%	0.00%
Fibulin 3	EFEMP1	Matricellular	0.09%	0.02%
Fibulin 5	FBLN5	Matricellular	0.08%	0.01%
Lumican	LUM	Matricellular	0.09%	0.33%
Periostin	POSTN	Matricellular	0.05%	0.01%
Thrombospondin 1	THBS1	Matricellular	0.08%	0.00%
TnxB Protein	TNXB	Matricellular	0.00%	0.00%
Versican	VCAN	Matricellular	0.00%	0.00%
Histone 2A(H2A-A-K)	H2A*	Other Cellular	0.08%	0.00%
Histone H1(H1.1,H1.2,H1.3,H1.4)	H1*	Other Cellular	0.36%	0.00%
Glyceraldehyde-3-phosphate dehydrogenase	GAPDH	Other Cellular	0.00%	0.03%
Matrix Gla Protein	MGP	Other ECM	0.04%	0.00%
Extracellular Matrix Protein 1	ECM1	Other ECM	0.00%	0.00%
Mimecan/Osteoglycin	OGN	Other ECM	0.00%	0.00%
Galectin-1	LGALS1	Other ECM	0.01%	0.00%
Transforming growth factor-beta-induced protein ig-h3	TGFBI	Secreted	0.06%	0.02%
Decorin	DCN	Structural ECM	0.00%	0.00%
Fibrillin 1	FBN1	Structural ECM	0.48%	0.27%
Fibrillin 2	FBN2	Structural ECM	0.06%	0.02%
Fibromodulin	FMOD	Structural ECM	0.00%	0.01%
Latent transforming growth factor beta binding protein 1	LTBP1	Structural ECM	0.00%	0.00%
Matrilin 1, Cartilage Matrix Protein	MATN1	Structural ECM	0.03%	0.00%
Aggrecan	ACAN	Structural ECM	0.19%	0.00%
Microfibrillar-associated protein 2	MFAP2	Structural ECM	1.95%	0.05%

4.3.2 Muscle-derived injectable hydrogel increases muscle repair after NTX injury

To investigate the difference in regenerative capacity of the two hydrogels *in vivo,* one of two decellularized hydrogels: tissue specific skeletal muscle, non-mesoderm-derived lung, or saline were injected intramuscularly two days after notexin injection in male adult C57BL/6 mice (n=7 per time point) and muscle was harvested at days 3, 7, and 12 post-treatment for histological and gene expression analysis.

At day 12, indeed skeletal muscle was observed to increase fiber cross sectional area (average fiber areas – saline: 564 ± 64 μm^2; lung ECM: 545 ± 65 μm^2; skeletal muscle ECM: 695 ± 94 μm^2) (Figure 4.2). This increase is evident through a significant decrease in fibers of smaller areas and a shift in distribution towards larger areas. This result suggested that skeletal muscle ECM hydrogels are able to improve muscle regeneration over saline and lung ECM hydrogels.

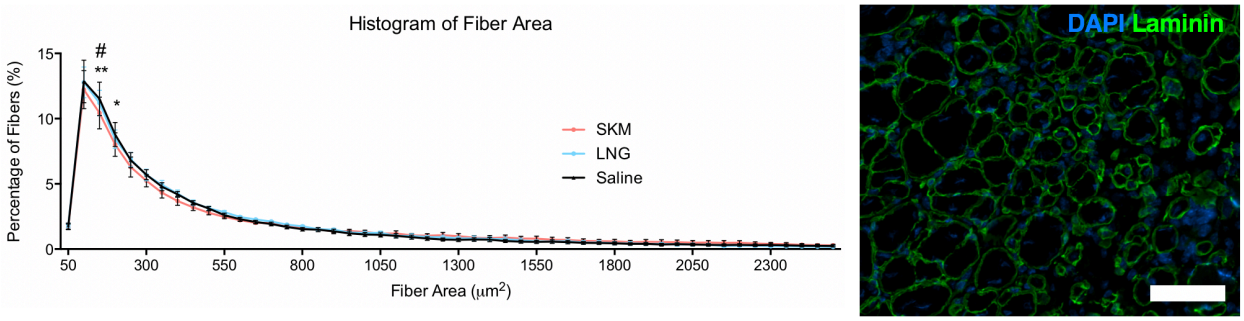

Figure 4.2. Muscle hydrogel improves muscle fiber cross-sectional area over non-matched tissue source. Histogram of fiber areas indicates SKM has fewer small fibers than saline and LNG. Right – representative image of fiber area quantified by laminin staining. *p<0.05 SKM versus saline, **p<0.01 SKM versus saline, #p<0.05 SKM versus LNG by two-way ANOVA with Fisher's post-hoc test. Scale bar is 70 μm.

To better understand what processes could drive increases in muscle regeneration, we histologically-analyzed muscle repair processes during the regeneration process. At day 3, the skeletal muscle ECM hydrogel significantly increased the density of Pax7+ satellite cells and differentiating myogenin+ cells in the muscle (Figure 4.3). This effect has also been previously

shown in response to the skeletal muscle matrix [3,22], but interestingly this effect was not seen with the non-matched lung ECM source. This is thus strong evidence that SKM is important for skeletal muscle progenitor activity *in vivo*.

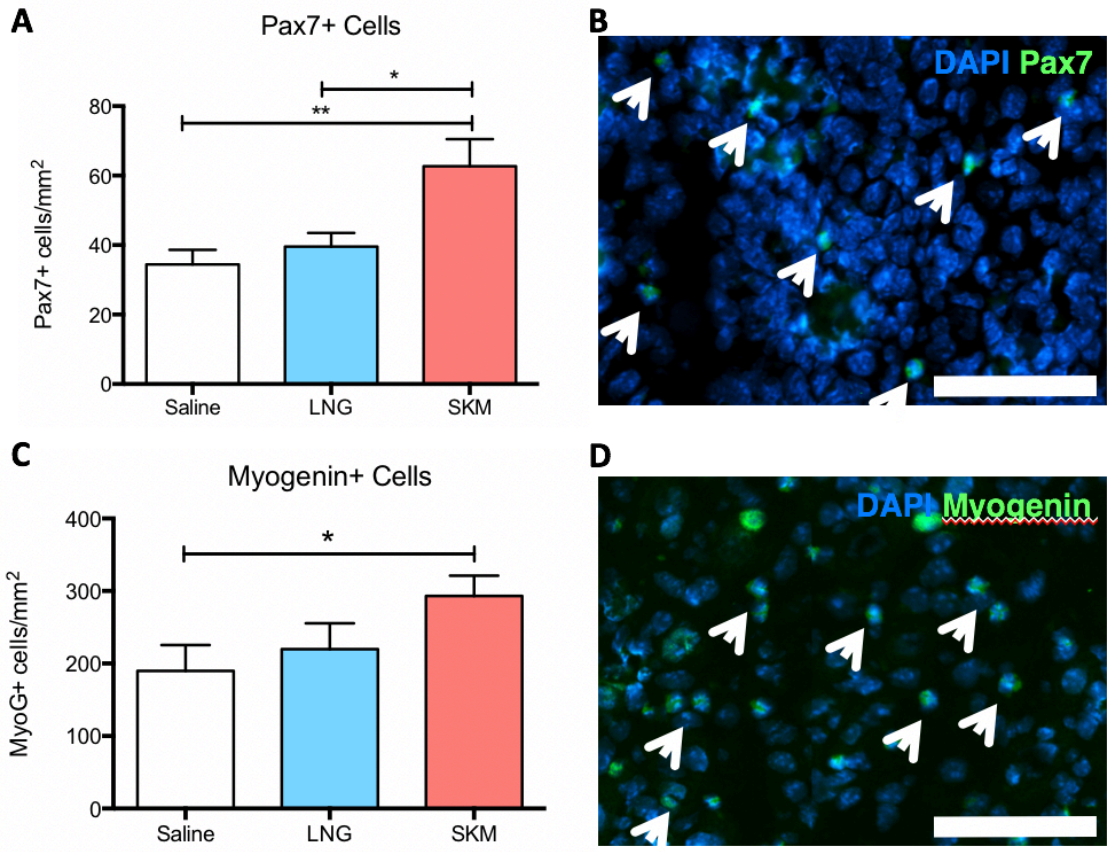

Figure 4.3. Skeletal muscle ECM hydrogel increases density of skeletal muscle progenitors. Quantification of quiescent (Pax7+, A) and activated (Myogenin+, C) skeletal muscle progenitors. Arrows indicate Pax7+ (B) or Myogenin+ (D) nuclei. *p<0.05, **p<0.01 using one-way ANOVA with Tukey's (Pax7) or Fisher's (Myogenin) post-hoc test. Scale bar is 70 μm.

4.3.3 Gene expression indicates muscle hydrogel improves muscle contractility pathways

Differences in transcriptomic regulation due to material injection were investigated using RNAseq. Whole muscle RNA was isolated at 3 and 7 days post-injection, sequenced, and normalized to saline control injection. Differentially expressed (DE) genes relative to saline were biologically interpreted using DAVID functional annotation clustering analysis. Differentially regulated genes and pathways between SKM-saline and LNG-saline were then compared to

assess how the different biomaterials were altering the transcriptomic response *in vivo.* At day 3 post-injection, both materials clustered differently from saline using principal component analysis (PCA) (Figure 4.4). While there were 222 DE genes for SKM-saline and 552 DE genes for LNG-saline at day 3, this dropped down to 4 and 8 DE genes at day 7, respectively. Groups also did not cluster separately on PCA at day 7, suggesting most of the transcriptomic effects of ECM injection occur during the first week post-injection. It has also been shown in previous transcriptomic studies that major differences due to ECM injection occur at shorter time points post-injection [3].

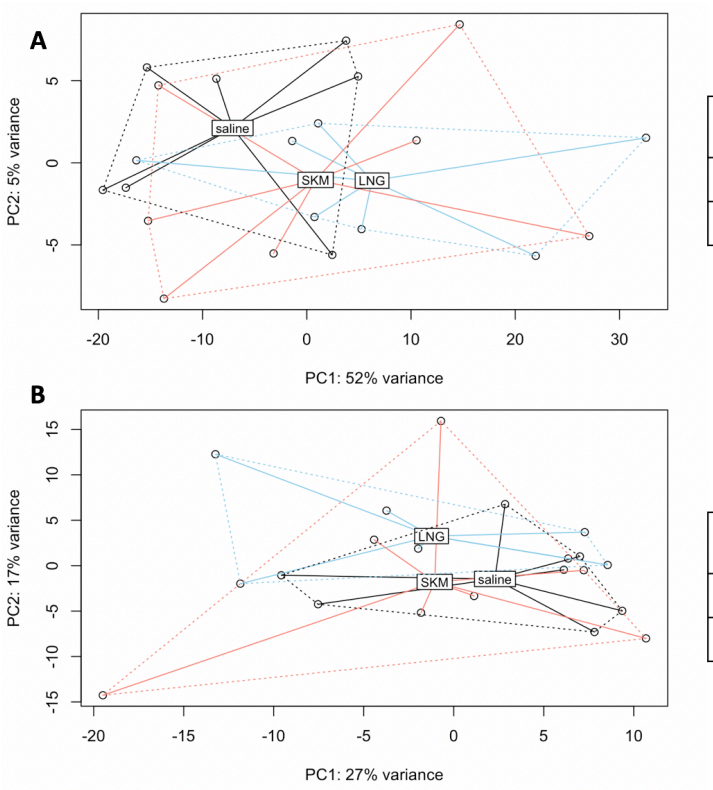

FDR < 0.1, Fold Change > 1.5	SKM v. saline	LNG v. saline
Up	182	429
Down	40	123

FDR < 0.1, Fold Change > 1.5	SKM v. saline	LNG v. saline
Up	2	5
Down	2	3

Figure 4.4. Differential expression analysis of notexin-injured and ECM-treated muscles. Gene expression analysis was conducted using DESeq2 negative binomial generalized linear models.

DAVID functional annotation clustering at day 3 post-injection shows that most DE pathways are related to metabolism, immune response, and skeletal muscle function (Table 4.2). Closer investigation of the overlapping and distinct DE genes was performed using Venn diagrams (Figure 4.5). Interestingly, the skeletal muscle matrix showed, distinct from LNG, upregulation of genes related to skeletal muscle contraction (*Tnnt3, Tcap, Jsrp1, Mylk2*). This suggests a tissue specific effect of the muscle hydrogel on muscle contractility pathways, which is strong evidence that tissue specific ECM source is an important consideration in regenerative applications. Also interesting, LNG showed most distinct expression of genes related to metabolism and immune response, specifically upregulation of oxidative phosphorylation genes (ATP synthases *Atp5f1* and *Atp5j*, NADH dehydrogenases, and cytochrome c oxidases) and downregulation of inflammatory response genes (*Cd163, Adam8, S1pr3, Csf1, Il4ra*) relative to saline. Interestingly, some of these genes are implicated in the pro-regenerative response, suggesting the response to LNG hydrogels may be more shifted to pro-inflammatory response at this time point [23–26]. Overlapping pathways between the two materials include upregulation of c-type lectin (*Klr* family) and immune response (*Ccl5, Cd27*). Both gene sets are suggestive of a natural killer cell and innate inflammatory response, which is expected at this early time point after injection of naturally derived biomaterials before the shift towards a pro-remodeling phenotype [27,28]. Interestingly, some signal/secreted transcripts were downregulated in both ECM groups (*Mmp9, Igtb3, Cxcl10, Osm*) which suggests regulation of ECM deposition and inflammatory response. However, as these genes are involved with many pathways, it is important to further validate their role in the tissue response to ECM hydrogels, especially since harnessing the inflammatory response is vital for successful skeletal muscle regeneration [26,29,30].

Table 4.2: DAVID functional annotation analysis of differentially expressed genes at day 3 post-injection. Top six up- and down-regulated pathways were reported by enrichment score.

SKM		LNG	
Up-regulated vs. saline			
Annotation Cluster	**Enrichment Score**	**Annotation Cluster**	**Enrichment Score**
C-type lectin, cell adhesion	3.76	C-type lectin, cell adhesion	5.90
Skeletal muscle contraction	3.35	Mitochondrion	5.81
Transmembrane	2.49	Oxidative phosphorylation	4.80
Disulfide bond/glycoprotein	1.52	Disulfide bond/signal/secreted	3.51
Ion channel activity	1.37	T cell receptor complex	3.00
Glycogen/carbohydrate metabolism	1.20	Transmembrane	1.80
Down-regulated vs. saline			
Disulfide bond/signal peptide	3.03	Cadherin/cell adhesion	6.85
Cholesterol metabolic process	1.88	Signal/secreted/glycoprotein	3.67
Oxidation-reduction	1.54	Lipid metabolic process	2.35
Cytokine activity	1.35	Cytokine activity	1.68
Transmembrane	1.28	Oxidation-reduction	1.65
Protease binding	1.20	Cell division	1.54

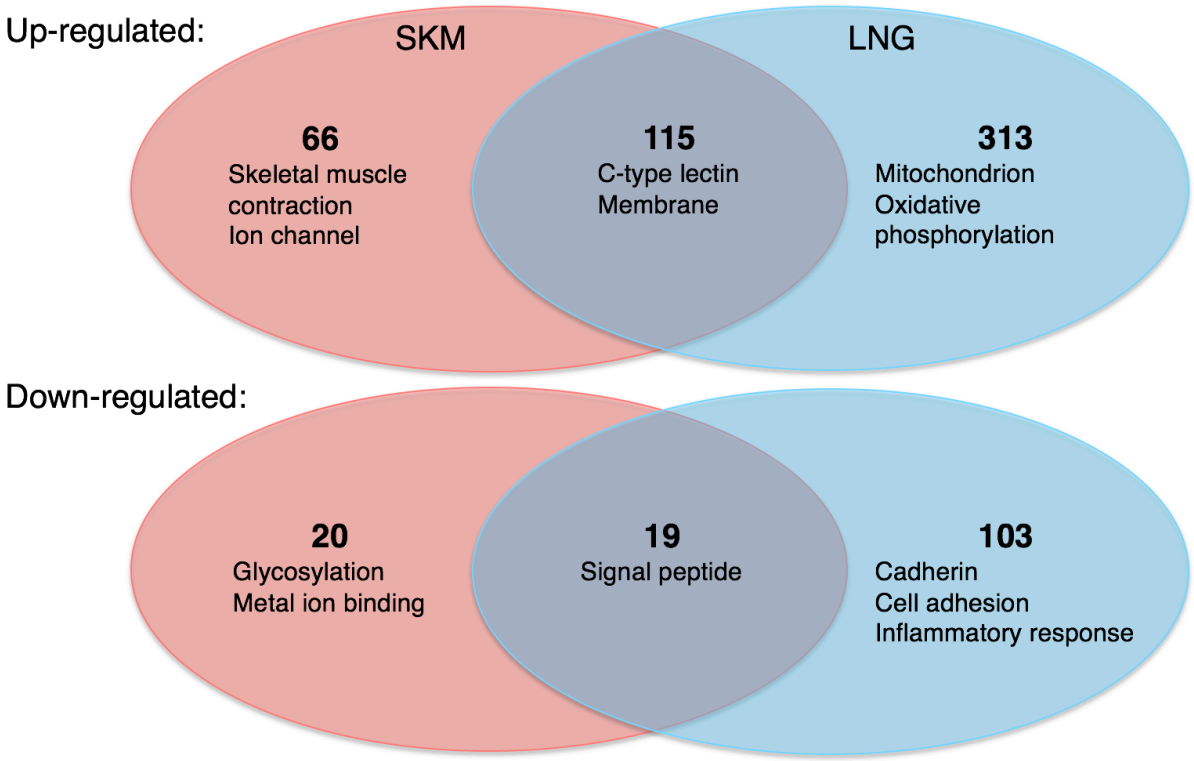

Figure 4.5: Overlapping and distinct differentially expressed genes between LNG and SKM. Number of DE genes intersecting between SKM-saline and LNG-saline contrasts are shown as well as the top pathways. Pathways are gene ontology or Kegg pathways with the lowest p values as determined by DAVID at day 3 post-injection.

Overall, RNAseq analysis suggests that both ECM hydrogels induce non-specific effects such as differential regulation of metabolism and inflammatory response. However, there are some subtle differences in inflammatory cell response (i.e., downregulation of pro-regenerative genes in LNG) which may indicate a tissue-specific response in not only muscle regeneration and contractility response but also inflammation, which is known to have a lot of cross-talk with muscle regeneration pathways *in vivo.* Future studies should focus on elucidating these complex responses to ECM biomaterials. However, distinct upregulation of muscle contractility genes, along with supporting histological evidence of skeletal muscle progenitor cell recruitment, activation, and shift in increased fiber area all indicate that tissue specific ECM hydrogels are critical for inducing tissue specific regenerative responses *in vivo.*

4.4 Discussion

In this study, we sought to investigate the effect of tissue-specific decellularized ECM hydrogels on skeletal muscle regeneration. We first characterized the ECM hydrogels derived from adult porcine tissue sources, either tissue-specific skeletal muscle or functionally and developmentally non-specific lung. Both ECM hydrogels had similar mechanical properties, but biochemically they had distinct proteomic compositions. We next sought to determine the importance of tissue-specificity of decellularized hydrogels for *in vivo* regeneration in an acute muscle injury model. Muscle fiber cross-sectional area, an important metric of functional regeneration, was increased in the SKM treated animals at day 12 post-treatment. We also quantified satellite cells and differentiating progenitors at day 3 post-injection and found that the SKM hydrogel increased density of both cell types in the muscle over LNG and saline injected muscles. Finally, whole muscle transcriptomics revealed that most differences due to ECM injection (normalized to saline-injected control muscles) were seen at day 3 post-injection with upregulation of skeletal muscle contraction genes in the SKM group and not in the LNG group.

The importance of tissue-specific ECM hydrogels on regenerative cell types and pathways has previously been rigorously studied *in vitro* [4,5,7], but with limited confirmatory evidence *in vivo* [3,12]. This study for the first time demonstrated the importance of tissue specificity *in vivo* while rigorously controlling for decellularization species, age, method, and mechanical properties of the resultant material. This is an important finding, because many non-specific materials are routinely used for regenerative medicine such as sub-intestinal submucosa (SIS) and urinary bladder matrix (UBM). These materials have shown efficacy *in vivo,* but our study suggests that tissue-specific materials may be more beneficial for regenerative medicine applications. Benefits seen with SIS and UBM *in vivo* could be explained by the non-specific pathways we consistently see being differentially regulated by ECM materials (i.e. inflammation and metabolism). The impact of these non-specific pathways should

be further elucidated with detailed mechanistic studies. Depending on the application, the polarization of these non-specific pathways may be sufficient alone (e.g., in wound healing [31,32]).

In this study both ECM hydrogels had similar mechanical properties so *in vivo* response were likely due to biochemical effects induced by differences in hydrogel proteomic composition. ECM has been shown to be an important regulator of skeletal muscle satellite cell response *in vivo* [33]. For example, collagen VI is a basement membrane protein known to be important for the muscle satellite cell self-renewal [21]. However, this effect was also reported to be mediated by collagen VI-dependent changes in mechanical properties, which are not different in our ECM hydrogels. Thus, it is difficult to deconvolute the contributions due to mechanical versus biochemical differences. Glycosaminoglycan and proteoglycan composition is also known to be important for the satellite cell niche due to their ability to bind and sequester growth factors [34–36]. Thus, differences in proteoglycan composition between the two materials could also have an effect on regeneration *in vivo.* Previous studies have shown that the SKM hydrogel may act directly on skeletal myoblasts by increasing proliferation and differentiation [3,37], so a complex distribution of proteins and proteoglycans may be more important than the presence or absence of a single component. Studies have shown that decellularized ECM hydrogels are more regenerative than a single ECM component such as collagen [7,22], which supports this finding *in vivo*.

4.5 Conclusions

In this study, we demonstrated that a skeletal muscle ECM hydrogel induced beneficial effects on muscle regeneration and hypertrophy after acute injury *in vivo.* This data indicates a potential role for muscle-specific regenerative capacity of decellularized, injectable muscle hydrogels. Because viscoelastic properties of the hydrogels were similar, it is likely that biochemical differences between the materials guide the differences in endogenous cellular behavior and increase muscle regeneration *in vivo.* Future studies should correlate differences

in muscle morphology with functional outcomes (e.g., muscle tetanic force generation), which was difficult to obtain in this study due to the gross anatomy of the TA muscle. Also, studies could be performed on more clinically relevant muscle regeneration models. This will lead to a greater understanding of the need for tissue specificity in regenerative medicine applications and further elucidate potential ECM-mediated tissue repair mechanisms *in vivo*.

Chapter 4, in full is currently being prepared for submission for publication of the material. The authors are Jessica Ungerleider and Karen Christman. The dissertation author was the primary investigator and author of this material.

4.6 References

1. Kuswanto, W., Burzyn, D., Panduro, M., Wang, K. K., Jang, Y. C., Wagers, A. J., Benoist, C. & Mathis, D. Poor Repair of Skeletal Muscle in Aging Mice Reflects a Defect in Local, Interleukin-33-Dependent Accumulation of Regulatory T Cells. *Immunity* **44,** 355–367 (2016).

2. Seif-Naraghi, S. B., Singelyn, J. M., Salvatore, M., Osborn, K. G., Wang, J., Sampat, U., Kwan, O. L., Strachan, G. M., Wong, J., Schup-Magoffin, P. A., Braden, R. L., Bartels, K., DeQuach, J. A., Preul, M., Kinsey, A. M., Demaria, A. N., Dib, N. & Christman, K. L. Safety and Efficacy of an Injectable Extracellular Matrix Hydrogel for Treating Myocardial Infarction. *Sci Transl Med* **5,** 173ra25 (2013).

3. Ungerleider, J. L., Johnson, T. D., Hernandez, M. J., Elhag, D. I., Braden, R. L., Dzieciatkowska, M., Osborn, K. G., Hansen, K. C., Mahmud, E. & Christman, K. L. Extracellular Matrix Hydrogel Promotes Tissue Remodeling, Arteriogenesis, and Perfusion in a Rat Hindlimb Ischemia Model. *J Am Coll Cardiol Basic Transl Sci* **1,** 32–44 (2016).

4. Skardal, A., Smith, L., Bharadwaj, S., Atala, A., Soker, S. & Zhang, Y. Tissue specific synthetic ECM hydrogels for 3-D in vitro maintenance of hepatocyte function. *Biomaterials* **33,** 4565–4575 (2012).

5. Zhang, Y., He, Y., Bharadwaj, S., Hammam, N., Carnagey, K., Myers, R., Atala, A. & Van Dyke, M. Tissue-specific extracellular matrix coatings for the promotion of cell proliferation and maintenance of cell phenotype. *Biomaterials* **30,** 4021–4028 (2009).

6. Medberry, C. J., Crapo, P. M., Siu, B. F., Carruthers, C. A., Wolf, M. T., Nagarkar, S. P., Agrawal, V., Jones, K. E., Kelly, J., Johnson, S. A., Velankar, S. S., Watkins, S. C., Modo, M. & Badylak, S. F. Hydrogels derived from central nervous system extracellular matrix. *Biomaterials* **34,** 1033–1040 (2013).

7. French, K. M., Boopathy, A. V, DeQuach, J. A., Chingozha, L., Lu, H., Christman, K. L. &

Davis, M. E. A naturally derived cardiac extracellular matrix enhances cardiac progenitor cell behavior in vitro. *Acta Biomater* **8,** 4357–4364 (2012).

8. DeQuach, J. A., Mezzano, V., Miglani, A., Lange, S., Keller, G. M., Sheikh, F. & Christman, K. L. Simple and high yielding method for preparing tissue specific extracellular matrix coatings for cell culture. *PLoS One* **5,** e13039 (2010).

9. Merna, N., Fung, K. M., Wang, J. J., King, C. R., Hansen, K. C., Christman, K. L. & George, S. C. Differential beta3 Integrin Expression Regulates the Response of Human Lung and Cardiac Fibroblasts to Extracellular Matrix and Its Components. *Tissue Eng Part A* **21,** 2195–2205 (2015).

10. Cortiella, J., Niles, J., Cantu, A., Brettler, A., Pham, A., Vargas, G., Winston, S., Wang, J., Walls, S. & Nichols, J. E. Influence of acellular natural lung matrix on murine embryonic stem cell differentiation and tissue formation. *Tissue Eng Part A* **16,** 2565–2580 (2010).

11. Sellaro, T. L., Ravindra, A. K., Stolz, D. B. & Badylak, S. F. Maintenance of hepatic sinusoidal endothelial cell phenotype in vitro using organ-specific extracellular matrix scaffolds. *Tissue Eng* **13,** 2301–2310 (2007).

12. Keane, T. J., DeWard, A., Londono, R., Saldin, L. T., Castleton, A. A., Carey, L., Nieponice, A., Lagasse, E. & Badylak, S. F. Tissue-Specific Effects of Esophageal Extracellular Matrix. *Tissue Eng Part A* **21,** 2293–2300 (2015).

13. Ungerleider, J. L., Johnson, T. D., Rao, N. & Christman, K. L. Fabrication and characterization of injectable hydrogels derived from decellularized skeletal and cardiac muscle. *Methods* **84,** 53–59 (2015).

14. Hill, R. C., Calle, E. A., Dzieciatkowska, M., Niklason, L. E. & Hansen, K. C. Quantification of Extracellular Matrix Proteins from a Rat Lung Scaffold to Provide a Molecular Readout for Tissue Engineering. *Mol. Cell. Proteomics* (2015). doi:10.1074/mcp.M114.045260

15. Kim, D., Langmead, B. & Salzberg, S. L. HISAT: a fast spliced aligner with low memory requirements. *Nat. Methods* **12,** 357 (2015).

16. Pertea, M., Kim, D., Pertea, G. M., Leek, J. T. & Salzberg, S. L. Transcript-level expression analysis of RNA-seq experiments with HISAT, StringTie and Ballgown. *Nat. Protoc.* **11,** 1650 (2016).

17. Pertea, M., Pertea, G. M., Antonescu, C. M., Chang, T.-C., Mendell, J. T. & Salzberg, S. L. StringTie enables improved reconstruction of a transcriptome from RNA-seq reads. *Nat. Biotechnol.* **33,** 290 (2015).

18. Love, M. I., Huber, W. & Anders, S. Moderated estimation of fold change and dispersion for RNA-seq data with DESeq2. *Genome Biol.* **15,** 550 (2014).

19. Huang, D. W., Sherman, B. T. & Lempicki, R. A. Systematic and integrative analysis of large gene lists using DAVID bioinformatics resources. *Nat. Protoc.* **4,** 44–57 (2009).

20. Huang, D. W., Sherman, B. T. & Lempicki, R. A. Bioinformatics enrichment tools: paths toward the comprehensive functional analysis of large gene lists. *Nucleic Acids Res.* **37,**

1–13 (2009).

21. Urciuolo, A., Quarta, M., Morbidoni, V., Gattazzo, F., Molon, S., Grumati, P., Montemurro, F., Tedesco, F. S., Blaauw, B., Cossu, G., Vozzi, G., Rando, T. A. & Bonaldo, P. Collagen VI regulates satellite cell self-renewal and muscle regeneration. *Nat. Commun.* **4,** 1964 (2013).

22. DeQuach, J. A., Lin, J. E., Cam, C., Hu, D., Salvatore, M., Sheikh, F. & Christman, K. L. Injectable skeletal muscle matrix hydrogel promotes neovascularization and muscle cell infiltration in a hindlimb ischemia model. *Eur Cell Mater* **23,** 400–412 (2013).

23. Awojoodu, A. O., Ogle, M. E., Sefcik, L. S., Bowers, D. T., Martin, K., Brayman, K. L., Lynch, K. R., Peirce-Cottler, S. M. & Botchwey, E. Sphingosine 1-phosphate receptor 3 regulates recruitment of anti-inflammatory monocytes to microvessels during implant arteriogenesis. *Proc. Natl. Acad. Sci.* **110,** 13785 LP-13790 (2013).

24. Bullers, S. J., Baker, S. C., Ingham, E. & Southgate, J. The Human Tissue–Biomaterial Interface: A Role for PPARγ-Dependent Glucocorticoid Receptor Activation in Regulating the CD163+ M2 Macrophage Phenotype. *Tissue Eng. Part A* **20,** 2390–2401 (2014).

25. Tidball, J. G. & Villalta, S. A. Regulatory interactions between muscle and the immune system during muscle regeneration. *Am. J. Physiol. Integr. Comp. Physiol.* **298,** R1173–R1187 (2010).

26. Sadtler, K., Estrellas, K., Allen, B. W., Wolf, M. T., Fan, H., Tam, A. J., Patel, C. H., Luber, B. S., Wang, H., Wagner, K. R., Powell, J. D., Housseau, F., Pardoll, D. M. & Elisseeff, J. H. Developing a pro-regenerative biomaterial scaffold microenvironment requires T helper 2 cells. *Science (80-.).* **352,** 366 LP-370 (2016).

27. Fishman, J. M., Lowdell, M. W., Urbani, L., Ansari, T., Burns, A. J., Turmaine, M., North, J., Sibbons, P., Seifalian, A. M., Wood, K. J., Birchall, M. A. & De Coppi, P. Immunomodulatory effect of a decellularized skeletal muscle scaffold in a discordant xenotransplantation model. *Proc. Natl. Acad. Sci.* **110,** 14360 LP-14365 (2013).

28. Mimura, K. K. O., Moraes, A. R., Miranda, A. C., Greco, R., Ansari, T., Sibbons, P., Greco, K. V & Oliani, S. M. Mechanisms underlying heterologous skin scaffold-mediated tissue remodeling. *Sci. Rep.* **6,** 35074 (2016).

29. Farup, J., Madaro, L., Puri, P. L. & Mikkelsen, U. R. Interactions between muscle stem cells, mesenchymal-derived cells and immune cells in muscle homeostasis, regeneration and disease. *Cell Death &Amp; Dis.* **6,** e1830 (2015).

30. Kharraz, Y., Guerra, J., Mann, C. J., Serrano, A. L. & Munoz-Canoves, P. Macrophage plasticity and the role of inflammation in skeletal muscle repair. *Mediators Inflamm.* **2013,** 491497 (2013).

31. Kimmel, H., Rahn, M. & Gilbert, T. W. The Clinical Effectiveness in Wound Healing With Extracellular Matrix Derived From Porcine Urinary Bladder Matrix: A Case Series on Severe Chronic Wounds. *J. Am. Col. Certif. Wound Spec.* **2,** 55–59 (2010).

32. Hodde, J. P. & Allam, R. Small Intestinal Submucosa Wound Matrix for Chronic Wound Healing. *Wounds a Compend. Clin. Res. Pract.* **19,** 157–162 (2007).

33. Thomas, K., Engler, A. J. & Meyer, G. A. EXTRACELLULAR MATRIX REGULATION IN THE MUSCLE SATELLITE CELL NICHE. *Connect. Tissue Res.* **56,** 1–8 (2015).

34. Cornelison, D. D. W., Wilcox-Adelman, S. A., Goetinck, P. F., Rauvala, H., Rapraeger, A. C. & Olwin, B. B. Essential and separable roles for Syndecan-3 and Syndecan-4 in skeletal muscle development and regeneration. *Genes Dev.* **18,** 2231–2236 (2004).

35. Gutiérrez, J. & Brandan, E. A Novel Mechanism of Sequestering Fibroblast Growth Factor 2 by Glypican in Lipid Rafts, Allowing Skeletal Muscle Differentiation. *Mol. Cell. Biol.* **30,** 1634 LP-1649 (2010).

36. Liu, C., McFarland, D. C., Nestor, K. E. & Velleman, S. G. Differential expression of membrane-associated heparan sulfate proteoglycans in the skeletal muscle of turkeys with different growth rates 1. *Poult. Sci.* **85,** 422–428 (2006).

37. Rao, N., Agmon, G., Tierney, M. T., Ungerleider, J. L., Braden, R. L., Sacco, A. & Christman, K. L. Engineering an Injectable Muscle-Specific Microenvironment for Improved Cell Delivery Using a Nanofibrous Extracellular Matrix Hydrogel. *ACS Nano* **11,** 3851–3859 (2017).

Chapter 5

Enzyme-Targeted Nanoparticles for Delivery to Ischemic Skeletal Muscle

5.1 Introduction

As outlined in Chapter 1, current treatments for PAD patients involve revascularization such as balloon angioplasty and arterial bypass. However, both options have high morbidity rates and low 5 year patency rates [1,2]. Thus, over 200,000 patients in the U.S. and Europe require lower extremity amputations annually [3]. There is a strong unmet clinical need for treating the ischemic muscle through improving blood perfusion and reducing muscle atrophy and tissue necrosis. Oftentimes the location of atherosclerotic lesions can prevent access via surgical or vascular intervention [4,5]. Moreover, treating a single atherosclerotic lesion may not desirable because the disease affects the entire tissue. Therefore, a desirable treatment for patients with PAD would involve a minimally invasive approach using angiogenic, arteriogenic, and/or myogenic therapies. Additionally, targeting molecular mechanisms of the disease would be beneficial for early stage treatment, since the patients treated with surgical interventions have already developed severe ischemia, atrophy and necrosis. Nanoparticle (NP) therapies would be desirable because they are minimally invasive, systemically deliverable, and can target to specific hallmarks of disease progression. One option could be to augment revascularization procedures through intra-arterial delivery of nanoparticles at the time of intervention (e.g., balloon angioplasty), or potentially intravenously (IV) via venipuncture for patients who are ineligible for vascular interventions.

NP drug delivery has recently shown promise in preclinical models of cardiovascular disease [6]. In a hindlimb ischemia model, Mooney and coworkers demonstrated effective delivery of vascular endothelial growth factor (VEGF) on gold NPs to ischemic tissue through the enhanced permeability and retention (EPR) effect known to be characteristic of both cancerous and ischemic tissues [7,8]. Another targeting strategy consists of ultrasound-microbubble rupturing to improve NP uptake into the ischemic limb [9]. However, neither of these particles was targeted to any particular molecular hallmarks of PAD tissue beyond leaky vasculature.

Recently, NPs comprised of peptide polymer amphiphiles (PPAs) were shown to aggregate in diseased tissue where matrix metalloproteinases (MMPs) are upregulated [10,11]. Specifically, these NPs consist of copolymers with hydrophobic and hydrophilic block regions that assemble into micellar nanoparticles [10,12,13]. The hydrophilic block contains a peptide sequence recognized and cleaved by MMP-2/9. Upon cleavage, the particles undergo a morphological switch from NPs to a micron scale aggregate-like scaffold at the tissue of interest because of the change in amphiphilicity of the PPA. MMP-9 is upregulated in the skeletal muscle of humans [14] and animals [15] with critical or hindlimb ischemia, respectively, thus indicating that this targeted nanoparticle system may be a clinically viable option for treatment of ischemic tissues in patients with PAD. We have previously shown that this system initially designed for cancer diagnosis and treatment can also be applied to non-invasive NP delivery to ischemic myocardium [11]. Furthermore, the system is easily tunable and has been conjugated to a variety of imaging and therapeutic functionalities [16–18], providing proof of concept for minimally-invasive drug delivery and subsequent targeted retention. Our goal was to design enzyme-targeted PPA NPs and demonstrate their delivery and optimal biodistribution for targeting to ischemic muscle in a preclinical model of PAD. We synthesized near-IR labeled enzyme-responsive micellar NPs and demonstrated their enzyme responsiveness and targeting capability *in vivo* in a rat hindlimb ischemia model. This is the first study to show proof-of-

concept for NP targeting and retention in ischemic muscle as a potential therapeutic vehicle for PAD patients.

5.2 Experimental

5.2.1 PPA synthesis and characterization

Detailed polymer synthesis and characterization methods are included in [19]. Briefly, PPAs were synthesized via ring opening metathesis polymerization (ROMP) using $(IMesH_2)(C_5H_5N)_sRu{=}CHPh$. PPAs were prepared by first polymerizing N-benzyl-*cis*-5-norbornene-*endo*-2,3-dicarboxyimide (phenyl monomer) until complete monomer consumption, followed by the addition of N-(Peptide)-*cis*-5-norbornene-*exo*-dicarboximide (peptide monomer; peptide = GPLGLAGGFGSGERDG). First order polymerization kinetics of N-(glycine)-*cis*-5-norbornene-*exo*-dicarboximide (glycine monomer) and peptide monomer were determined by monitoring polymerization by ^1H NMR. For blend copolymers, N-(Glycine)-*cis*-5-norbornene-*exo*-dicarboximide was added every 2 minutes. After complete monomer consumption, polymers were either quenched with ethyl vinyl ether (EVE), or labeled with a near IR cyanine dye monomer and quenched with EVE after complete monomer consumption. PPAs were characterized using size exclusion chromatography coupled with multiangle light scattering to determine molecular weight and dispersity indices.

5.2.2 NP synthesis and characterization

PPAs were dissolved in dry DMF at 2 mg/mL concentration. 1x DPBS was then added to the solution at 1 mL/hr with rapid stirring to reach a final concentration of 1 mg/mL. NPs were then dialyzed into 1x DPBS to remove organic solvent. NPs were analyzed by dynamic light scattering (DLS) and transmission electron microscopy (TEM) to determine size and morphology. Enzyme cleavage was determined by incubating NPs with thermolysin and characterizing the morphology by TEM.

5.2.3 Hindlimb ischemia surgery and perfusion imaging

All animal procedures were performed in accordance with the guidelines established by the Institutional Animal Care and Use Committee at the University of California, San Diego and the American Association for Accreditation of Laboratory Animal Care. Studies were done with 32 female Sprague Dawley rats ranging in weights from 200-250g. For the hindlimb ischemia surgery, animals were anesthetized with 2.5% isoflurane gas using a Kent Scientific PhysioSuite ventilator. Unilateral ischemia damage was applied to the animals' right limb by ligation and removal of segments from the femoral artery and vein starting proximal to the epigastric artery as described previously [20]. First, the surgical site was shaved and cleaned with betadine and isopropanol along with delivery of 1% lidocaine subcutaneously along the incision site. The contralateral skin was also shaved for equivalent IVIS imaging since fur can interfere with IVIS. The targeted vessels were visualized by creating an incision overlying the proximal, medial portion of the right hindlimb. The femoral artery and vein were dissected away from the femoral nerve and ligated to target the proximal removal of a 2 cm segment. Any major branches along the 2 cm segment, including the epigastric artery, were cauterized or ligated prior to excision to minimize bleeding. The entry incision through the skin was then closed using a mattress suture (5-O silk). Postoperatively, all animals were regularly monitored and analgesia (Buprenorphine at 0.05 mg/kg) was administered immediately upon regaining consciousness.

Immediately after surgery, perfusion measurements were made using a laser speckle contrast analysis system (PeriMed, Stockholm, Sweden) to ensure adequate ischemia compared to the healthy limb. All readings were done with the following settings: working distance of 20 cm. high point density, 0.42 images/s, frame rate of 25 images/s, recorded with averaging of 50 images, effective frame rate of 0.5 images/s, and intensity filter from 0.20-10.0. The animals were transferred to the PeriMed immediately after hindlimb ischemia surgery and were maintained at 2.5% isoflurane and on a heated insulated deck. Readings were

continuously taken for a minimum of 20 minutes or until the perfusion measurements reached a plateau. Regions of interest were utilized to target each hairless plantar sole region individually for assessment at the equilibrium time point. Percent perfusion was calculated as a ratio of the ischemic limb (right) to the healthy limb (left). Measurements were taken before and immediately after surgery.

5.2.4 NP injection and IVIS tracking

For all animal studies, animals were randomized after the hindlimb ischemia surgery. For the injection time point pilot study, animals were injected with Cy5.5-labeled NPs at 1 (n=2), 3 (n=2), 5 (n=2), or 7 (n=2) days post-ischemia. For the block versus blend study, animals were injected with Cy5.5-labeled block (n=3) or blend (n=3) NPs at 4 days post-ischemia. For the zwitterionic long term retention study, $NP_{5.5}$ (7 day retention: n=4; 28 day retention: n=4) or NP_{zw5} (7 day retention: n=4; 28 day retention: n=8) were injected 4 days post-ischemia. For all injections, NP concentration was 400nmol with respect to polymer in a 1mL injection volume. For the tail vein injections, animals were anesthetized using 2.5% isoflurane. Their tails were heated for 1 minute with a heating pad to induce vasodilation. Tails were sterilized by scrubbing with isopropanol. NPs were injected intravenously with a 27G needle through either the right or left tail vein after verifying the vein was accessed via flashback. Venous puncture attempts were not totaling more than 3 per side. Animals with failed injections were excluded from the study. NP targeting was monitored using an *In Vivo* Imaging System (IVIS) Spectrum 200 (Perkin Elmer). For *in vivo* monitoring, the transillumination mode was used to capture signal deeper in the tissue. Animals were anesthetized with 2.5% isoflurane and placed in the IVIS chamber in a supine position. Their legs were angled outward to expose the ischemic region. Excitation/emission and exposure was 675nm/720nm and 10 seconds for $NP_{5.5}$ and 640nm/680nm and 5 seconds for NP_{zw5}. Each leg (ischemic and healthy) was imaged individually using a 3x3 pinhole square (9 images per limb). Overview images were created

using the Perkin Elmer Living Image software. Ischemic to healthy muscle fluorescence ratios were calculated by drawing circular regions of interest around the thigh (gracilis) muscle, measuring the total normalized transmission fluorescence (NTF) efficiency for each limb, and normalizing to the healthy limb internally for each animal. After the final *in vivo* time point, animals were euthanized with lethal injection of sodium pentobarbital. For *ex vivo* fluorescence, organs were harvested after euthanasia, placed on a black laminated sheet, and read for fluorescence on IVIS using epi-fluorescence mode with the same excitation/emission filters as for *in vivo* imaging, but with an exposure time of 0.1 sec. Radiant efficiency for each organ ([p/s/cm^2/sr]/[μW/cm^2]) was internally normalized to the healthy muscle of each animal to be able to compare between different fluorescent dye species.

5.2.5 Immunohistochemistry and confocal imaging

After *ex vivo* IVIS imaging, both ischemic and healthy gracilis muscle from each animal was flash frozen in liquid nitrogen-chilled isopentane and blocked in OCT for cryosectioning in the transverse orientation. Sections of 10 μm thickness were taken at 4 locations spanning the majority of the muscle. For immunohistochemistry, sections were thawed, fixed with ice-cold acetone, blocked with 5% bovine serum albumin (Gemini Bio-Products), and permeabilized with 0.3% Triton X-100 (Sigma) before incubation with primary antibody (rabbit polyclonal anti-laminin 1:100, abcam), secondary antibody (AlexaFluor-488 goat anti-rabbit 1:500, Invitrogen), and Hoechst 33342 (ThermoFisher Scientific). Sections were mounted using FluorMount and were imaged on a Nikon A1R Confocal microscope using a 20x air objective. Confocal settings were as such: 1 frame/sec, simultaneous scan, 1.2 Airy unit pinhole, scan area of 1024x1024 pixels, 0.34 μm Nyquist pixel size. For each laser the hv, offset, and power were respectively: DAPI 85, -10, 0.85; FITC 66, -10, 0.4; Cy5 97, -9, 14.44 (Cy5.5 NPs); Cy5 84, -9, 14.44 (zwCy5 NPs).

5.2.6 Statistical analysis

For the injection time point pilot, data was analyzed with a two-way ANOVA with post-ischemia injection time point and post-injection imaging time point as factors with a post-hoc Tukey multiple comparisons test. Block versus blend data and zwitterionic versus charged data were analyzed with a Student's T-test at each time point post-injection. *Ex vivo* biodistribution data was analyzed with a Student's T-test for each organ. Data are means±SEM unless otherwise noted. Significance was accepted at $p < 0.05$.

5.3 Results and discussion

Herein, we sought to investigate the use of MMP responsive NPs for noninvasive targeting and retention in a preclinical model of PAD. Our group has previously developed MMP-targeted PPA NPs and shown these particles target effectively to damaged tissue in xenogeneic tumors [10,13] and myocardial infarction models [11], both of which are known to have upregulated MMPs. We sought to further investigate this targeting strategy in an animal model of PAD to determine if these particles could target ischemic skeletal muscle after intravenous injection. Because of the nature of the polymeric materials, we were able to tune the design of the NPs by optimizing enzyme cleavage efficiency, and by incorporating differentially charged dyes, which altered the targeting to ischemic tissue. We first demonstrated targeted assembly of our original PPA NP design in a rat hindlimb ischemia model. We then undertook the synthesis and conjugation of a zwitterionic Cy5 to investigate whether a zwitterionic charge on the particles could improve targeting to ischemic muscle.

5.3.1 Synthesis of PPA NPs

PPAs were synthesized via ROMP using a ruthenium based initiator ($(H_2IMES)(pyr)_2(Cl)_2Ru=CHPh$, I, Scheme 5.1). Similar to previous MMP responsive PPAs, we used a N-

benzyl-*cis*-5-norbornene-*endo*-2,3-dicarboxyimide (phenyl monomer) for the hydrophobic block. However, we chose to investigate the composition of the hydrophilic block. Previous MMP responsive nanoparticles were prepared from block copolymers where the hydrophilic block contained only the N-(Peptide)-*cis*-5-norbornene-*exo*-dicarboximide (peptide monomer; peptide = GPLGLAGGFGSGERDG). Recently, it was shown that homopolymers of peptides prepared via ROMP were resistant to proteolysis due to the dense packing of the peptide brush [21]. Proteolysis could be enhanced by preparing a copolymer of a peptide with a small "spacer". Inspired by these results, we were interested in comparing the original design (block copolymers) to a new design where the hydrophilic peptide monomer was co-polymerized with a small "spacer" monomer, N-(Glycine)-*cis*-5-norbornene-*exo*-dicarboximide (Scheme 5.1).

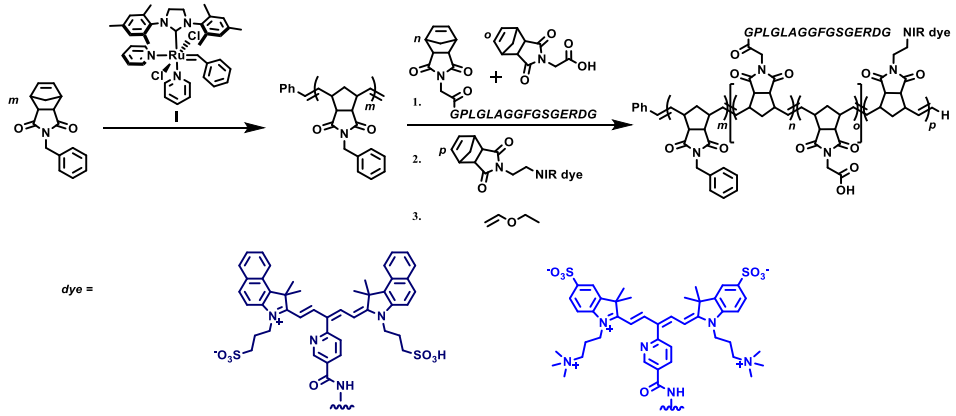

Scheme 5.1: Synthesis of blend PPAs. PPAs labelled either with the negatively charged Cy 5.5 or zwitterionic Cy5 using ROMP with the initiator **I**.

Block PPA (where the hydrophilic portion contains only the peptide monomer) and blend PPA (where the hydrophilic portion contains a random copolymer of peptide monomer and glycine spacer monomer) were prepared by ROMP (Figure 5.1A). To prepare blend PPAs, the first order polymerization kinetics of each monomer were determined by ^{1}H NMR. Initial rate of glycine spacer monomer was determined to be 17.4 hr^{-1} or 1 monomer every 0.20 minutes (Figure 5.1B). Initial rate of peptide monomer was determined to be 3.7 hr^{-1} or 1 monomer every

2.01 minutes (Figure 5.1C). Block and blend PPAs were analyzed by size exclusion chromatography coupled with a multi angle light scattering detector (SEC-MALS) to determine molecular weight (M_n) and dispersity index (M_w/M_n) (Figure 5.1D-E). The resulting PPAs assembled into micellar nanoparticles (NPs) through the slow addition of DPBS buffer to a polymer solution in DMF, followed by dialysis into DPBS buffer, and resulting NPs were characterized by dynamic light scattering (DLS) and TEM. Indeed, when incubated with thermolysin, a model protease, the blend PPAs reached ~35 percent cleavage over 14 hours whereas the block copolymer reached ~25 percent, which supports previous studies showing increased sensitivity to protease cleavage when the peptide block is less dense (Figure 5.2A) [21]. For our *in vitro* enzyme assays, we chose thermolysin as a proxy for MMP because it is more reliable that commercially available MMPs and we have shown that it can cleave the same recognition sequence as MMP2/9 [22]. Moreover, similar particle systems with the same enzymatic recognition sequences proved to be MMP responsive [10,11,13].

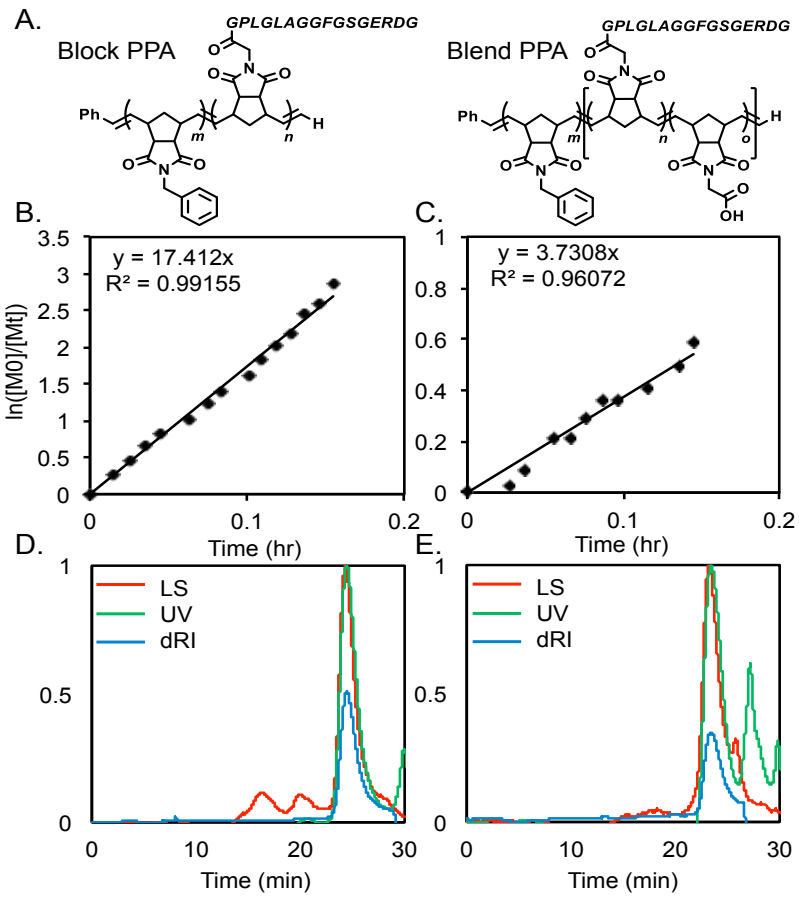

Figure 5.1: Preparation of polymer peptide amphiphiles (PPAs) for *in vivo* studies. (A) Chemical structure of block and blend PPAs. (B-C) First order polymerization kinetics for norbornene glycine monomer (B) and norbornene peptide monomer (C). (D-E) SEC-MALS trace for the block (D) and blend (E) polymers. Data acquired by Jacquelin Kammeyer.

For *in vivo* tracking of NPs, PPAs needed fluorescent labeling. We chose to utilize NIR fluorescent, polymethine cyanine fluorophores (Cy) as NIR fluorophores allow for deeper tissue imaging with minimal tissue autofluorescence. We synthesized a negatively charged Cy5.5 analog bearing a norbornene moiety (Nor-$Cy_{5.5}$) to incorporate the fluorophore into ROMP polymers (for synthesis, see [19]). Cy fluorophores can self-quench if positioned in close proximity [23–25], such as when fluorophore-labeled polymers assemble into micellar nanoparticles. Labeling each polymer in the particle could potentially lead to self-quenching and a reduced fluorescence signal. To prepare Cy-labeled PPAs, polymers were prepared as stated previously, then after complete monomer consumption of the hydrophilic block, Nor-$Cy_{5.5}$

monomer was added to the polymerization. To prepare NPs, labeled and unlabeled PPAs assembled at various ratios to determine the proper ratio to minimize self-quenching. Quenching was high with 1:0 ratio of labeled to unlabeled polymer, as seen with minimal fluorescent intensity (Figure 5.2B). Optimal fluorescence intensity was observed at a 1:1 ratio of labeled to unlabeled polymer, indicating this ratio exhibited the least amount of self-quenching while maintaining a high intensity fluorescent signal.

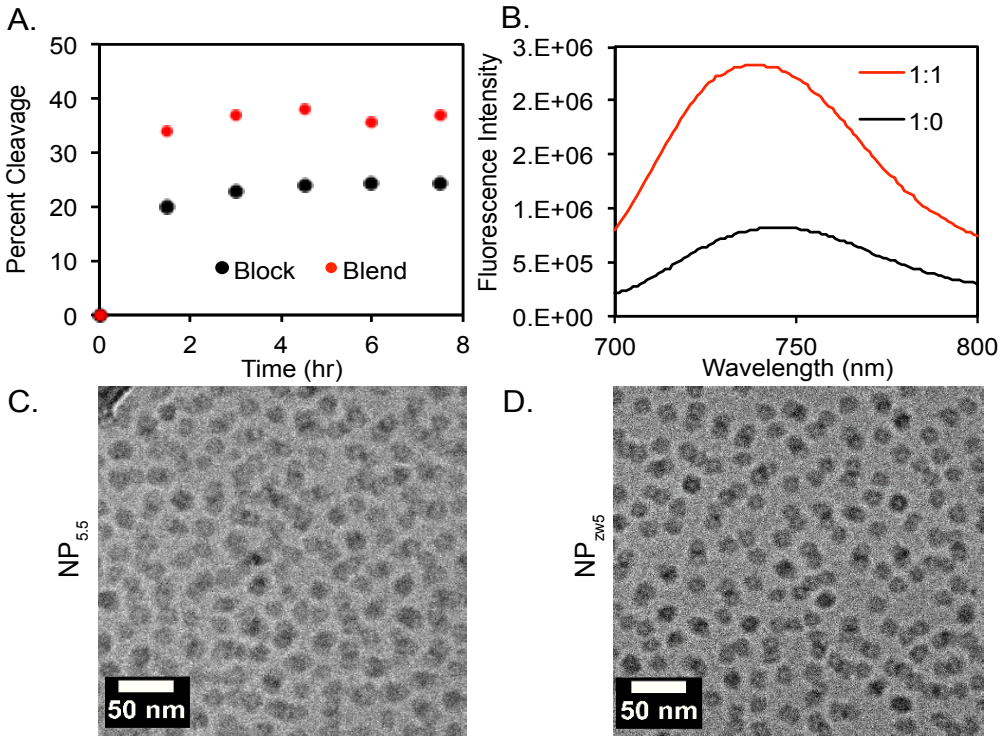

Figure 5.2: Preparation of near-IR labeled NPs. (A) Block vs. blend cleavage kinetics when incubated with thermolysin, a model protease, as determined by HPLC. (B) Fluorescence intensity of NPs with a ratio of labeled-to-nonlabeled PPAs of 1:1 or 1:0. PPAs were labeled with the negatively charged Nor-$Cy_{5.5}$, and fluorescence intensity was found to be the greatest when a 1:1 ratio of labeled-to-unlabeled NPs was prepared. (C-D) CryoEM of particles labeled with negatively charged Cy 5.5 (C) and particles labeled with zwitterionic Cy 5 (D). Scale bar is 50 nm. Data acquired by Jacquelin Kammeyer.

An additional zwitterionic near-IR Cy fluorophore (Nor-Cy_{zw5}) was also synthesized. It has been shown that zwitterionic materials can be "stealthy" *in vivo* due to less uptake in the monocyte phagocytic system (MPS) and overall better circulation half-life [26–29]. The current

polymer system contained an overall negative charge at neutral pH, therefore we were interested in creating a more zwitterionic polymer for NP preparation. For assembled materials, a completely zwitterionic polymer may not be desirable because of difficulty obtaining a stable morphology due to lack of charge repulsion [30]. Therefore, we envisioned labeling the polymer with a zwitterionic Cy5 monomer to improve the neutral charge character of the PPA and resulting surface of the assembled NPs. Full polymerization of either dye species into the PPAs was verified with ^{1}H NMR [19], and successful assembly of PPAs into NPs ($NP_{5.5}$ and NP_{zw5}) was characterized by TEM (Figure 5.2C-D). Note that due to the laser wavelength of the light scattering instrumentation, no DLS data could be obtained of dye-labeled particles. NPs were confirmed to be responsive to thermolysin enzyme cleavage by TEM (Figure 5.3). NPs underwent a morphological switch only in the presence of active enzyme but not denatured enzyme, indicating they could form micron-scale aggregates after cleavage of the enzyme-labile peptide substrate. The addition of near-IR dyes and optimization of fluorescence quenching in this enzyme-targeted NP system allowed for non-invasive monitoring of the particle aggregation *in vivo.*

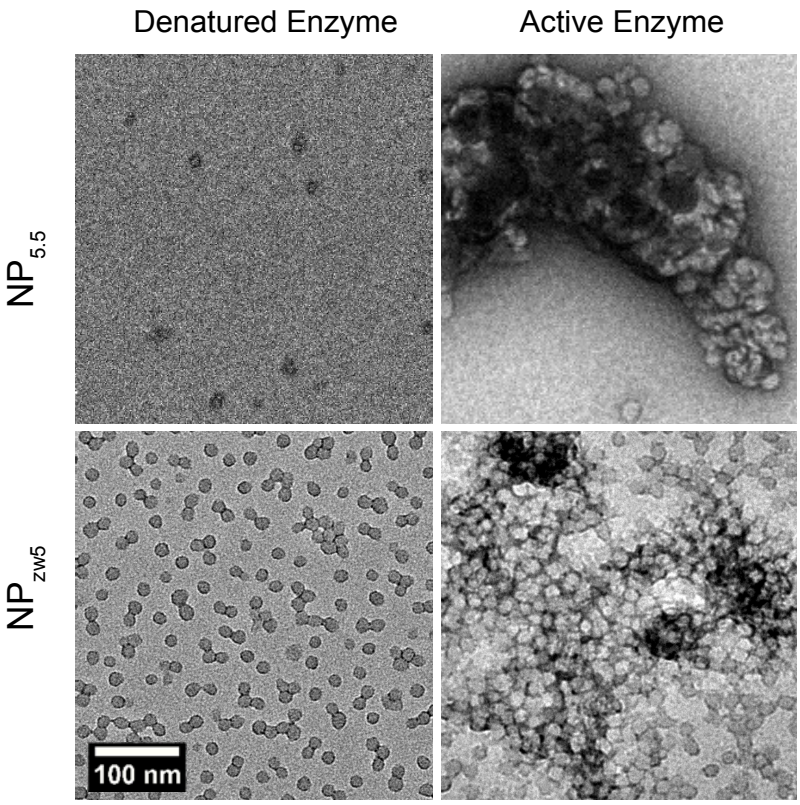

Figure 5.3: Characterization of morphology of NPs after treatment with thermolysin, a model protease. TEM images show monodispersed NPs after denatured enzyme treatment, but with active enzyme treatment NPs appear to be large micronscale aggregates. Scale bar is 100 nm. Data acquired by Jacquelin Kammeyer.

5.3.2 In vivo targeting

NPs were first tested in a hindlimb ischemia model pilot study to optimize the injection timepoint for optimal MMP activity and thus targeting. Ryu *et. al.* demonstrated that the highest MMP activity in the tissue would be around 5 days post-ischemia induction using an albumin based probe [31]. However, there is variation inherent to the hindlimb ischemia model originating with different surgical technique, species used, and even between animal strains of the same species [32,33]. We validated optimal targeting in a pilot study by delivering $NP_{5.5}$ at 1, 3, 5, or 7 days after the induction of hindlimb ischemia. Targeting to the ischemic limb was monitored through an *In Vivo* Imaging System (IVIS) by measuring fluorescence of the near-IR dye over 9 days post-injection. Targeting was determined by comparing the ratio of fluorescence of the

ischemic limb compared to healthy limb. It was found that particles delivered at 3 and 5 days post-ischemia had the highest NP targeting (Figure 5.4). Thus, we chose to inject our particles at 4 days post-ischemia for the remaining studies to ensure we were following the timecourse of maximum MMP activity and thus particle efficacy.

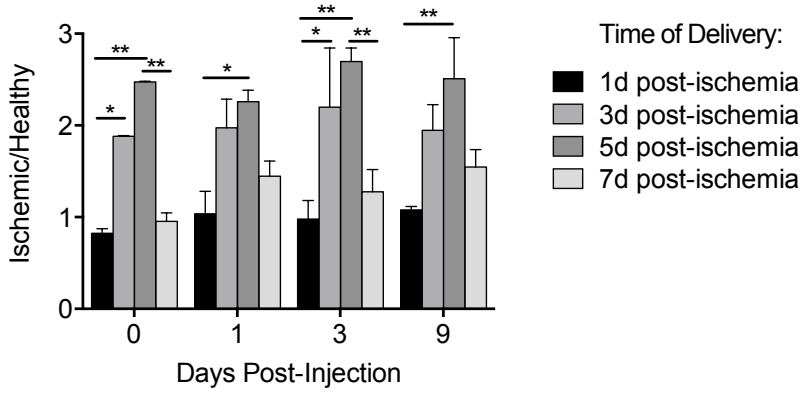

Figure 5.4: Delivery of PPA NPs after hindlimb ischemia. Cy5.5-labeled PPA NPs were injected at multiple time points (n=2 per group) after hindlimb ischemia and were monitored for 9 days post-injection to determine optimal delivery time point. Data is presented as mean±SEM. Analyzed with two-way ANOVA and post-hoc Tukey's multiple comparisons test. *p<0.05, **p<0.01.

We next sought to examine if improved enzyme cleavage *in vitro* would correlate with increased NP targeting *in vivo*. Cy-5.5-labeled block or blend NPs (same as those characterized in Figure 5.1 and Figure 5.2A) were injected IV 4 days post-ischemia and NPs were monitored for 7 days post-injection using IVIS. Blend particles showed a trend of better targeting than block particles to the ischemic muscle (Figure 5.5). Thus, this suggests that less dense peptide packing can cause increased enzyme cleavage *in vitro* and improved targeting *in vivo*.

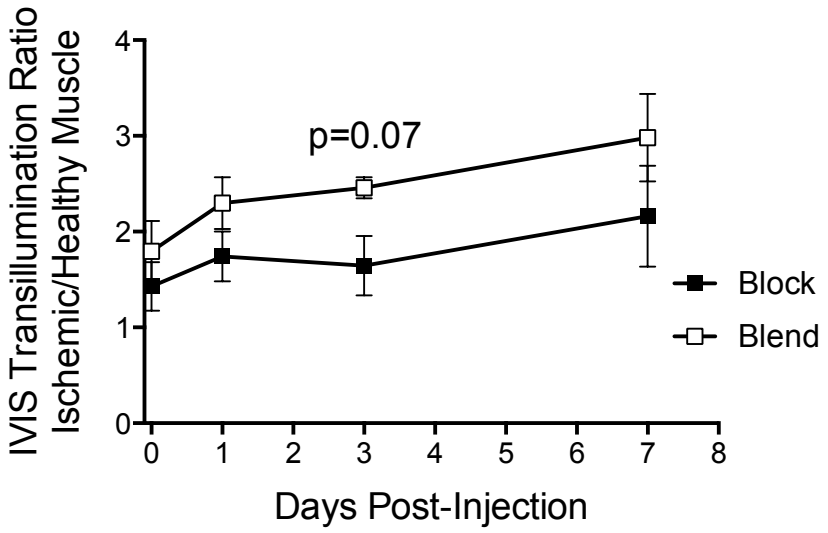

Figure 5.5: Targeting of block versus blend NPs after hindlimb ischemia. Cy5.5-labeled PPA NPs with the hydrophilic block consisting of just peptide ("block") or peptide mixed with spacer ("blend") were injected 4 days post-hindlimb ischemia (n=3). Animals were monitored for 7 days post-injection. Blend NPs targeted better than block NPs as indicated by a higher ischemic-to-healthy fluorescence ratio. Data is presented as mean±SEM. Data was analyzed with Student's T-test at each time point.

To examine the effect of NP surface charge on targeting and long term retention to the ischemic limb, $NP_{5.5}$ and NP_{zw5} were administered IV four days after hindlimb ischemia injury and monitored by IVIS to either 7 or 28 days post-injection. PeriMed laser speckle contrast imaging confirmed that the degree of ischemia was similar in both experimental groups (Figure 5.6). Through IVIS monitoring at regular intervals post-injection, we showed both NPs target to the ischemic limb as shown by an ischemic/healthy ratio above 1 (Figure 5.7A, Figure 5.8). The zwitterionic NPs targeted better to the ischemic limb at each time point, although this trend was not significant. This is the first study to show long term NP retention in ischemic skeletal muscle over at least 28 days, which will be significant for delivering therapeutics for prolonged release. This is consistent with previous studies showing enzyme responsive NP retention in infarcted myocardium for at least 28 days post-injection [11].

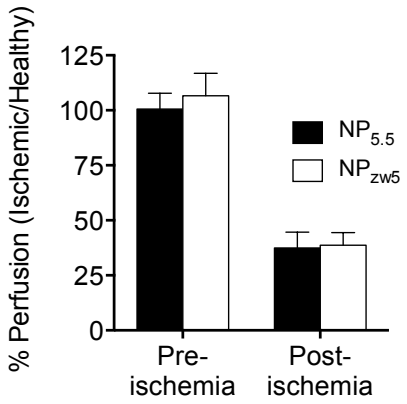

Figure 5.6: Blood perfusion pre- and post- hindlimb ischemia surgery as determined by laser speckle contrast analysis. Perfusion to the hindlimb was measured using laser speckle contrast analysis immediately before (pre-ischemia) and after (post-ischemia) the hindlimb ischemia surgery in order to ensure an adequate and similar degree of ischemia between experimental groups. N=8 for $NP_{5.5}$, n=12 for NP_{zw5}.

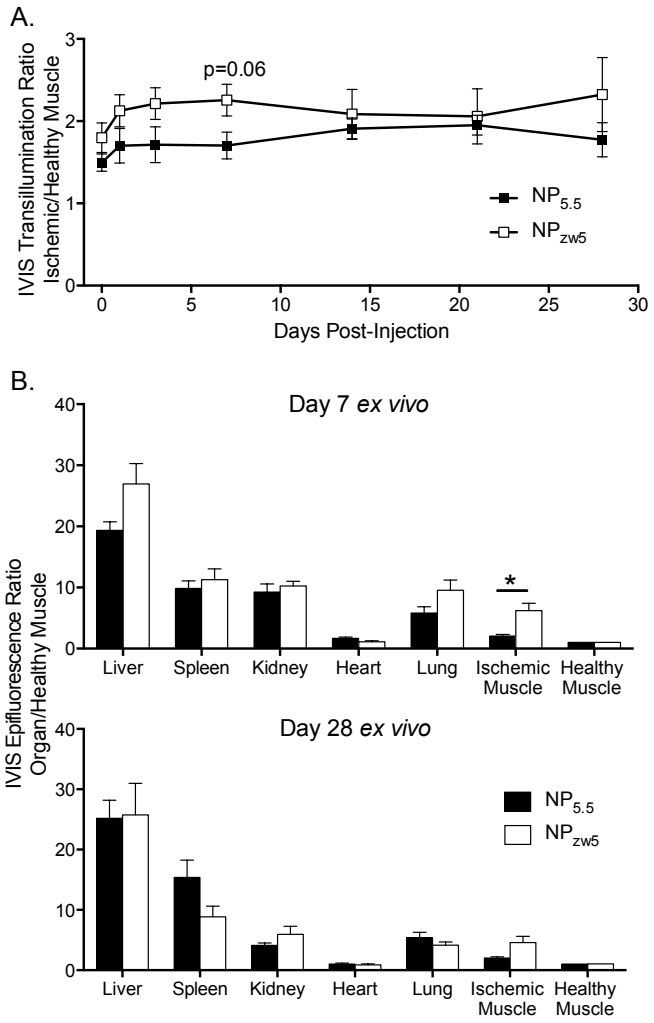

Figure 5.7: Targeting of near-IR NPs over 28 days. (A) PPA NPs were injected 4 days after hindlimb ischemia and monitored *in vivo* at 0, 1, 3, 7, 14, 21, and 28 days post-injection using IVIS. Half of the animals (n=4 for each group) were harvested at day 7; n=4 ($NP_{5.5}$) and n=8 (NP_{zw5}) animals were followed for the full 28 day study. Data is reported as the ratio of ischemic to healthy muscle fluorescence as measured through the IVIS transillumination setting. (B) *Ex vivo* organs were analyzed using IVIS epifluorescence to determine biodistribution. Average radiant efficiency [(P/sec/cm^2/sr)/(μW/cm^2)] was measured for each organ and internally normalized to the healthy muscle to account for differences in fluorescent intensity between cyanine dyes. $NP_{5.5}$ and NP_{zw5} were compared using Students t-test at each time point or for each organ. *p<0.05.

After 7 or 28 days, organs were analyzed *ex vivo* using IVIS and normalized to healthy muscle fluorescence to make comparisons between dyes (Figure 5.7B, Figure 5.8). As expected with any NP therapy, the PPA NPs have significant accumulation in the liver and spleen. In agreement with *in vivo* IVIS data, we observed significantly higher fluorescence in the

ischemic gracilis muscle of animals treated with NP_{zw5} compared to $NP_{5.5}$ at 7 days post-injection, but this only trended higher at 28 days. This could be because zwitterionic NPs have a longer half-life, thus allowing for more efficient targeting to the ischemic limb through longer circulation time. Furthermore, there were no differences in fluorescent signal in any of the satellite organs between dye species, although we expected to see less NP_{zw5} trafficking to the liver and spleen. However, similar PPA NPs were shown not to cause any inflammatory reaction in off target organs through histopathological analysis [11], suggesting there are no significant toxicity concerns, although more through safety evaluation will be needed.

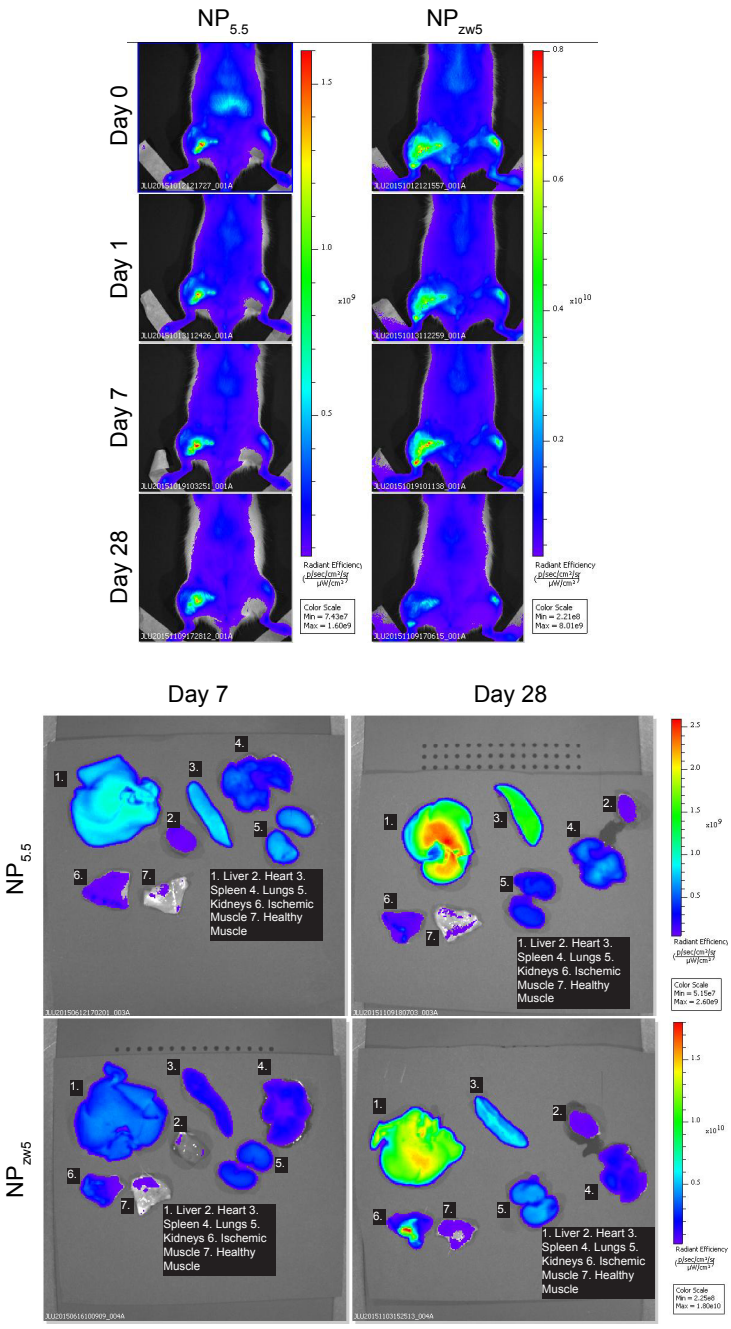

Figure 5.8: Representative IVIS images. Top: representative IVIS timecourse images for $NP_{5.5}$ (left) and NP_{zw5} (right) groups. Bottom: representative IVIS *ex vivo* images at day 7 (left) and day 28 (right) post-injection. Each image represents a single animal throughout the time course. Cy5.5 and Cy5 are shown on different intensity scales to account for the differences in fluorescent intensity between the different dyes at their unique excitation/emission filters.

Immunohistochemistry of cross sections from ischemic and healthy muscle confirmed the presence of NPs in the ischemic muscle at a greater frequency than their presence in healthy contralateral muscle (Figure 5.9, Figure 5.10). Fluorescence from NP aggregates was apparent in the extracellular space of the endomysium and perimysium, which was visible through co-staining with laminin, a basement membrane protein ubiquitously expressed in skeletal muscle. This spatial localization is expected due to NP aggregation in the presence of extracellular MMP activity. NP fluorescence was present in the ischemic muscle at both 7 (Figure 5.9) and 28 days (Figure 5.10) post-injection for both $NP_{5.5}$ and NP_{zw5}. Aggregates colocalized with extracellular laminin seen out to 28 days post-injection shows proof of concept of scaffold formation for possible prolonged, slow release of therapeutics.

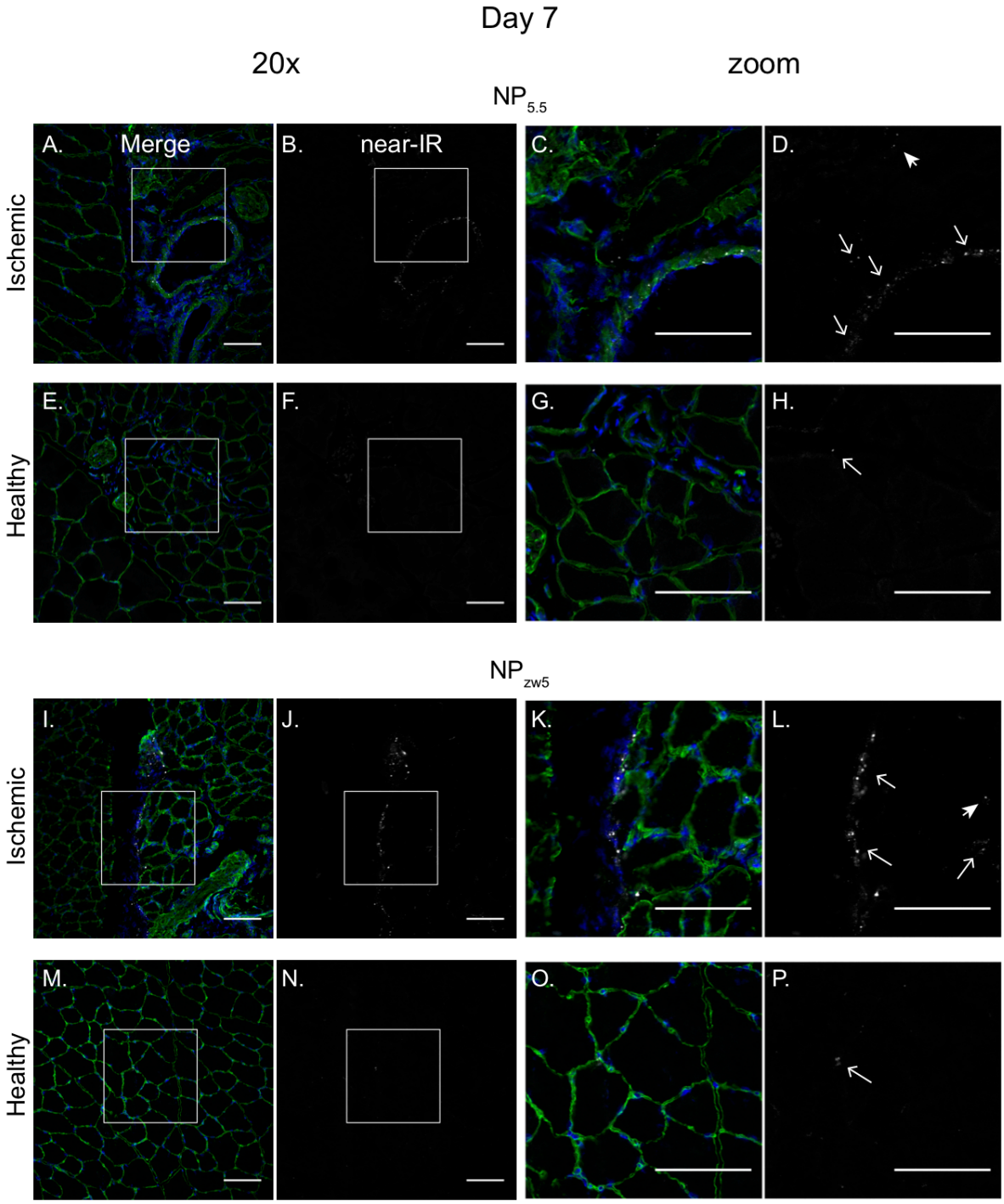

Figure 5.9: *Ex vivo* histology of ischemic and healthy muscle at 7 days post-injection. Immunohistochemistry of fresh frozen muscle cross sections stained for laminin (green) and nuclei (blue) shows NPs (white) dispersed primarily through ischemic, and not healthy, muscle in both $NP_{5.5}$ (A-H) and NP_{zw5} (I-P) treated groups. Images on the left (A, B, E, F, I, J, M, N) show 20x views and images on the right (C, D, G, H, K, L, O, P) are zoomed in from the corresponding boxes on the left. (A, C, E, G, I, K, M, O) Three channel images. (B, D, F, H, J, L, N, P) Near-IR channel only. Thin arrows indicate perimysial localization while thick arrowheads indicate endomysial localization. Scale bars are 100 μm.

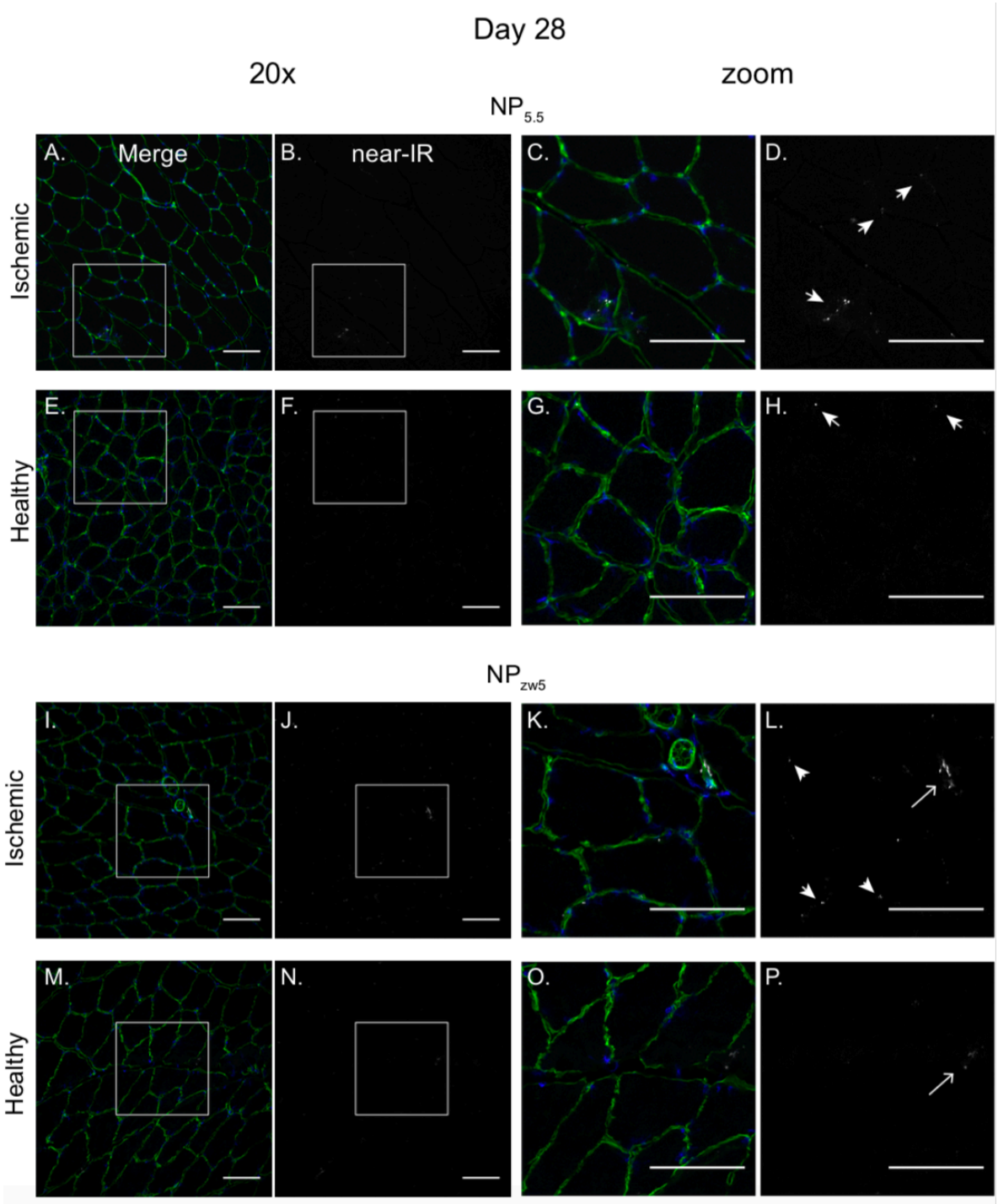

Figure 5.10: *Ex vivo* histology of ischemic and healthy muscle at 28 days post-injection. Immunohistochemistry of fresh frozen muscle cross sections stained for laminin (green) and nuclei (blue) shows nanoparticles (white) dispersed primarily through ischemic, and not healthy, muscle in both $NP_{5.5}$ (A-H) and NP_{zw5} (I-P) treated groups. Images on the left (A, B, E, F, I, J, M, N) show 20x views and images on the right (C, D, G, H, K, L, O, P) are zoomed in from the corresponding boxes on the left. (A, C, E, G, I, K, M, O) Three channel images. (B, D, F, H, J, L, N, P) Near-IR channel only. Thin arrows indicate perimysial localization while thick arrowheads indicate endomysial localization. Scale bars are 100 μm.

5.3.3 Limitations

Although this study is a promising advance in the field of targeted NP delivery, there are several limitations. First, the NP system in its current form shows off target accumulation in the liver and the spleen. Although this is a common hallmark of NP therapeutics, safety studies with therapeutic conjugated NPs will need to be evaluated in these organs to confirm no off target side effects. Second, the enzyme responsive NPs used for this study are not degradable; future studies will need to evaluate degradable systems. This study only examined a single delivery time point, but multiple injections over the course of months or years could be desirable for certain therapeutic regimens or for patients with chronic lesions. However, the long-term retention of our NP system could reduce the need for multiple injections due to the potential for long term, sustained release from NP aggregates. Lastly, although we did not explore therapeutic molecule delivery here, it is important to note that the PPA system is amenable to the incorporation of a variety of therapeutics. In our hands, similar types of PPA particles have been prepared that contain small molecule drugs in the core [16], or other peptides or nucleic acids in the shell [18]. Thus, this system can be easily modified for future therapeutic delivery.

5.4 Conclusions

MMPs are upregulated in animal models of hindlimb ischemia as well as ischemic skeletal muscle of human patients with PAD [14,15]. This study demonstrated that these enzymatic biomarkers of damaged ischemic muscle can be harnessed for systemic delivery, intramuscular targeting, and long term retention of an enzyme responsive NP. In this study, we synthesized MMP-responsive, PPA NPs with varied surface charge. We demonstrated that surface charge of the NPs had a significant effect on targeting to ischemic tissues. This study demonstrates proof of concept for the utility of enzyme-targeted vehicles for noninvasive delivery to ischemic skeletal muscle.

Chapter 5, in part, is a reprint of the material as it appears in *Polymer Chemistry*, 2017, 8(34): 5212-5219. The authors are Jessica Ungerleider, Jacquelin Kammeyer, Rebecca Braden, Karen Christman, and Nathan Gianneschi. The dissertation author was the primary investigator and co-first author of this paper.

5.5 References

1. Aihara, H., Soga, Y., Mii, S., Okazaki, J., Yamaoka, T., Kamoi, D., Shintani, Y., Ishikawa, T. & Investigators, R. R. Comparison of long-term outcome after endovascular therapy versus bypass surgery in claudication patients with Trans-Atlantic Inter-Society Consensus-II C and D femoropopliteal disease. *Circ. J.* **78,** 457–464 (2014).

2. van de Weijer, M. A. J., Kruse, R. R., Schamp, K., Zeebregts, C. J. & Reijnen, M. M. P. J. Morbidity of femoropopliteal bypass surgery. *Semin. Vasc. Surg.* **28,** 112–121 (2015).

3. Lawall, H., Bramlage, P. & Amann, B. Stem cell and progenitor cell therapy in peripheral artery disease. A critical appraisal. *Thromb. Haemost.* **103,** 696–709 (2010).

4. Dormandy, J., Heeck, L. & Vig, S. The fate of patients with critical leg ischemia. *Semin Vasc Surg* **12,** 142–147 (1999).

5. Marston, W. A., Davies, S. W., Armstrong, B., Farber, M. A., Mendes, R. C., Fulton, J. J. & Keagy, B. A. Natural history of limbs with arterial insufficiency and chronic ulceration treated without revascularization. *J Vasc Surg* **44,** 108–114 (2006).

6. Suarez, S., Almutairi, A. & Christman, K. L. Micro- and Nanoparticles for Treating Cardiovascular Disease. *Biomater. Sci.* **3,** 564–580 (2015).

7. Kim, J., Cao, L., Shvartsman, D., Silva, E. A. & Mooney, D. J. Targeted Delivery of Nanoparticles to Ischemic Muscle for Imaging and Therapeutic Angiogenesis. *Nano Let.* **11,** 694–700 (2011).

8. Weis, S. M. Vascular permeability in cardiovascular disease and cancer. *Curr. Opin. Hematol.* **15,** 243–249 (2008).

9. Chappell, J. C., Song, J., Burke, C. W., Klibanov, A. L. & Price, R. J. Targeted Delivery of Nanoparticles Bearing Fibroblast Growth Factor-2 by Ultrasonic Microbubble Destruction for Therapeutic Arteriogenesis. *Small* **4,** 1769–1777 (2008).

10. Chien, M. P., Thompson, M. P., Barback, C. V, Ku, T. H., Hall, D. J. & Gianneschi, N. C. Enzyme-directed assembly of a nanoparticle probe in tumor tissue. *Adv Mater* **25,** 3599–3604 (2013).

11. Nguyen, M. M., Carlini, A. S., Chien, M.-P., Sonnenberg, S., Luo, C., Braden, R. L., Osborn, K. G., Li, Y., Gianneschi, N. C. & Christman, K. L. Enzyme-Responsive Nanoparticles for Targeted Accumulation and Prolonged Retention in Heart Tissue after Myocardial Infarction. *Adv. Mater.* **27,** 5547–5552 (2015).

12. Chien, M.-P., Thompson, M. P., Lin, E. C. & Gianneschi, N. C. Fluorogenic Enzyme-Responsive Micellar Nanoparticles. *Chem. Sci.* **3,** 2690–2694 (2012).

13. Chien, M. P., Carlini, A. S., Hu, D., Barback, C. V, Rush, A. M., Hall, D. J., Orr, G. & Gianneschi, N. C. Enzyme-directed assembly of nanoparticles in tumors monitored by in vivo whole animal imaging and ex vivo super-resolution fluorescence imaging. *J Am Chem Soc* **135,** 18710–18713 (2013).

14. Baum, O., Ganster, M., Baumgartner, I., Nieselt, K. & Djonov, V. Basement membrane remodeling in skeletal muscles of patients with limb ischemia involves regulation of matrix metalloproteinases and tissue inhibitor of matrix metalloproteinases. *J Vasc Res* **44,** 202–213 (2007).

15. Muhs, B. E., Plitas, G., Delgado, Y., Ianus, I., Shaw, J. P., Adelman, M. A., Lamparello, P., Shamamian, P. & Gagne, P. Temporal expression and activation of matrix metalloproteinases-2, -9, and membrane type 1—matrix metalloproteinase following acute hindlimb ischemia. *J. Surg. Res.* **111,** 8–15 (2003).

16. Callmann, C. E., Barback, C. V, Thompson, M. P., Hall, D. J., Mattrey, R. F. & Gianneschi, N. C. Therapeutic Enzyme-Responsive Nanoparticles for Targeted Delivery and Accumulation in Tumors. *Adv. Mater.* **27,** 4611–4615 (2015).

17. Rush, A. M., Thompson, M. P., Tatro, E. T. & Gianneschi, N. C. Nuclease Resistant DNA via High-Density Packing in Polymeric Micellar Nanoparticle Coronas. *ACS Nano* **7,** 1379–1387 (2013).

18. Rush, A. M., Nelles, D. A., Blum, A. P., Barnhill, S. A., Tatro, E. T., Yeo, G. W. & Gianneschi, N. C. Intracellular mRNA Regulation with Self-Assembled Locked Nucleic Acid Polymer Nanoparticles. *J. Am. Chem. Soc.* **136,** 7615–7618 (2014).

19. Ungerleider, J. L., Kammeyer, J. K., Braden, R. L., Christman, K. L. & Gianneschi, N. C. Enzyme-targeted nanoparticles for delivery to ischemic skeletal muscle. *Polym. Chem.* **8,** 5212–5219 (2017).

20. Ungerleider, J. L., Johnson, T. D., Hernandez, M. J., Elhag, D. I., Braden, R. L., Dzieciatkowska, M., Osborn, K. G., Hansen, K. C., Mahmud, E. & Christman, K. L. Extracellular Matrix Hydrogel Promotes Tissue Remodeling, Arteriogenesis, and Perfusion in a Rat Hindlimb Ischemia Model. *J Am Coll Cardiol Basic Transl Sci* **1,** 32–44 (2016).

21. Blum, A. P., Kammeyer, J. K., Yin, J., Crystal, D. T., Rush, A. M., Gilson, M. K. & Gianneschi, N. C. Peptides Displayed as High Density Brush Polymers Resist Proteolysis and Retain Bioactivity. *J. Am. Chem. Soc.* **136,** 15422–15437 (2014).

22. Ma, C. D., Adamiak, L., Miller, D. S., Wang, X., Gianneschi, N. C. & Abbott, N. L. Liquid Crystal Interfaces Programmed with Enzyme-Responsive Polymers and Surfactants. *Small* **11,** 5747–5751 (2015).

23. Weissleder, R., Tung, C.-H., Mahmood, U. & Bogdanov, A. In vivo imaging of tumors with protease-activated near-infrared fluorescent probes. *Nat Biotech* **17,** 375–378 (1999).

24. Mahmood, U. & Weissleder, R. Near-Infrared Optical Imaging of Proteases in Cancer.

Mol. Cancer Ther. **2,** 489–496 (2003).

25. Ogawa, M., Kosaka, N., Choyke, P. L. & Kobayashi, H. In vivo Molecular Imaging of Cancer with a Quenching Near Infrared Fluorescent Probe Using Conjugates of Monoclonal Antibodies and Indocyanine Green. *Cancer Res.* **69,** 1268–1272 (2009).

26. Choi, H. S., Nasr, K., Alyabyev, S., Feith, D., Lee, J. H., Kim, S. H., Ashitate, Y., Hyun, H., Patonay, G., Strekowski, L., Henary, M. & Frangioni, J. V. Synthesis and In Vivo Fate of Zwitterionic Near-Infrared Fluorophores(). *Angew. Chem. Int. Ed. Engl.* **50,** 6258–6263 (2011).

27. Ladd, J., Zhang, Z., Chen, S., Hower, J. C. & Jiang, S. Zwitterionic Polymers Exhibiting High Resistance to Nonspecific Protein Adsorption from Human Serum and Plasma. *Biomacromolecules* **9,** 1357–1361 (2008).

28. Chang, Y., Liao, S.-C., Higuchi, A., Ruaan, R.-C., Chu, C.-W. & Chen, W.-Y. A Highly Stable Nonbiofouling Surface with Well-Packed Grafted Zwitterionic Polysulfobetaine for Plasma Protein Repulsion. *Langmuir* **24,** 5453–5458 (2008).

29. Xiao, W., Lin, J., Li, M., Ma, Y., Chen, Y., Zhang, C., Li, D. & Gu, H. Prolonged in vivo circulation time by zwitterionic modification of magnetite nanoparticles for blood pool contrast agents. *Contrast Media Mol Imaging* **7,** 320–327 (2012).

30. Barnhill, S. A., Bell, N. C., Patterson, J. P., Olds, D. P. & Gianneschi, N. C. Phase Diagrams of Polynorbornene Amphiphilic Block Copolymers in Solution. *Macromolecules* **48,** 1152–1161 (2015).

31. Ryu, J. H., Shin, J. Y., Kim, S. A., Kang, S. W., Kim, H., Kang, S., Choi, K., Kwon, I. C., Kim, B. S. & Kim, K. Non-invasive optical imaging of matrix metalloproteinase activity with albumin-based fluorogenic nanoprobes during angiogenesis in a mouse hindlimb ischemia model. *Biomaterials* **34,** 6871–6881 (2013).

32. Helisch, A., Wagner, S., Khan, N., Drinane, M., Wolfram, S., Heil, M., Ziegelhoeffer, T., Brandt, U., Pearlman, J. D., Swartz, H. M. & Schaper, W. Impact of mouse strain differences in innate himdlimb collateral vasculature. *Arterioscler. Thromb. Vasc. Biol.* **26,** 520–526 (2006).

33. Chalothorn, D. & Faber, J. E. Strain-dependent variation in collateral circulatory function in mouse hindlimb. *Physiol. Genomics* **42,** 469–479 (2010).

Chapter 6

Conclusions

6.1 Summary and Significance

The works presented in this thesis highlight the development and translational potential of two injectable biomaterial therapies for skeletal muscle regeneration. Skeletal muscle regeneration, whether ischemic peripheral artery disease or acute injury represents a leading cause of disability and pain in adults. Pharmacologic and surgical interventions are largely ineffective, and the field of regenerative medicine is developing approaches to ameliorate muscle regeneration strategies. Specifically, injectable hydrogels or nanoparticles can deliver a therapeutic payload or be used as a material alone approach as a supportive, bioactive scaffold to initiate endogenous repair mechanisms. Taken together, these studies demonstrate the efficacy and promising future translational outlook of these materials for improving clinically meaningful skeletal muscle regeneration.

The first chapter, “Injectable biomaterials for the treatment of peripheral artery disease: translational challenges and progress,” outlines the approaches the biomaterials field has taken for therapeutic delivery strategies of growth factors, cells, or material-alone systems for peripheral artery disease. Moreover, this work highlights the specific translational concerns that need to be considered when developing injectable biomaterials for the clinic – namely, regulatory challenges, delivery challenges, and manufacturing challenges. Consideration of these factors early on in the development of injectable biomaterials will help facilitate their rapid clinical translation.

The second chapter, “Fabrication and Characterization of Injectable Hydrogels Derived from Decellularized Skeletal and Cardiac Muscle,” demonstrates common methods for fabricating decellularized hydrogels in an attempt to present a standardized set of methods for

the field. Especially given the translational nature of these materials, it is important to consider all of the factors that must be evaluated to ensure consistency of decellularized materials including decellularization verification, biochemical characterization, and mechanical characterization.

The third chapter, “Extracellular Matrix Hydrogel Promotes Tissue Remodeling, Arteriogenesis, and Perfusion in a Rat Hindlimb Ischemia Model,” is the first study to demonstrate efficacy of a skeletal muscle matrix hydrogel in a preclinical peripheral artery disease model. The study also examines possible mechanisms of action behind functional improvements using novel transcriptomic analysis and confirmatory histological analysis. Evidence suggests that the skeletal muscle matrix hydrogel promotes cell survival, arteriogenesis, and skeletal muscle progenitor cell recruitment. This is a significant study for the field to demonstrate how acellular hydrogels can act as bioactive scaffolds with beneficial effects on vasculogenesis and myogenesis *in vivo,* which is translationally much more cost-effective, easy to manufacture, and easy to deliver than alternative regenerative medicine approaches (i.e., growth factors, cells).

The fourth chapter, “Tissue specific muscle extracellular matrix hydrogel improves skeletal muscle regeneration *in vivo* over non-matched tissue sources,” is the first study to rigorously examine the effects of tissue source of decellularized hydrogels *in vivo.* Specifically, mechanistic studies demonstrate that the skeletal muscle ECM hydrogel increases muscle hypertrophy and growth and skeletal muscle progenitor recruitment. This study demonstrates that the tissue source of decellularized ECM hydrogels is an important consideration for regenerative medicine applications *in vivo.* Although many groups have investigated the importance of tissue specificity of decellularized ECM materials *in vitro* on tissue specific progenitor and primary cells, their tissue specific qualities have not been rigorously validated *in vivo*, which presents a much more complex milieu of cells and synergistic microenvironmental

cues. It is hoped that the field will take this important finding about tissue specific ECM hydrogel cues to design more optimal injectable therapeutic scaffolds.

The fifth chapter, “Enzyme-Targeted Nanoparticles for Delivery to Ischemic Skeletal Muscle,” is the first study to demonstrate minimally invasive nanoparticle targeting in a preclinical peripheral artery disease model by harnessing the upregulation of matrix metalloproteinase enzyme activity in ischemic skeletal muscle. Targeting was achieved and modulated by altering the design of the nanoparticles. This study provides proof-of-concept for a targeted system for minimally invasive delivery of therapeutic payload. Although groups have aimed to passively target cardiovascular tissues with various options (enhanced permeability and retention effect, ultrasound-enabled delivery), no groups have targeted molecular hallmarks of ischemic skeletal muscle until this work.

Taken together these chapters demonstrate proof-of-concept of efficacy and mechanism of action of injectable hydrogel and nanoparticle therapies for skeletal muscle regeneration. Naturally derived and synthetic scaffolds provide flexible platforms for injectable delivery of therapeutic payloads or bioactive material-alone approaches. These novel treatment modalities will enable future translational development of minimally invasive approaches for today’s unmet clinical needs.

6.2 Future Outlook

In order to continue developing injectable hydrogel and nanoparticle approaches for clinical translation for treating peripheral artery disease and skeletal muscle regeneration, there is much work still to be done.

Although investigated in depth here, the mechanism of action of decellularized ECM hydrogels has just begun to be studied in the past ~5 years. Many seminal works have been recently published which detail the complex endogenous biological response to decellularized materials [1–4]. These studies, along with the work presented in this thesis, demonstrate that the

endogenous response is comprised of many cell types including inflammatory populations, tissue specific progenitors, vascular cell types, and stromal cells. However, conclusions have been mainly discerned through whole tissue gene expression, which lacks the resolution of behavior on a single cell or cell-type level, or through investigations of the phenotypes of single cells or maybe interactions between 1-2 cell types, interactions which while thoroughly characterized are overly simplistic. Thus, future work should focus on the systems-level interaction of multiple cell types and extracellular cues in the tissue- and organism-level coordination of regenerative responses *in vivo.* By better understanding the complex biological response, perhaps a future decellularized material can be envisioned that can specifically modulate pathways and interactions known to be important for successful tissue regeneration. Furthermore, most mechanistic studies have been completed in young, healthy animal models. Future studies should focus on regenerative medicine in the context of aging, fibrosis, and chronic inflammation. Unique microenvironmental obstacles to regeneration exist in these states, and understanding the systems-level response to decellularized ECM in these more clinically relevant microenvironments will help ensure these injectable materials are successful upon clinical translation. Still, the promising preclinical data and translation to clinical trials of certain injectable decellularized ECM hydrogels (NCT02305602) indicates that the clinical translation of these materials is imminent.

On the other hand, the enzyme-targeted nanoparticles studied in this thesis have many hurdles to overcome before clinical translation is possible. The data presented here focus on proof-of-concept of MMP-targeted NPs to ischemic muscle. However, these NPs are solely targeting systems; they had no therapeutic payload for delivery to the tissue once targeted. Current work is focusing on evaluating a variety of compounds for conjugation to and delivery from the targeted NPs, including small molecules and therapeutic peptides. In the case of peripheral artery disease, most therapeutics are focused on ameliorating the ischemia and restoring functional blood flow to the muscle. The benefit of the polymer peptide amphiphilic

system is that a variety of therapeutics can be theoretically conjugated to the polynorbornene backbone due to the ease of the ring opening metathesis polymerization strategy. Once therapeutic candidates are selected and validated *in vitro*, preclinical studies will need to be conducted to ensure targeting, efficacy, and safety *in vivo*. Another limitation of the nanoparticle system is that it is not degradable and was thus seen in studies from this thesis and unpublished data to reside in the target tissue for up to 40 days post-injection. This property may not be desirable for therapeutic delivery or long term biological responses to the NPs. Thus, degradable systems are now being investigated to improve the therapeutic delivery window and prevent long term side effects of the aggregated NPs. Aggregation/degradation dynamics will need to be optimized, and the parameters may be different depending on which therapeutic is being delivered or between preclinical animal models and human patients. Another limitation of enzyme-targeted NPs is the specificity of the enzyme-cleavable substrate to the diseased target tissue of interest. For example, MMP-2/9 are upregulated in cardiovascular disease, but also may be implicated in other tissues (e.g., cartilage in the joints). Thus, a more specific targeted system could avoid aggregation in tissues that are not intending to be targeted or in patients with multiple comorbidities where elevated MMP activity may be present (e.g., arthritis). Other groups have used different targeting modalities than enzyme specificity such as ROS activity or pH. Incorporating a dual targeting component into the nanoparticles, or making them more specific to enzymes active in ischemic muscle, could improve targeting and limit off-target accumulation. In conclusion, if these limitations are addressed, enzyme-targeted NPs would be a desirable therapeutic delivery strategy for PAD patients due to their minimally invasive nature and ability to target to molecular hallmarks of the disease without off target effects.

In summary, injectable biomaterials represent a promising new treatment modality in PAD to mitigate the unmet clinical need. Naturally derived hydrogels act as self-assembling viscoelastic scaffolds that have pro-survival, pro-regenerative effects *in vivo* to restore perfusion

and improve muscle regeneration. Targeted nanoparticles can be a more minimally invasive approach that aggregate and are retained for drug delivery approaches.

6.3 References

1. Wassenaar, J. W., Gaetani, R., Garcia, J. J., Braden, R. L., Luo, C. G., Huang, D., DeMaria, A. N., Omens, J. H. & Christman, K. L. Evidence for Mechanisms Underlying the Functional Benefits of a Myocardial Matrix Hydrogel for Post-MI Treatment. *J. Am. Coll. Cardiol.* **67,** 1074–1086 (2016).

2. Sadtler, K., Estrellas, K., Allen, B. W., Wolf, M. T., Fan, H., Tam, A. J., Patel, C. H., Luber, B. S., Wang, H., Wagner, K. R., Powell, J. D., Housseau, F., Pardoll, D. M. & Elisseeff, J. H. Developing a pro-regenerative biomaterial scaffold microenvironment requires T helper 2 cells. *Science (80-.).* **352,** 366 LP-370 (2016).

3. Williams, C., Quinn, K. P., Georgakoudi, I. & Black, L. D. Young developmental age cardiac extracellular matrix promotes the expansion of neonatal cardiomyocytes in vitro. *Acta Biomater.* **10,** 10.1016/j.actbio.2013.08.037 (2014).

4. Williams, C., Sullivan, K. & Black, L. D. Partially Digested Adult Cardiac Extracellular Matrix Promotes Cardiomyocyte Proliferation in Vitro. *Adv. Healthc. Mater.* **4,** 1545–1554 (2015).